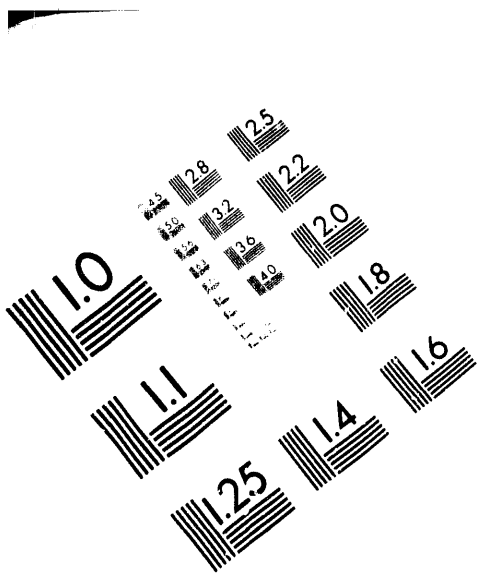

Association for Information and Image Management

1100 Wayne Avenue, Suite 1100
Silver Spring, Maryland 20910

301/587-8202

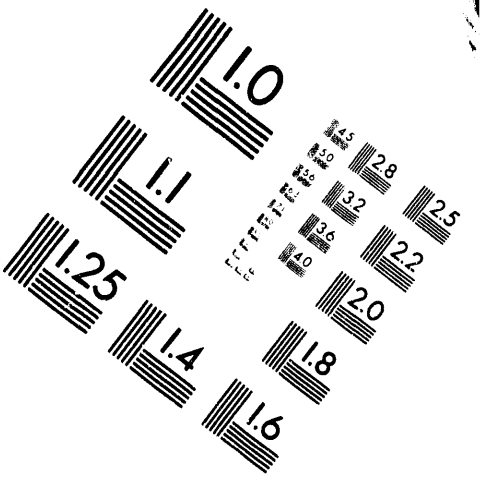

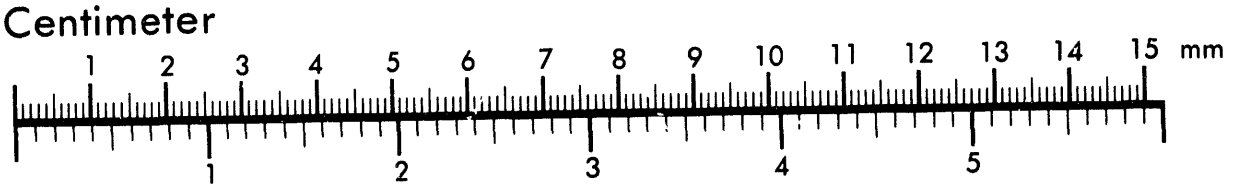

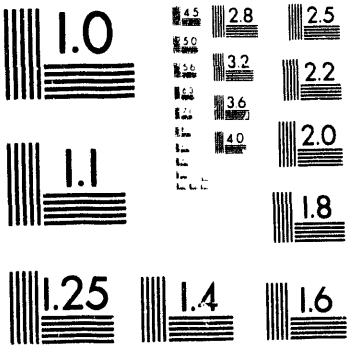

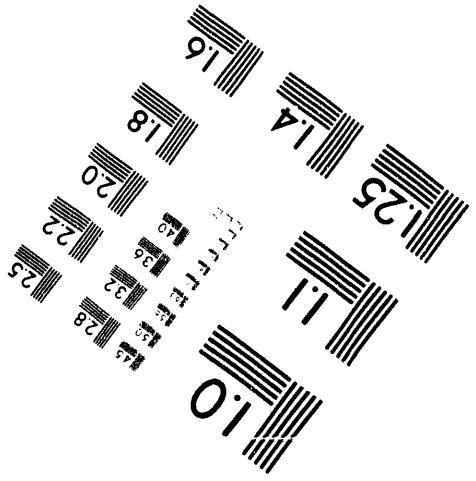

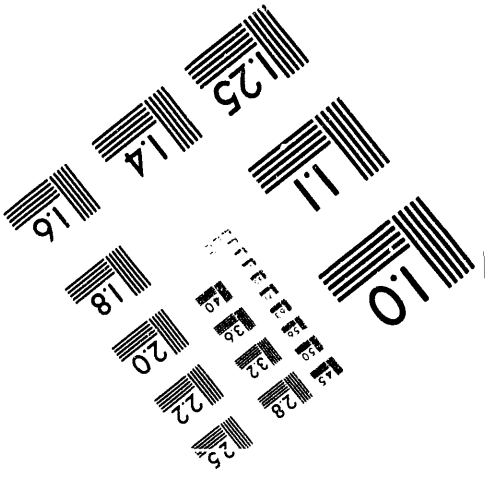

1 of 1

ORNL/TM-12254

INSTRUMENTATION AND CONTROLS DIVISION

DEVELOPMENT OF A NEURAL NET PARADIGM THAT PREDICTS SIMULATOR SICKNESS

G. O. Allgood

Date Published—March 1993

Prepared by
OAK RIDGE NATIONAL LABORATORY
Oak Ridge, Tennessee 37831-6285
managed by
MARTIN MARIETTA ENERGY SYSTEMS, INC.
for the
U.S. DEPARTMENT OF ENERGY
under contract DE-AC05-84OR21400

CONTENTS

FIGURES

TABLES

ABSTRACT

A disease exists that affects pilots and aircrew members who use Navy Operational Flight Training Systems. This malady, commonly referred to as simulator sickness and whose symptomatology closely aligns with that of motion sickness, can compromise the use of these systems because of a reduced utilization factor, negative transfer of training, and reduction in combat readiness. A report is submitted that develops an artificial neural network (ANN) and behavioral model that predicts the onset and level of simulator sickness in the pilots and aircrews who use these systems. It is proposed that the paradigm could be implemented in real time as a biofeedback monitor to reduce the risk to users of these systems.

The model captures the neurophysiological impact of use (human-machine interaction) by developing a structure that maps the associative and nonassociative behavioral patterns (learned expectations) and vestibular (otolith and semicircular canals of the inner ear) and tactile interaction, derived from system acceleration profiles, onto an abstract space that predicts simulator sickness for a given training flight.

1. INTRODUCTION

The usefulness of a major innovation in the history of flight training is being compromised by a rather poorly understood phenomenon known as simulator sickness, whose symptoms closely parallel those of motion sickness. This disease creates a negative environment where the undesirable reputation of a simulator to cause sickness/discomfort is enhanced and the utilization decreased by the lack of training conformity. Experts have noted an increase in the incidence of this malady and believe it to be the result, at least in part, of the increase in sophistication or fidelity of flight simulators. This report discusses the phenomenon of simulator sickness and develops an artificial neural network (ANN) method to measure and predict the onset and level of the disease in pilots and aircrews who use these systems. By providing a capability such as an on-line feedback monitoring system, the discomfort and risk for those who train on these devices can be reduced or eliminated.

Simulator sickness is defined as the sickness that is produced in the simulator, but not in the aircraft, while performing particular flight profiles or training hops. Interestingly, in the past it has been assumed that more experienced pilots have a higher incidence of simulator sickness than do less experienced pilots. (This assumption has come under scrutiny in light of this research.) On the surface, this statement may appear paradoxical. However, intuition provides an explanation: the more experienced pilots have a greater neural store of expectations and therefore are more sensitive to subtle differences between aircraft and simulator motion and visual cues. These expectations and awareness create an environment of sustained sensitivity to those stimuli that act as a genesis of the disease. This finding is particularly disconcerting to military training commands responsible for these devices because experienced pilots usually are in the more influential position to create negative impressions of simulators. Figure 1.1 is a diagrammatical representation of the attributes of simulator sickness whose interactions impact the fidelity and training effectiveness of these devices. The quadrants represent three functional attribute classes [**system dynamics** (motion/visual), **behavioral** (situational awareness/associative behavior), and **training** (flight syllabus)] that can alter the human's environmental perception, combining to enhance or degrade the interpretative capabilities of the human during training sessions.

Other concerns are associated with the use of these systems. Adaptation, a process by which the neural store of information is altered, can lead to a negative transfer of training to the aircraft in the form of inappropriate control responses. After-effects including postural instability, dizziness, and flashbacks can influence product liability of use. Flashbacks are particularly problematic because of their sudden and unexpected onset manifested by illusory sensations of climbing and turning, sensations of negative gravity (g), and perceived inversions of the visual field.

Investigators researching this problem note that, while the symptoms of simulator sickness resemble those of motion sickness, they are not identical. While the most explicit sign of simulator sickness is vomiting, a constellation of signs and symptoms exist: dizziness, drowsiness, postural changes, confusion, headaches, apathy, fatigue, and disorientation. Reports suggest that the incidence rate for simulator sickness, depending on the specific device, can reach as high as 60% (Allgood et al. 1987b). Figure 1.2 shows an overall incidence of simulator sickness vs six helicopter simulators studied (Kennedy, Allgood, and Lilienthal 1989). The incidence reporting is based on at least one minor

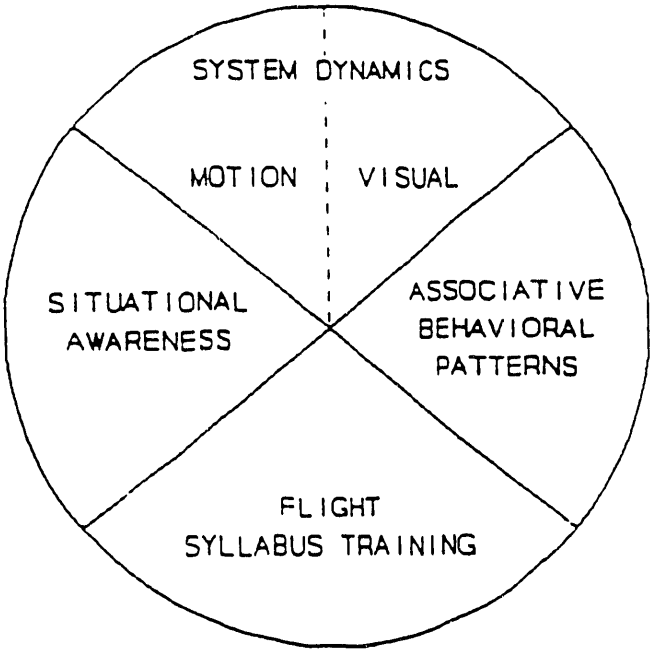

Fig. 1.1. Attributes of simulator sickness.

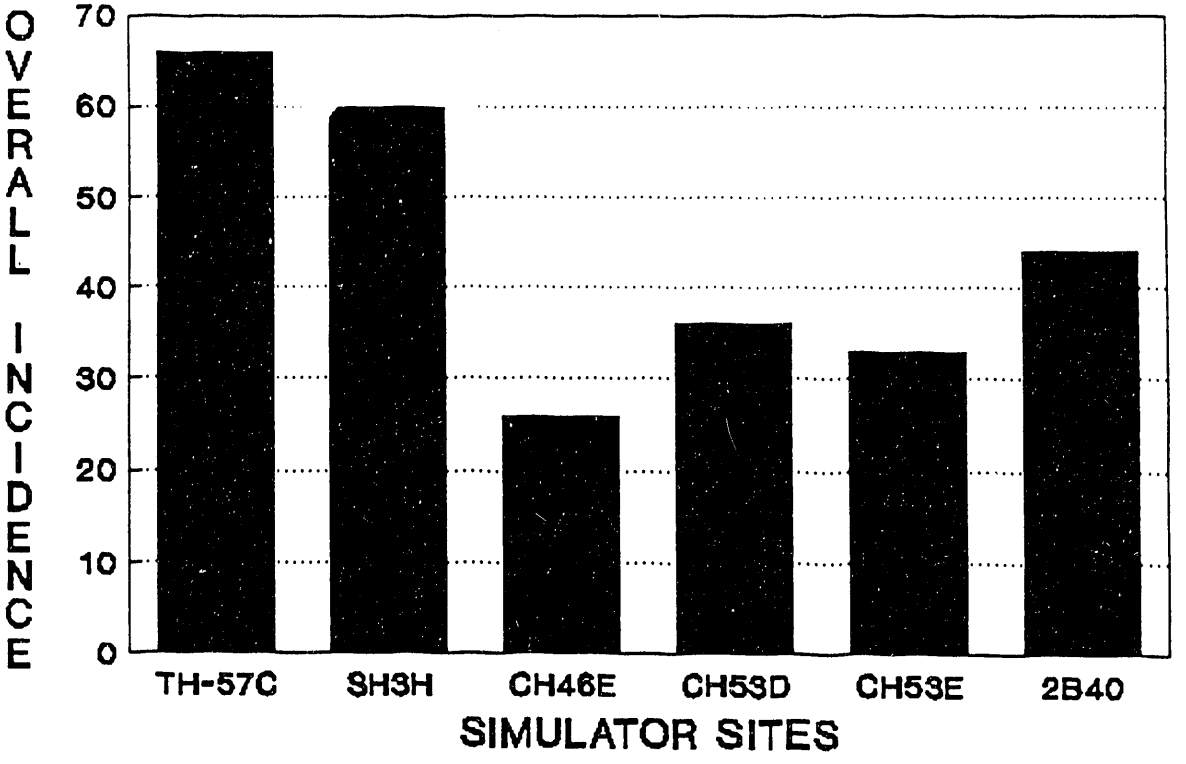

Fig. 1.2. Comparison of pilots reporting key symptomatology in six helicopter simulators.

symptom reported on a motion sickness questionnaire. As indicated, simulator sickness exists at some level in several of these systems currently active in the U.S. Navy's training inventory. Since these devices represent large capital outlays, the presence of the malady in any system can translate into a reduction in the use recovery cost.

Conversations (1988) with R. S. Kennedy, recognized expert in the field of simulator sickness (Essex Corporation, Orlando, Florida), confirmed agreement that among field experts the satisfactory solution to the problem will not be in the form of one fix, but many. They base their conclusions on the belief that simulator sickness is a convolution of system dynamics and behavioral processes, each requiring its own solution. Current research efforts are directed toward the systematic identification of these causal relationships and establishment of corrective actions for each. The causes include, among others: (1) engineering performance of both visual and motion system(s), (2) properties of the visual/motion coordination (synchronization and transport delay), (3) nature of flight profiles for simulated mission scenarios, (4) length and scheduling of simulator exposure and recovery periods, and (5) pilot associative and nonassociative behavioral patterns. Previous attempts to identify these simulator sickness attributes have omitted the most important relationship that exists in these systems—the human-machine interaction—in support of a classical systems approach to identification. Figure 1.3 is a diagram of the overall system showing the pilot as an integral part of the cascaded loop. By ignoring the pilot, his skills level, and task/syllabus structure, the feedback path is cut, reducing the system to a simple feedforward network (G2*G3). This omission will not excite the unstable modes of operation that exist with the pilot-in-the-loop. These instabilities are a result of pilot-induced oscillation (PIO) that occurs when excessive time delays (nonminimum phase system) are present in the system.

The emphasis of this research is on supplementing these efforts by providing a means to characterize and predict in real time the effects of human-machine interaction as it relates to simulator sickness. This emphasis infers a capability to implement the paradigm in an

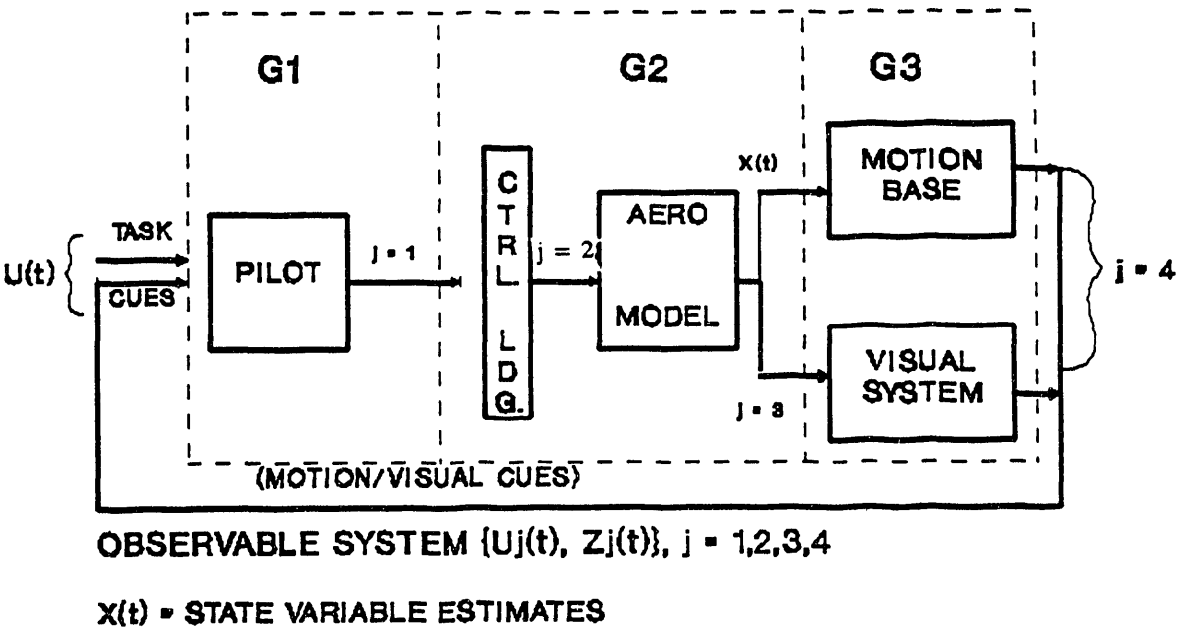

Fig. 1.3. System measurement paradigm cascaded system with feedback = G1*G2*G3.

existing or deployable system. The benefits from this research can extend to areas in which humans are exposed to environments such as ships, amphibious craft, tanks, personnel carriers, and aircraft that may induce motion-type sicknesses. The results also have applicability for test and evaluation criteria for systems (information feedback providing revisions of standards for human limits to vibration exposure).

An interesting exercise supporting this research outlines the potential payoff as outlined by Kennedy. Training a single combat pilot costs upwards of $1M. The cost distribution is 60% for the simulator and 40% for the aircraft. The average cost ratio of military aircraft time to simulator is 10:1, indicating that an hour of aircraft time costing $1500 is equivalent to an hourly cost of $150 for the simulator. This cost ratio equates to a potential savings of $4.2M through the use of training devices. This is based on a 6-day-week, 10-hour-day usage rate. The cost ratio for commercial airline simulators ranges between 15:1 and 20:1, resulting in an increasingly larger payoff. Unfortunately, depending on the device, simulator sickness can affect from 25% to over 60% of the pilots who train in them, which can substantially reduce the savings realized by the government and industry through a reduced usage factor. The impact will be increased training costs; a higher at-risk use for training in the aircraft instead of in the simulator; reduced pilot readiness; and poor training that will jeopardize pilots, aircrews, and passengers. In support of simulator training, the ANN paradigm could provide a real-time assessment of the probability of the onset and level of simulator sickness and allow a means to institute safeguard policies for simulator training. This information could be extended to provide an ongoing quality assurance assessment. Major simulator manufacturers such as CAE, Link, and Rediffusion are extremely interested in how the simulators they produce impact pilot operational readiness.

1.1 A HISTORY OF SIMULATOR SICKNESS (KENNEDY 1989)

Flight training is a multimillion-dollar-a-year business that draws its technical talent from the fields of experimental and behavioral psychology, human factors, engineering, mathematics, artificial intelligence, and medicine. As such, it has many facets that span a multitude of requirements. One is wargaming, where predictive models of combat are integrated to provide a learning environment for tactics, strategy, and logistic support for military personnel. Another is interrogation and diagnostic systems to train personnel to repair complex devices. These systems provide an interactive computer environment where the user asks questions, reviews literature, and views video images to train and/or repair these systems. A third is part-task trainers. These systems provide selective elements of training and present them to the user. An example is the Stand-Off Land Attack Missile part-task trainer, which provides an ability for the pilot/weapons officer to practice weapon deliveries on selected targets by using a portable computer. A fourth system is the static instrument trainers used to teach switchology to personnel. For the future, virtual environment trainers exist where humans train in a projected three-dimensional world. Finally, there are simulators. In this context, simulators are defined as those systems that provide visual cues, motion cues, or combinations of the two for training purposes. These systems provide a mechanism by which pilots and aircrews can train for tactics, emergency procedures, basic flight skills, or even transition to new systems without the need of the real aircraft. Their strengths are in an ability to simulate the motion, visual, acoustic, and environmental parameters that would accompany the pilot's interaction with the aircraft and

the world. In addition, they provide a platform where mistakes are not measured in terms of aircraft and pilot loss—only in terms of training effectiveness.

The number and types of these devices are quite numerous and include driving simulators, aircraft simulators for both helicopter and fixed-wing aircraft, air cushion devices, NASA shuttles, tanks, and ship navigation. The importance of these systems is described in a recent article in a trade magazine (PM Trade 1991) that alludes to the fact that the success of Desert Storm can be attributed to the training that our military personnel received on these devices. In view of this, these systems will become more important in light of declining training dollars.

The development of these flight and automobile simulators appears to have been guided by an assumption that the more realistic a simulation is, the better training will be (Kennedy, Hettinger, and Lilienthal 1990). Early flight simulators (1950s) were fixed base with limited noise and vibration cues (Kennedy et al. 1991). Cockpits were open with limited projected screen visuals (260 × 75°). Luminance was dim and resolution was poor. Their visual model was based solely on sky and earth. Current simulators are fixed based or motion with 6-degree-of-freedom (DOF) movement. Their cockpits are enclosed with computer imaging graphics provided by CRTs. The visual model incorporates sky/earth and targets. These systems have good contrast luminance and can have a visual projection > 300° horizontal × 180° vertical. The early driving simulators (1960s) had terrain-board closed-circuit TV systems for visuals with a field-of-view projection of 50° horizontal and 39° vertical and were fixed based (Barrett and Nelson 1965). Current conceptual designs by the U.S. Department of Transportation (Allgood 1991) call for wide-field-of-view computer imaging graphics or head slaved projection with the possibility of a full 6-DOF motion base. As seen, technology has focused on creating a higher fidelity simulation environment. This does not materialize without cost. There is strong belief that increased realism results in an increase in the incidence of simulator sickness (Kennedy, Hettinger, and Lilienthal 1990). Although the relationship between fidelity, training effectiveness, and simulator sickness is not well known, empirical evidence (Casali 1986) supports this assumption.

The presence of simulator sickness is accompanied by concerns for safety and health, compromised training, and operational readiness (Kennedy et al. 1991). Among the implications of simulator sickness for safety and health are the presence of physiological discomfort, visual aftereffects, flashbacks, and interference with motor skills. Aftereffects are of particular importance because they bear a strong resemblance to the disturbances individuals experience when wearing reversing, displacing, or inverting lenses (Dolezal 1982) and also resembles astronauts's experience with space adaptation (Homick 1982) or space sickness. The occurrence of these symptoms poses a significant threat to pilot safety following the use of the simulator. To alleviate this, mandatory grounding policies have been enforced in some training commands (FITRON 1981). For compromised training, the impact is poor training and the development of an adverse attitude toward the use of a simulator. The presence of symptoms can interfere with learning because of distractions caused by physiological disturbances. Finally, the impact on operational readiness is flying downtime and the acquisition of habits inappropriate in the control of the environment. In some U.S. Navy and Marine Training Commands, a pilot is required to be grounded for 12–24 hours following a simulator exercise. As an example of inappropriate behavior, in an effort to minimize the effects of the pseudo-Coriolis effects (Dichgans and Brandt 1973), a pilot may restrict head movement in the simulator. If this behavior is taken into a combat situation, it could result in pilot death. As seen, the presence of simulator sickness has significant implications for training and pilot safety.

Most literature on simulator sickness consists of surveys documenting the occurrence of the malady during simulator training. The earliest reported case is the Bell HTL-4 helicopter simulator (Havron and Butler 1957). This fixed-base device was designed to train pilots in hovering and other close-to-ground plane coupling events. An evaluation was undertaken to study training effectiveness in the device. It was determined, though, that the lack of fidelity in a number of display-control relationships contributed to simulator sickness (78% of 36 student pilots) and negative transfer of training. Although the study was not targeted for simulator sickness, it was such an acute problem that a questionnaire was developed to determine the severity and occurrence of the malady.

A subsequent study of this same simulator (Miller and Goodson 1960) identified a number of potential hypotheses for the sickness problem. (An important point about this study is that the observations are based on personal experiences.) One was that the cyclic control input/output lag was two to three times that of the actual helicopter. Another observation was visual disparity in low-altitude flight. In all cases, the resulting simulator sickness problem was attributed to conflicts within the visual presentation.

In a 1967 report, Sinacori identified the V/STOL simulator, a fixed-based system, as problematic because of the incidence of simulator sickness. Later, a motion base was added (roll, pitch, and yaw) to alleviate the sickness and improve simulator utility. Overall, the addition of the motion base appeared to reduce the incidence of simulator sickness. In addition to identifying the presence of the malady, this study also offered countermeasures to reduce the level of the disease. These included eyeshades, procedures for pilots, and operational considerations for the system.

During the following 10 years, very little research was carried out on simulator sickness until a study (Hartman and Hatsell 1976) was undertaken to document the occurrence of simulator sickness in the U.S. Air Force Simulator for Air-to-Air Combat (SAAC) at Luke Air Force Base. It was determined that as high as 50% of the pilots experienced some form of simulator sickness while training. Further analysis identified that most of the moving base energy was in the 0.2-Hz energy range. In a subsequent survey of the simulator (Kellog, Castore, and Coward 1980), it was found that 88% of the pilots who used the simulator experienced some symptoms.

In a training evaluation of a P3-C simulator (Ryan, Scott, and Browning 1978) motion sickness-like symptoms were recorded during both on- and off-motion conditions. The Canadian counterpart of this simulator was also studied (Money 1980) with published guidelines to minimize the symptoms.

Investigations of Air Combat Maneuvering fighter simulators (Frank 1981; Casto 1982) identified that the F-14 Weapons Systems Trainer (WST) had an incidence rate of 10% for the users. Based on this readjustment, guidelines for use were issued. For the Navy Air Combat Maneuvering simulator, sickness symptoms were experienced by both the pilot and the radio intercept officer. As with the F-14 WST, guidelines were issued to reduce or eliminate the incidence of simulator sickness.

True simulator sickness research in the early 1960s concentrated on individual differences among subjects (Barrett and Nelson 1965; Barrett and Thornton 1968) as related to driving simulators. These experiments were aimed at determining the relationship among perceptual style, simulator sickness, and other related issues. Based on this rationale, it was hypothesized that simulator sickness was due to sensory conflict between the visual presentation of motion and the lack of any corresponding body motion. By using field independence-dependence as a measure of sensitivity for the human test subjects, the study showed that those more susceptible to motion cues did, in fact, experience a higher

incidence of simulator sickness. In another experiment (Reason and Diaz 1971), subjects were asked to rate the fidelity or realism of the simulator. In this, a negative correlation was shown to exist between reported sickness and rated simulator realism.

Other research efforts addressed simulator sickness in an experimental framework. One looked at the causal relationship between retinal disparity and poor depth of convergence in a fixed-based simulator (Miller and Goodson 1958). The study found that distortion in distance cuing was probably insufficient in itself to elicit simulator sickness. In an experiment designed to determine the effects of driving simulator design variables on simulator sickness (Casali and Wierwille 1980), it was determined that computational delays have an influence on the incidence of the disease and that enclosures (cab design) can also influence the onset of symptoms. Another experiment was developed to determine design parameter impact on simulator sickness (Hartman and Hartsell 1976), in which a structured rating scale was administered to instructor pilots after they flew the SAAC simulator. It was determined that 50% of the pilots experienced eye strain, possibly due to CRT raster line generation; 33% experienced headaches, possibly a result of eye strain; 38% experienced tiredness due to workload; and 14% reported nausea with or without motion. In the P3-C studies mentioned earlier (Ryan, Scott, and Browning 1978), one was conducted to investigate the effects of cockpit motion vs no motion on simulator sickness as measured by a Motion Sickness Questionnaire (MSQ). According to the MSQ, subjects in the motion and no-motion groups appeared to be about average among pilots with regard to simulator sickness. Neither group produced significant evidence of simulator-induced sickness during training. Experiments were designed to investigate the incidence of symptoms accompanying purely visual stimulation (Crampton and Young 1953) and wide-field-of-view displays (Parker 1971). Included in this group was an experiment which showed that large-field patterns of high-velocity linear motion created disturbing effects in the test subjects (Lestienne, Soechting, and Herthoz 1977) and one which showed the effects of visual influences on vestibular function (Precht 1979).

Experiments were also conducted to determine the impact of simulator system design parameters on simulator sickness. In one study (Uliano et al. 1986), the effects of a synchronous visual delay on a simulated helicopter hover and air taxi were investigated. The results indicated that no effect on either illness or performance was observable over the testing parameters (215, 177, and 126 ms). In another experiment, in which the role of visual-motion coupling delays and cuing order was investigated (Frank, Casali, and Wierwille 1987), it was observed that visual delay was far more disruptive to control performance and physical comfort. Furthermore, it was observed that performance was increased and a better feeling of well-being observed when the visual system led the motion system. Another experiment investigated the effects of energy spectra in moving- base simulators on simulator sickness (Allgood et al. 1987b). The results showed that the incidence of simulator sickness was greater in a simulator with energy spectra in the region guarded against by MILSTD 1472C (see Fig. 1.4) (McCauley and Kennedy 1976). Although a significant finding, there was no extension of the arguments to include the time-domain dependencies (see Fig. 1.5). There was also an experiment to determine what effects dynamic visual distortions had on the incidence of simulator sickness (Rosinski 1982). This study investigated the effects of viewing visual displays from other than the design eye of the system. The results supported a previous conclusion that aircrew who viewed a simulator's visual display from off-axis experienced a greater incidence of simulator sickness.

As seen from this literature review of simulator sickness, the research has focused primarily on simulator site surveys or partitioned elements of the causal parameters that are implicated in simulator sickness. What is missing is a unifying model that acts as a stable predictor of simulator sickness incorporating all available information. This model must provide a memory of the time history of interactive dynamics between subject and simulator and account for such. I base this model hypothesis on my own experience in the simulator. As I flew the device, I became more aware of the neural-physiological sensitivities of dynamic events that occurred during the flight. Events that happened at the beginning of the hop did not affect me later if I maintained the simulator's acceleration profiles below some subjected level that was accommodating to me (a forced control action driven by the task at hand). In instances such as this, I flew the simulator without any physical problems. If I exceeded this perceived threshold during the flight and continued to do so, then I experienced a cumulative effect that I was unable to shed before departing the simulator. At

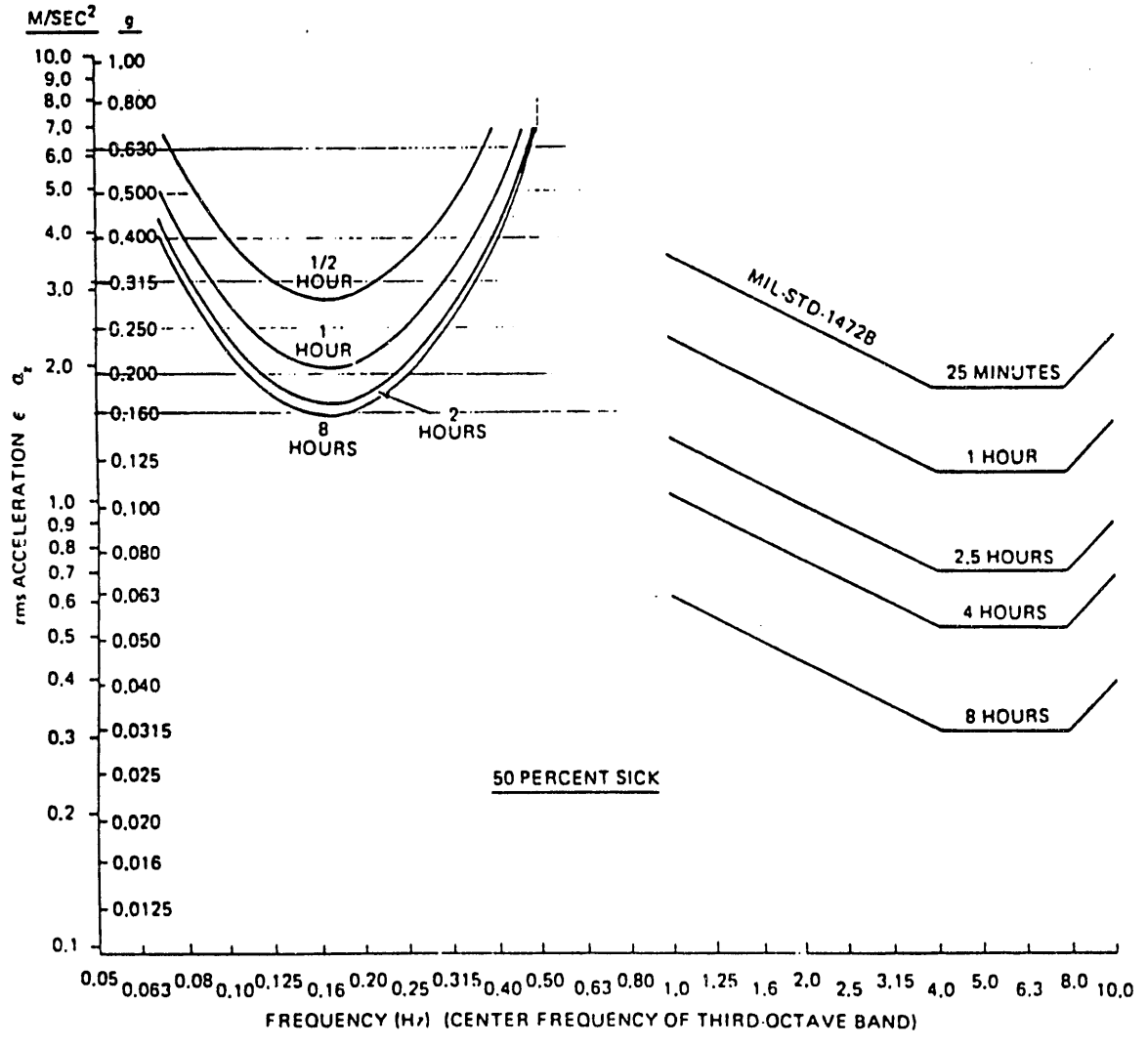

Fig. 1.4. Fifty percent motion sickness protection limits for human exposure to very low frequency vibration.

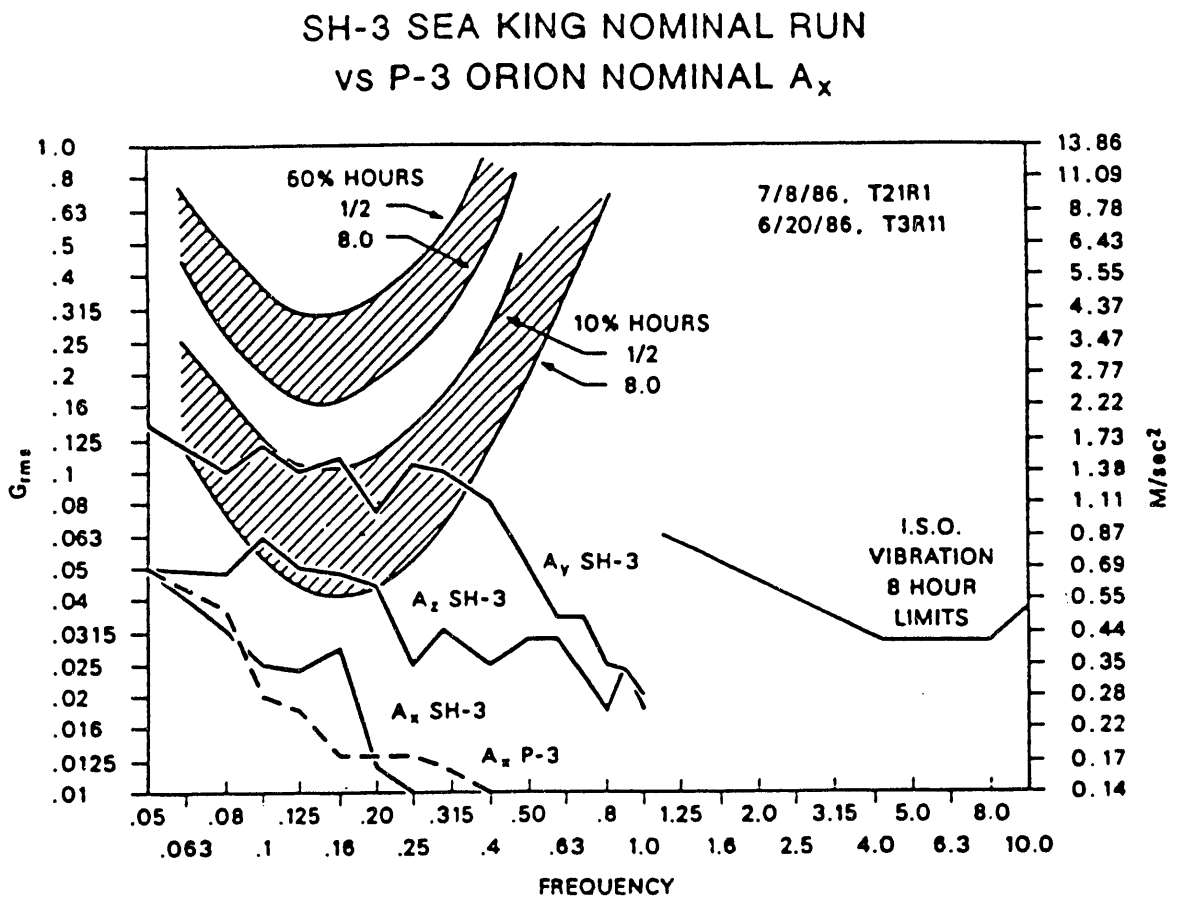

Fig. 1.5. Comparative acceleration vs frequency profiles for the 2F64C and 2F87 simulator systems.

these times, I flew the simulator with symptoms. In the course of my recovery, I also noticed that my recovery period was directly related to the amount of acceleration energy (defined as the integral of acceleration squared) I absorbed during my simulated flight. This experience led to the basic structure of the model, a charge/discharge relationship functionally related to the activity of the simulator. By providing two of these models in cascade, the nonlinear interaction between visual and vestibular systems could be accommodated. It was also known from previous experiments (Allgood et al. 1987b) that a strong correlation exists between distinct elements of the energy spectra of each linear axis of acceleration and simulator sickness. To develop this in the model, a frequency domain integration was performed over defined limits and for select center frequencies of the acceleration-per-hertz squared for each axis. This variable was then used as the input to the second filter at each discrete time step. This model forms the structure for what the author classifies as the Whole Body Energy Absorption Model for simulator interactive dynamics.

The dynamics of this model will provide the time history of events for each flight and provide the select features needed to capture the nonlinear aspects of human-simulator interaction.

1.2 DEVELOPMENT OF THE NEURAL NET PARADIGM

The complex system interaction between pilot and simulator has created problems when attempts have been made to characterize the relationship in terms of simulator sickness. Difficulties have arisen when time has been taken into account. Most paradigms assume that temporal sensitivity is uniform across the event, that is, initial events have as much impact/weight as those that occur at the end of a training session. What has been overlooked is that the human is a variable gain system whose sensitivity increases with both magnitude and temporal occurrence of stimuli. It is my hypothesis that humans exhibit a form of interpretive memory for whole-body energy absorption, which we continue to accumulate as long as the stimuli competing for attention remains above a threshold functionally related to the individual. Once the energy spectrum drops below the threshold, the body begins to shed or discharge the effects of interaction with the simulator, forcing the body into a recovery period and reducing the level of sickness. This threshold, charge/discharge, and variable sensitivity compound any attempt to characterize the malady since no efforts have been made to experimentally validate these attributes.

This hypothesis for a functional model of the human-machine interaction led to the development of a set of nonlinear difference equations whose dynamics are characterized by temporal differences associated with the charge/discharge time constants [functionally related to behavioral differences (Allgood 1989)]. This model overcomes limitations associated with paradigms that ignore magnitude and temporal influences of stimuli that act as a genesis of the disease, and it possesses accountability, in a limited sense, for the behavioral differences in pilots.

Although the model identified the temporal aspects of stimuli overlooked in previous works and functionally described behavioral class structures that could provide predictive capabilities for measures of simulator sickness, it still lacked the formalization of the biological process that is active in the human-machine interaction. Particularly missing are how a pilot's associative and nonassociative behavioral patterns (or learned expectations and sensitivities and previous experience in a particular simulator) color that pilot's perceptions of the simulator environment and how these perceptions, in turn, are affected by situational awareness. An example would best serve to point out the implications of this statement.

Most people have extensive experience with driving cars and, as such, a strong neural store of expectations or memory of this activity. If this experience is taken to an arcade where a driving simulator (game) exists, the probability of invoking stimuli that induce simulator sickness due to cue conflict are minimal (although anecdotes are reported of induced sickness, which may be extreme cases). This is largely because the system presents such a gross approximation of a car that our experiences, reinforced by our situational awareness, do not lead us to assume anything else. In addition, our senses collaborate the assessment that, indeed, we are in a world of make-believe and should not expect it to be otherwise. For the full-motion base driving simulator, this is not the case. Because of its fidelity in replicating our driving experience, we subconsciously expect a collaboration between our visual, vestibular, and proprioceptive senses. And unless overridden by a conscious thought process, these expectations, which do not match our neural store, create an environment of cue-conflict. Our senses are bombarded with discordant information that, when mapped to the cerebral cortex, creates conflicting sensory experiences. Compounding this conflict are engineering attributes that are artifacts of the system's performance and/or poor design. Included are excessive time delays, asynchronous motion and visual systems, display problems (e.g., convergence, resolution, and alignment), and minimal cue capabilities

(e.g., simulator washout where the system returns to a neutral position and propreoceptic feedback), all of which contribute to providing inappropriate cues or information.

Figure 1.6 is a behavioral/systems paradigm developed to model the interactive processes of a pilot and simulator. This paradigm is used as a basis for the proposed research and represents the model simulated by the neural network. The physiological aspects of the model are developed around the visual and vestibular systems interaction coupled with tactile senses feedback. This model provides the experience modifying the nervous system that reveals itself later as altered behavior.

The primary function of the vestibular apparatus is to provide information in conjunction with the visual system about the head's angular and linear acceleration and to signal its attitude relative to gravity vertical. This regulation of motor activity is at a subcortical level. The visual system also plays an important role in the equilibrium system, becoming the overriding input in the control hierarchy in certain situations. Certainly, the visual and vestibular mechanisms are interdependent. Information about head movement from the vestibular system is used to stabilize eye position and preserve vision during transient head movements, while the detectors of retinal motion project to the vestibular nuclei and contribute both postural adjustments and perception of body attitude and motion. Thus, the sensory precepts of the visual and vestibular systems along with tactile feedback provide the pilot with an environmental interpretation of world, aircraft, and cognition. In the real world, the learned expectations reinforce this perception, which is not the case in the simulated environment. Cues are perceived as discordant information violating expectations. The pilot is then forced to deal with the new information in one of two ways: (1) it can be interpreted as new information about the environment and dealt with as altered behavior [it can also be considered nonassociative behavioral adaptation (habituation and sensitization)] or (2) it can be interpreted as a "poisoning" of the pilot's system. In the latter case, the result would be simulator sickness.

The form of the neural network and the development of the behavioral/system model are the major emphases of this research. A possible biological structure is shown in Fig. 1.7, in which levels of abstraction account for the associative behavioral patterns (categorization level), vestibular and visual (tactile) interdependence (interpretive level), perception (perception level), nonassociative behavioral patterns (adaptation level), and the abstract space associated with prediction of simulator sickness (predictive level). This particular net is presented for discussion only but is realized in some form as the model structure.

Input for the associative and nonassociative behavior is gathered from syllabus hop dynamics and questionnaires administered at simulator test sites which include answers to a Motion History Questionnaire and a Motion Sickness Questionnaire (developed in 1987 by R. S. Kennedy, Essex Corporation). A behavioral structure is developed after a literature search where input stimuli are categorized and a proper sense for the sensory interaction is developed. The vestibular and tactile information is the recorded output from the feed of linear acceleration data, recorded for each syllabus hop, to the set of nonlinear difference equations representing the whole-body energy absorption model. Since no visual information exists (except in the form of CPU timing signals), the functional aspects of interaction are inferred from the model's response to the acceleration data. Although this may seem lacking, close examination of the operational characteristics of a simulator shows a strong correlation between motion dynamics (stick movement) and visual screen projection (especially in the absence of any dynamics data).

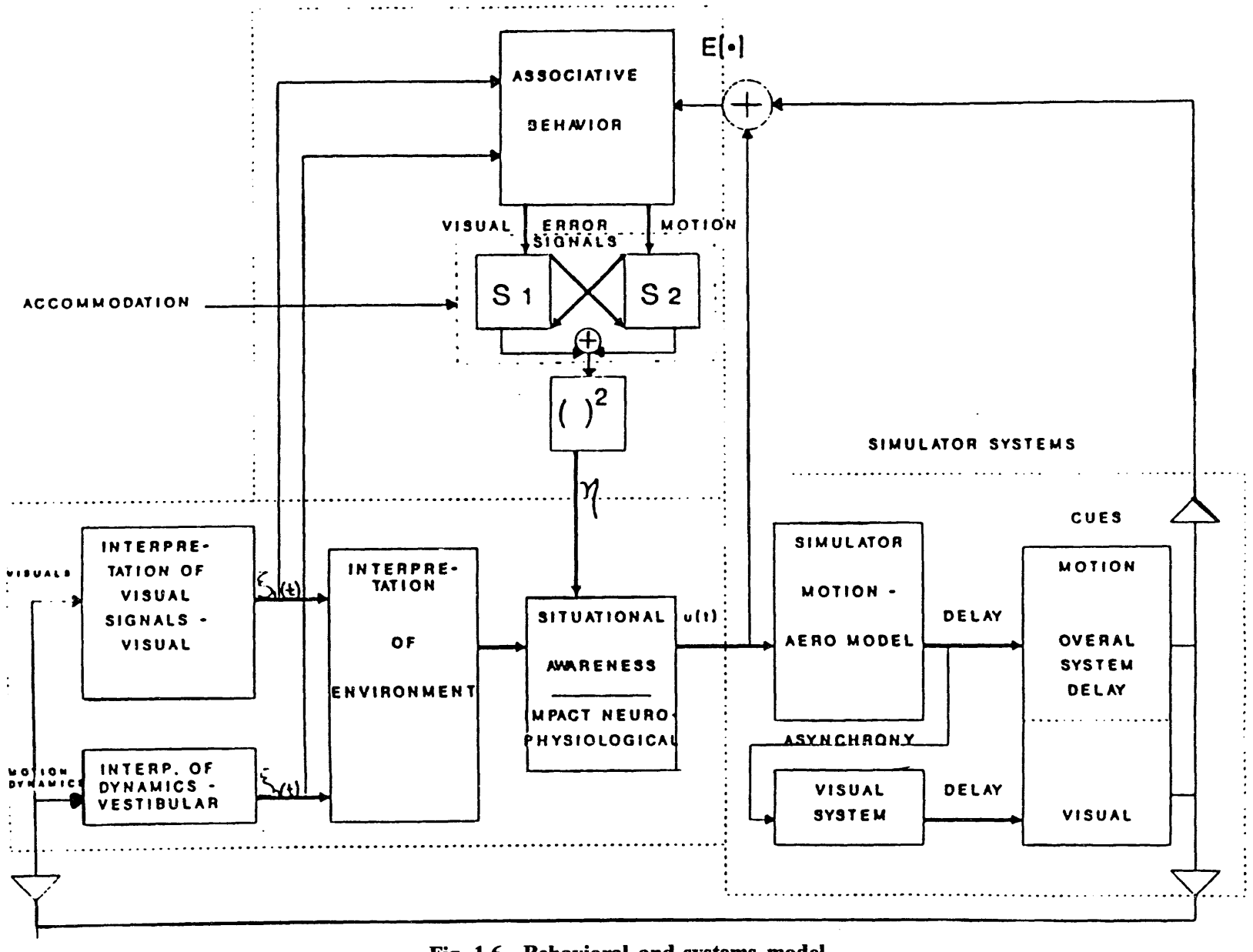

Fig. 1.6. Behavioral and systems model.

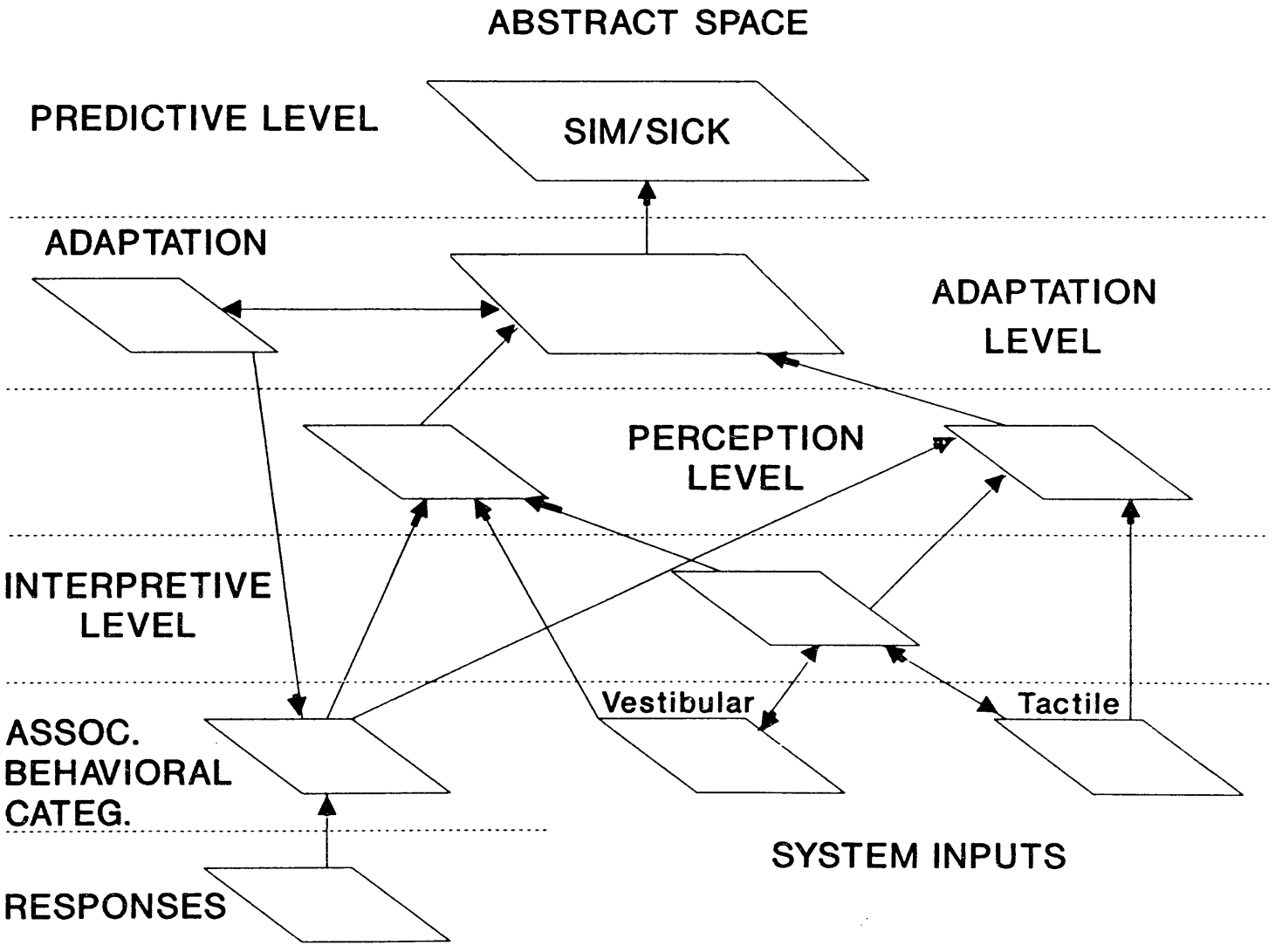

Fig. 1.7. Proposed biological model for net.

The N-tuple is chosen as the net structure for the paradigm. Its capability for feature extraction and ease of mapping for temporal, spatial, and spectral attributes makes it ideal for real-time applications. It also overcomes issues of saturation, convergence/stability, scale-up, and speed that eliminate most other nets.

The remaining chapters are devoted to the development of the neural network paradigm and behavioral model and its predictive capabilities. Chapter 2 describes, in some detail, the simulator where experiments were conducted and outlines, in a broad sense, the data acquisition techniques employed. Chapter 3 analyzes the biological neural structure of the human central nervous system and develops supporting arguments for the structure/form correlates that must exist in the artificial neural network. Chapter 4 describes additional analytic techniques, including the whole-body energy absorption model, employed as supportive work, correlating findings with the development of the simulator sickness predictor. Chapter 5 provides a description of artificial neural nets with emphasis on the N-tuple formulation. Chapter 6 discusses issues associated with the development of the simulator sickness N-tuple. Finally, Chapter 7 presents the results and conclusions from the application of data collected at a simulator site to the predictor.

2. FACILITY, EXPERIMENTAL DESIGN, AND DATA ACQUISITION TECHNIQUES

2.1 INTRODUCTION

In August 1987, an evaluation was performed on the U.S. Navy's TH57C (2B42) Operational Flight Trainer (OFT) to assess the health of the simulator through tests designed to correlate system dynamics with reported (incidence of) simulator sickness. At issue was the perception by instructor pilots that the simulator induced a high incidence of simulator sickness in the user community.

The results of the experiment confirmed the suspicion that a high incidence of symptomatology, defined as the presence of at least one minor simulator sickness symptom, was indeed present in the student pilot population. The tests were conducted under normal training procedures for student pilots: 72-min flights, one student each in the left and right seats, and a normal training syllabus (cal-sites, shipboard, and field landings). The results pointed to the inability of the device to protect sensory modalities from conflicting information (cues) that act as the genesis of the disease.

Figure 2.1 compares the 2B42s incidence of simulator sickness (total severity score) against those of other systems that have been investigated. As shown, the 2B42 has the second highest reported incidence. In this figure, the ordinate represents an overall

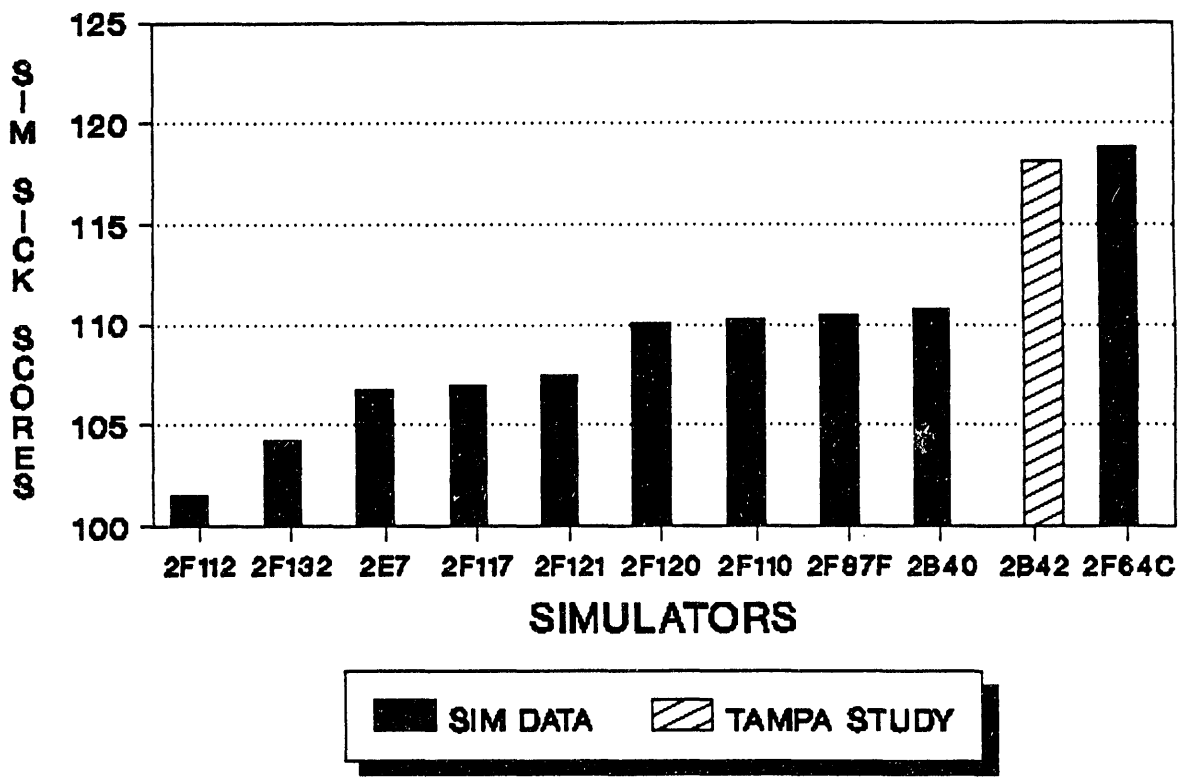

Fig. 2.1. Severity score comparisons of 2B42 operational flight trainer study with other investigated simulators.

discomfort across all events (syllabus training hops) and is a performance variable indicative of simulator sickness. The scale is normalized to a score of 100 (absence of symptomatology) to values presented, with severe cases of simulator sickness scoring in excess of 107. In this study, the sample population was represented by 32 distinct test cases distributed over 16 student pilots on 2 different training hops, all under instructor pilot supervision.

An executive summary (Allgood et al. 1987a) was issued outlining the procedures and results of this study. In it, fatigue, sweating, nausea, dizziness, vertigo, fullness of head, and stomach awareness were identified as the most prevalent symptoms in the students. These data were correlated with system anomalies, resulting in recommendations for system upgrades and enhancements that would alleviate or reduce the incidence of simulator sickness in the user community. These recommendations were taken under advisement by the Navy and issued as 2B42 system upgrades to be implemented by the manufacturer before the device was accepted into the Navy's training inventory.

In the spring of 1988, the TH57C simulator was delivered to the U.S. Naval Air Station (NAS) Whiting Field, Pensacola, Florida, for Navy acceptance testing. The Navy requested that another experiment similar to the one employed during the evaluation be developed and implemented. This plan, in addition to a behavioral study, would check for compliance of all system upgrades. After review of the evaluation test, an enhanced experimental plan was recommended to take advantage of the system's availability. This new test would not only provide baseline symptomatology scores, spectral energy distributions, and conformity checks on all upgrades but also extend the test to provide for a comparative analysis between the Bell Ranger Helicopter and the TH57C (2B42) simulator. A plan along with a flight syllabus profile for the study were submitted to the Navy and approved as the NAS Whiting Field Acceptance Test.

This experiment, when compared with the previous one, had a major difference in the philosophy employed for the behavioral study. Instead of implementing the baseline test case as before, testing would attempt to identify operational profiles (syllabus hops) that would alleviate enforced restrictions (movements) on the student pilots after training. This philosophical departure from the original behavioral study would negate any valid comparison between the two and prohibit extrapolation of reduced symptomatology to any system enhancements. A diagrammatical representation can best describe the impact of this decision. Figure 2.2 is a slice through the R^n operational space of the simulator, showing four possible (but not all-inclusive) operating regimes. The hypothesis is that the system can exhibit a reduction in the incidence of simulator sickness by simply eliminating from training those hops that act as the genesis of the disease—in this case, elements requiring close ground-plane coupling. Thus, any scenario that requires a high degree of interaction between the human's visual, tactile, and vestibular systems for extended periods of time would be eliminated from training. The dichotomy that results is one in which the simulator can exhibit a reduction in the incidence of simulator sickness without significant changes to the system's operational performance.

This hypothesis cannot be completely substantiated by the 2B42 simulator tests, but it can be supported by the results of the Acceptance Test experiment. As shown in Fig. 2.3, the incidence was reduced from a high of 118.1 (second worst) to a level of 106.2 (third best). When considering secondary and higher order effects, it becomes increasingly difficult to determine whether engineering enhancements, if performed, contributed solely to the reduction in symptomatology or whether changes in the syllabus structure were the primary cause. What is known is that the initial data set evaluation represents a baseline test

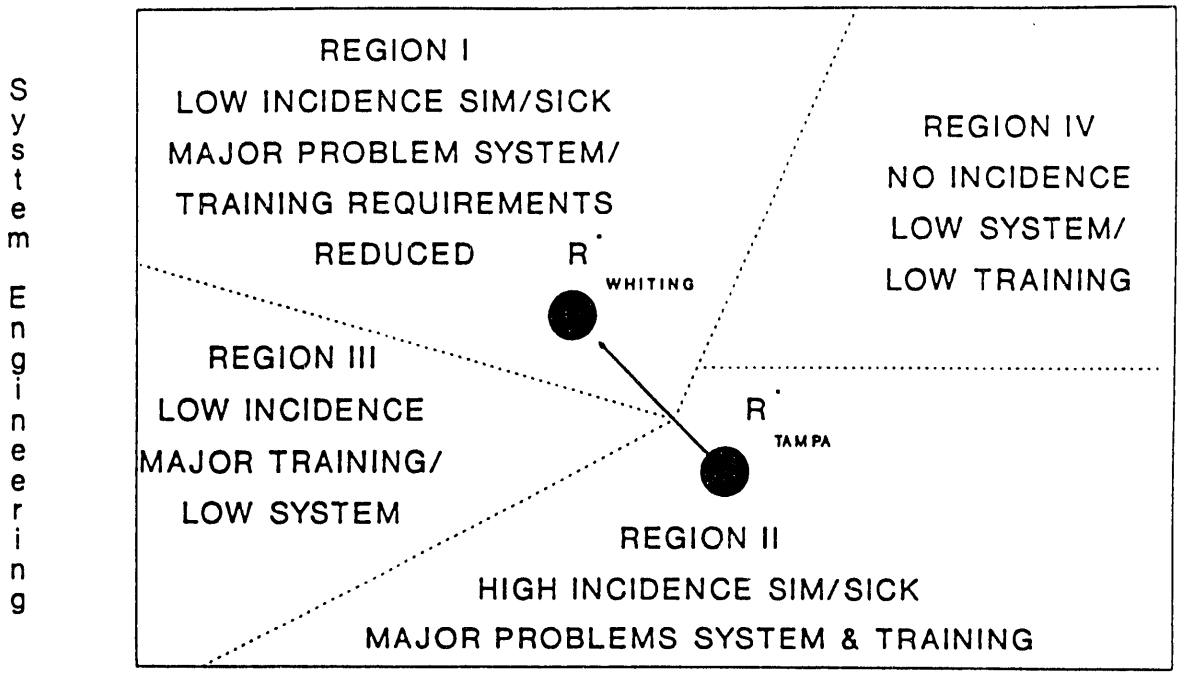

Fig. 2.2. Simulator sickness dichotomy—results of transitioning from one operational space to another.

case for the neural net predictor since the paradigm would reflect those compounding effects due to sensory conflict in the pilots.

2.2 FACILITY

The 2B42 was originally developed as a flight instrument trainer (FIT) to provide student pilots the basic skills in instrument training. As such, the simulator was designed with a full six-degree-of-freedom motion base [roll, pitch, and yaw angular acceleration and x, y, and z linear acceleration (see Fig. 2.4)]. (The importance of these systems is seen in the skills acquired by the student and the fact that human and/or equipment are not put at risk in the training environment.) A decision was made during the system's development cycle to expand its definition to an operational flight trainer (OFT) through the addition of a color graphics image (CGI) visual system (full right-seat visuals). This enhancement would provide skills acquisition by the students in close ground-plane coupling tasks such as landings and approaches. This added dimension would require the student to process sensory information at levels not previously encountered in training—in particular, the interaction of the visual, tactile, and vestibular systems. This interaction and the resulting *sensory conflict* are widely believed to cause simulator sickness, partly because of the latency in the system and the asynchronous operation between the visual and motion base subsystems.

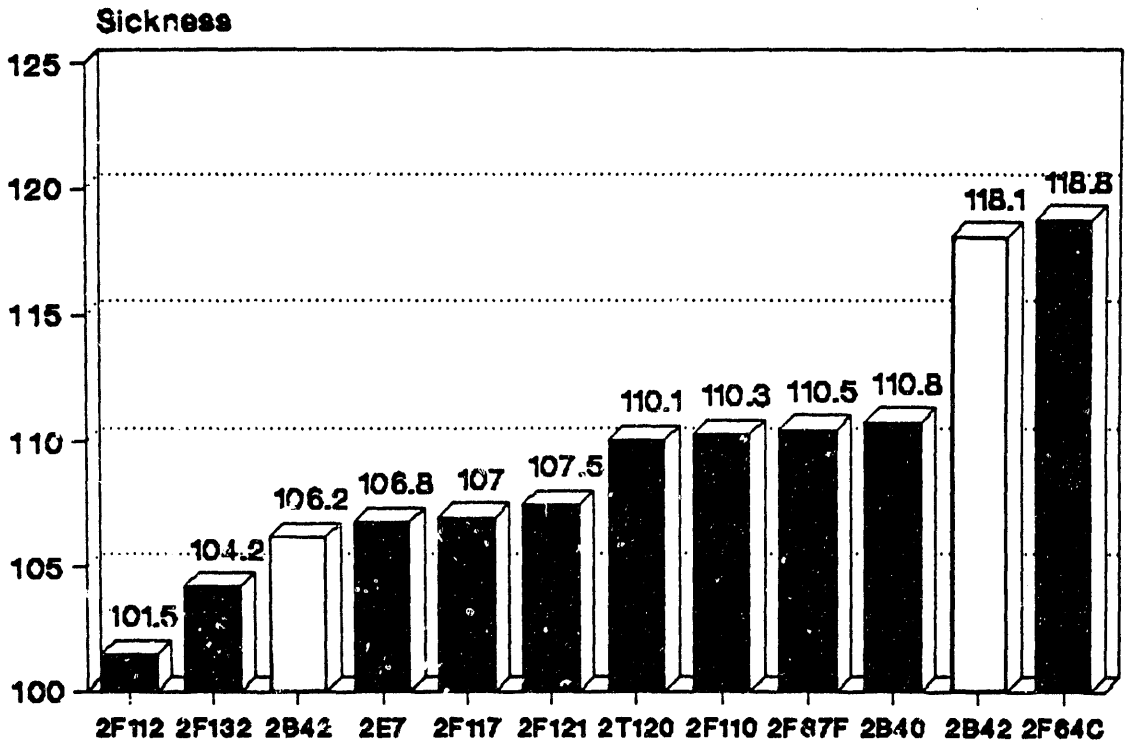

Fig. 2.3. Comparison between 2B42 simulator severity scores for test/checkout and Acceptance Test.

Latency is defined as the time delay in the response of a system or subsystem and is normally independently characterized for both the motion and visual systems. That is, measured dynamic responses from stick (longitudinal and lateral) movements will include onset of acceleration (measured for the motion base), graphic image updates (for the visual system), and the difference between the two. The reader is referred to Chap. 1 and Fig. 1.6 for review.

By using analogies from system theory to link system performance with sensory processing, an intuitive model can be developed that predicts pilot/simulator instabilities in the presence of excessive time delays and relates the prediction through sensory (cue) conflict and MILSTD 1472D to the incidence of simulator sickness. For this discussion, this paradigm will be labeled the *Latency/Cue-Conflict Model.* It should be noted that similar models based on laboratory data gathered under other than facility operational conditions have been postulated by other researchers.

Figure 2.5 is a block diagram of the overall cascaded system, showing the pilot in the loop. Of particular importance is the role that the pilot and his task skills play in characterizing the system's dynamic response. Arguments can be made that the pilot, a nonlinear controller, has a transfer function that is conditioned upon real-world expectations and personal limitations. Thus associative behavior will condition the pilot's ability to maintain and control the aircraft in a stable flight envelope.

Normally, the cascade system of pilot and simulator is expected to have dominant poles located away from the narrow-band, low-frequency region identified by

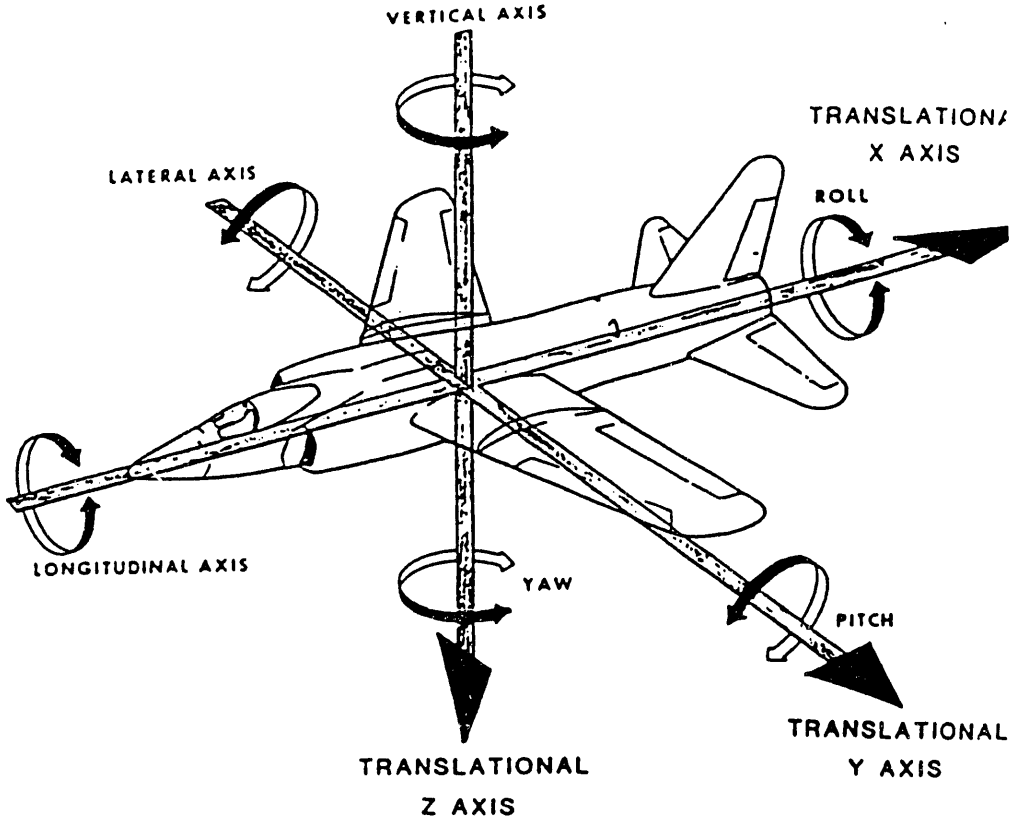

Fig. 2.4. Aircraft (simulator) measurement axis.

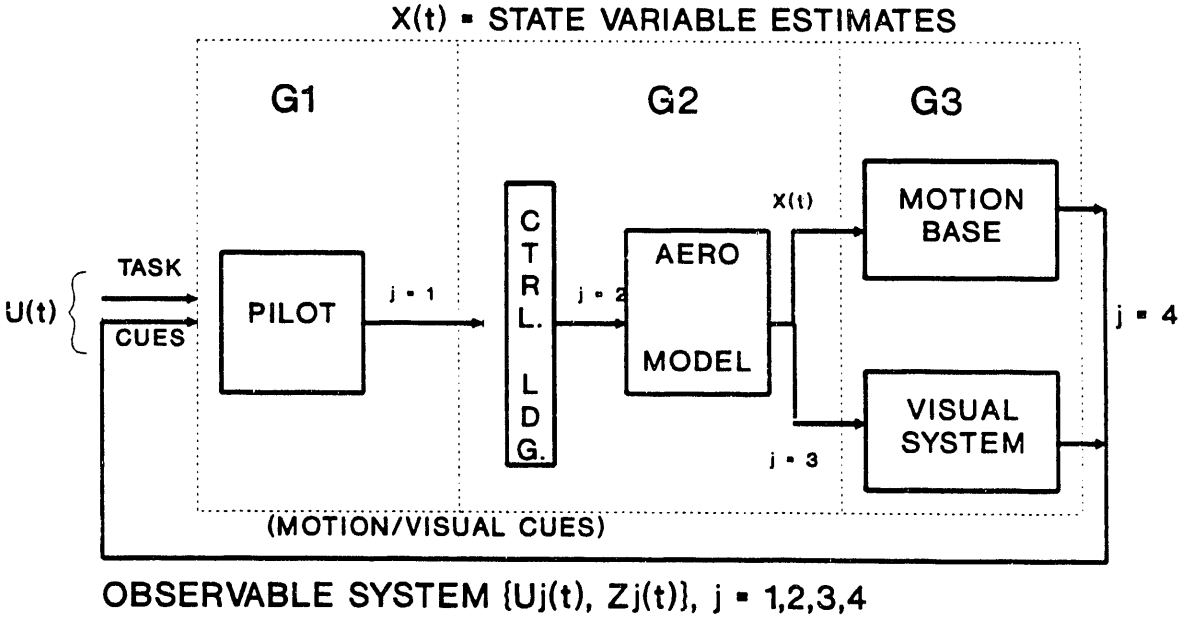

Fig. 2.5. System measurement paradigm.

MILSTD 1472D. If excessive time delays (latency) occur, it is argued by the author that the simulator, acting as a nonminimum phase system, interacts with the pilot in such a way as to drive the system into an operating regime where the overall gain (sensitivity) is increased and instabilities (oscillations) occur at frequencies guarded against by MILSTD 1472D. The hypothesis is that the delays introduced by the system's design interact with the human to create an environment of sustained sensitivity to interpretative errors. Since the human sensory modalities (visual, tactile, and vestibular systems) act as a unifying feedback control signal, violation of the conditional expectation acts as a positive feedback sending the system into sustained oscillations. The oscillations that result have been categorized by the simulator community as *Pilot-Induced Oscillations* (PIO). This anomaly has the undesirable effect of reducing the system's fidelity, known to be suboptimal when compared with the actual aircraft, to a point where system performance resulting from the human/machine interaction is unacceptable.

The following series of figures provides an overview of the 2B42 simulator and Bell Ranger helicopter analysis and presents supporting evidence for the hypothesis stated above. It should be noted that this is not the complete analysis but only those elements that are key to the arguments presented above.

Figures 2.6–2.8 are the x-, y-, and z-axis acceleration step response to cyclic inputs for the simulator. These inputs were created by using a software patch in the aeromodel, which initiated a defined g-loading in one of six axes of the motion base. It is obvious from these response curves that the system has excessive delay times in the x- and y-axes. (Excessive delay times are defined as >60 ms, a figure of merit developed from the Bell Ranger helicopter study presented later). The latencies (>500 ms) create cue conflicts in the sensory input channels of the human, a qualified statement supported by the 2B42/Bell Ranger helicopter comparative analysis.

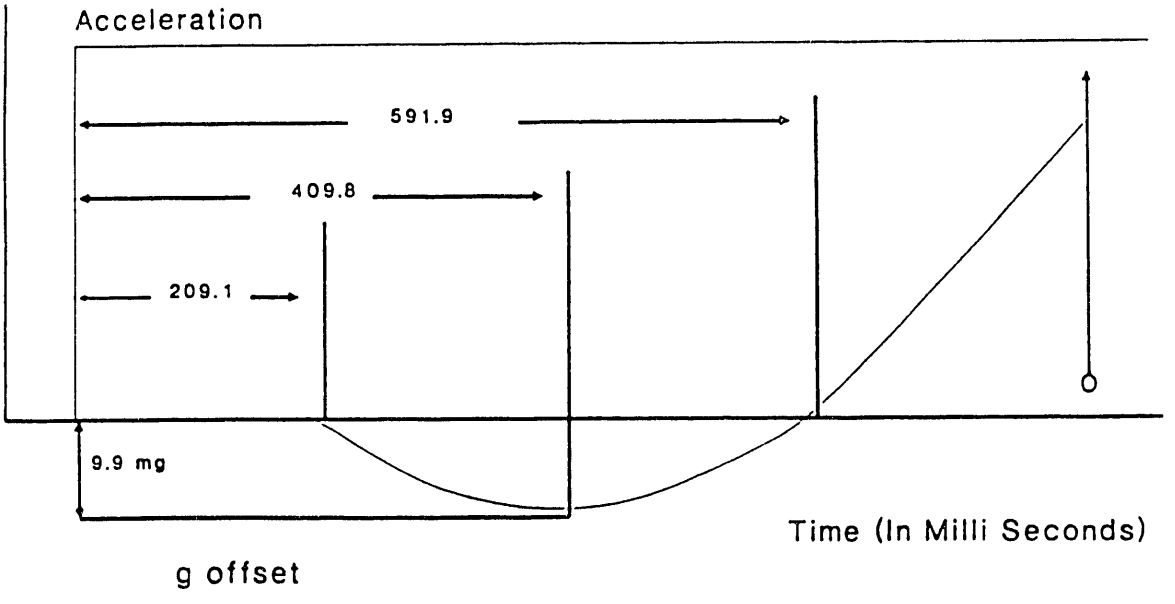

Fig. 2.6. The x-axis acceleration step response to cyclic inputs.

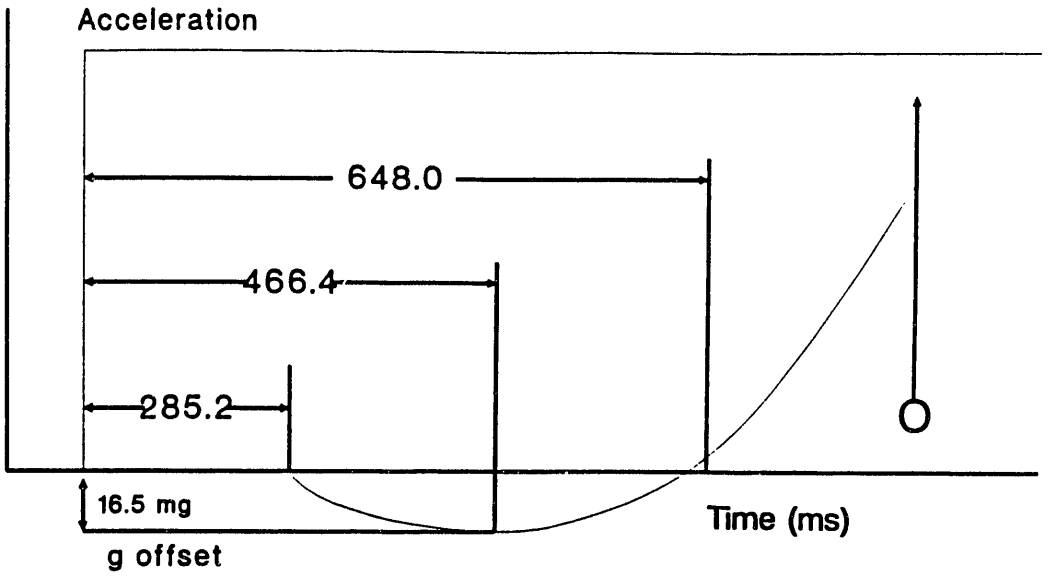

Fig. 2.7. The y-axis acceleration step response to cyclic inputs.

The *Comparative Study* was developed around a flight syllabus that would exercise perceived anomalies that exist in the simulator. Although it would not help identify the contributing elements of each subsystem (e.g., aeromodel, signal path delays, and hydraulic response), it would provide an overall system characterization. Each event (1 in. lateral left, 0.5 in. lateral left, 1 in. longitudinal aft, 0.5 in. longitudinal aft) was designed to characterize temporal responses initiated through the movement of the cyclic (stick). Flight Test School located at Patuxent Naval Flight Center flew the test syllabus in both systems. Their participation ensured replication of tasks across all events and systems. The tests were

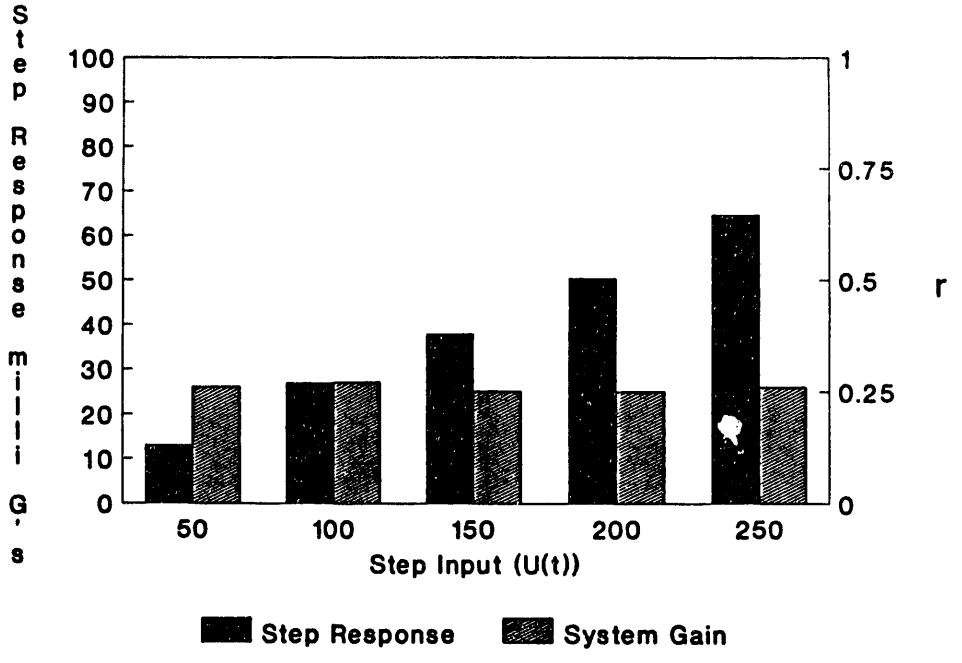

Fig. 2.8. The x-axis temporal response.

conducted under ambient weather conditions, fuel burns, and flight envelopes. The combination of pilot and attention to testing ensured the validity of the comparison. As shown in Fig. 2.9, the helicopter exhibited an average delay of ~45-50 ms across all events. The simulator, on the other hand, experienced delay times (statistical average) on the order of 125 ms. This difference, according to the *Latency/Cue-Conflict Model*, would establish sensory conflict, a result of the error propagation due to inconsistencies in learned expectations, and act as a genesis of simulator sickness driving the system (human/simulator) into sustained oscillations.

2.3 SYSTEM DELAY TO FIRST RESPONSE—STATISTICAL AVERAGE

The data that have been presented are necessary but not sufficient to support the *Latency/Cue Conflict* hypothesis. Corroborating data from the visual system are needed so that a sensory stimulus mapping can be developed showing flow of information and its convolution in space-time. A test was designed to capture this information using timing pulses on the x- and y-deflection amps of the CGI graphic screens. During a preliminary test, the simulator motion base system developed errors in the aero model, which drove the positioning vectors 180° out of phase. This negated any attempts to correlate visual and motion base latency. However, the experiment did provide information on the visual timing sequences. These results are shown in Figs. 2.10 and 2.11, where lag time and lag time distribution vs events are presented for information purposes only.

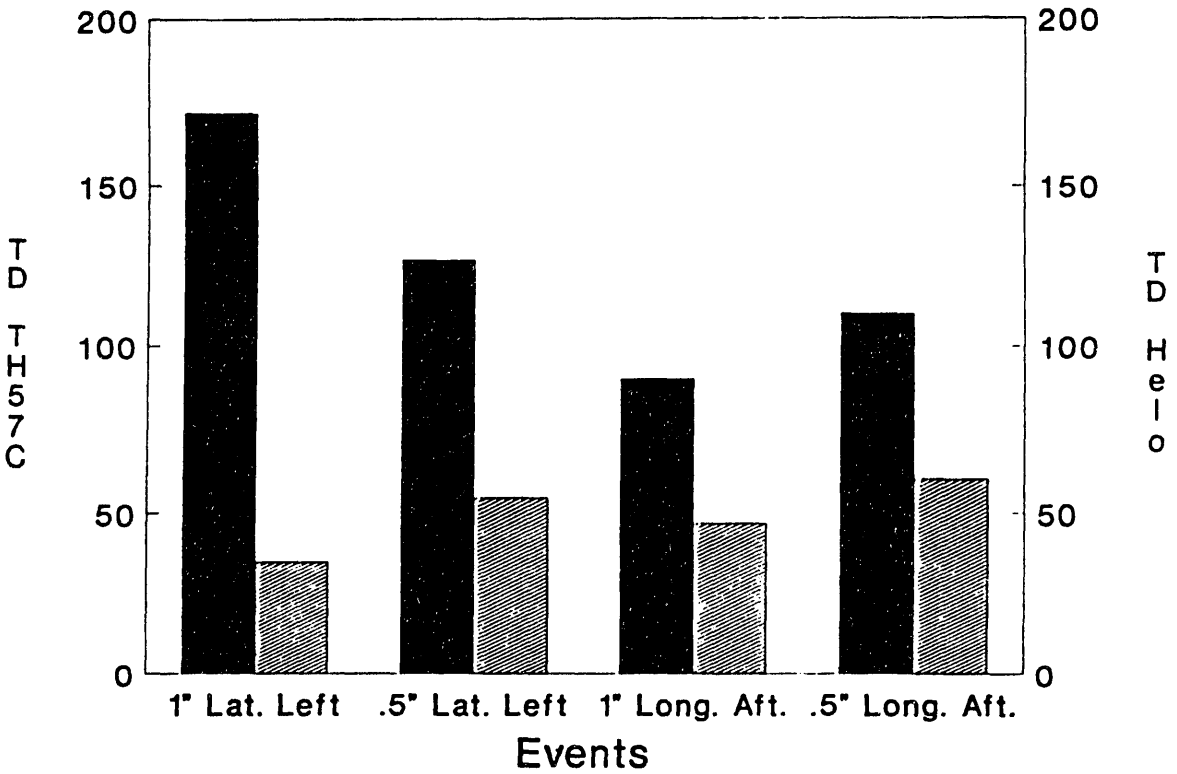

Fig. 2.9. Comparative analysis of helo vs TH57C system delay to first response—statistical average (all times are in milliseconds).

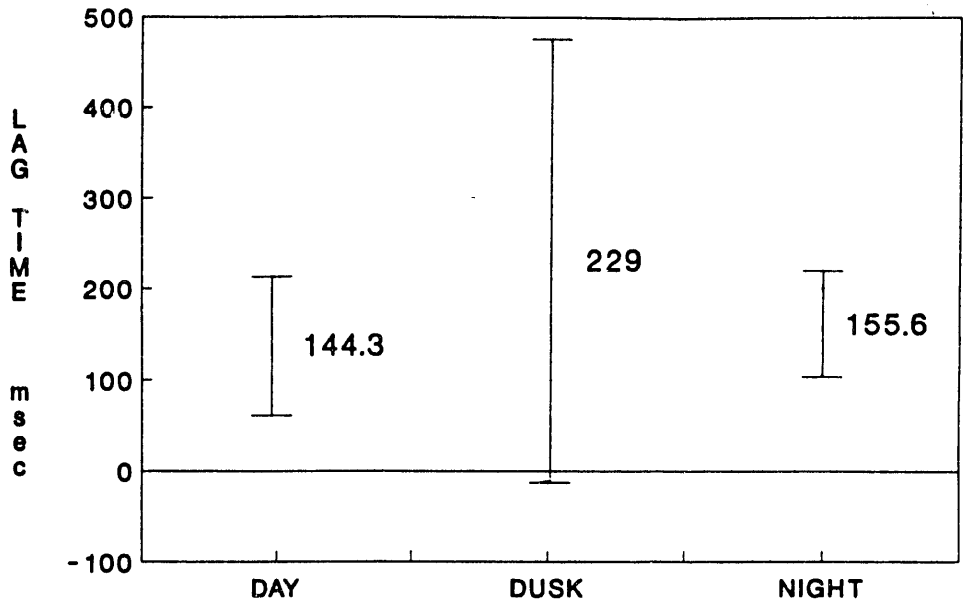

Fig. 2.10. Visual scenes.

To establish support for the sensory convolution argument, an additional set of events was specified that would require a high degree of visual-ground plane coupling. The resulting interaction between the human, the system, and the task skills requirements resulting from these tasks, would exercise those sensory modes (visual, vestibular, and tactile) that, in the presence of perceptual errors, cause simulator sickness. If, as predicted by the model, conflicts in sensory input occur, the system will transition into an unstable operating regime identified by MILSTD 1472D. The events, normal approach, hover, left

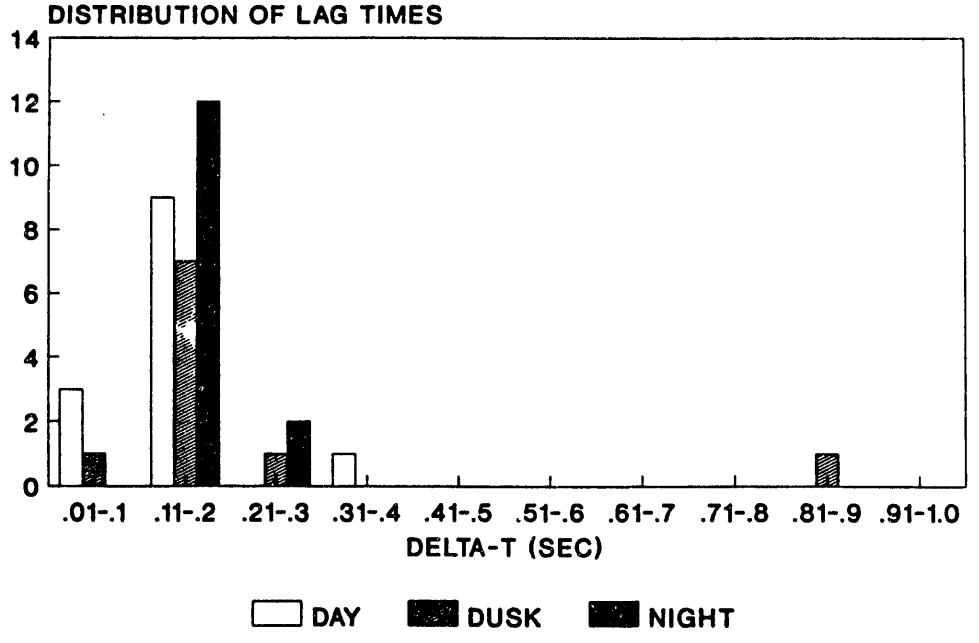

Fig. 2.11. Visual cue sync study—day, dusk, and night scenes.

clearing turn, and hover/land/hover were flown under replicate conditions in both systems to establish a valid comparison base.

The results of the experiment are shown in the following series of figures. The first is the comparison of the flight characteristics of the simulator and helicopter in the Hover Task. Figures 2.12 and 2.13 are plots of the Bell Ranger's x- and y-axis acceleration and y- and z-axis stick acceleration vs time respectively. (The stick was instrumented with PCB accelerometers to measure acceleration. The configuration is described in the Data Acquisition Techniques subsection.) Very little movement in either the stick or helicopter platform is shown. Some cycling of the ship does occur (more prevalent in the x- than in the y-direction), but this is to be expected under normal flight operations. On the other hand, the simulator (see Fig. 2.14) shows a pronounced oscillation coupled with dead time (the estimated delay is on the order of 860 ms). Figure 2.15 compares the spectral components of y-acceleration for both systems. As shown, the simulator has a peaked narrow-band distribution in the low-frequency range between 0.080 and 0.380 Hz, the peak occurring at ~0.16 Hz. This energy distribution occurs in the region guarded against by MILSTD 1472D (see Fig. 1.4). The helicopter, on the other hand, shows no significant contributions in this region. It is characterized by a flat, uniform distribution two orders of magnitude down from the peak value of the simulator. The other event, hover-land-hover, is shown in Figs. 2.16 and 2.17, where the spectral estimates of the x- and y-acceleration of the helicopter and simulator are compared. Similar to the hover task, the simulator has a peaked distribution of energies in the guarded region where the helicopter does not.

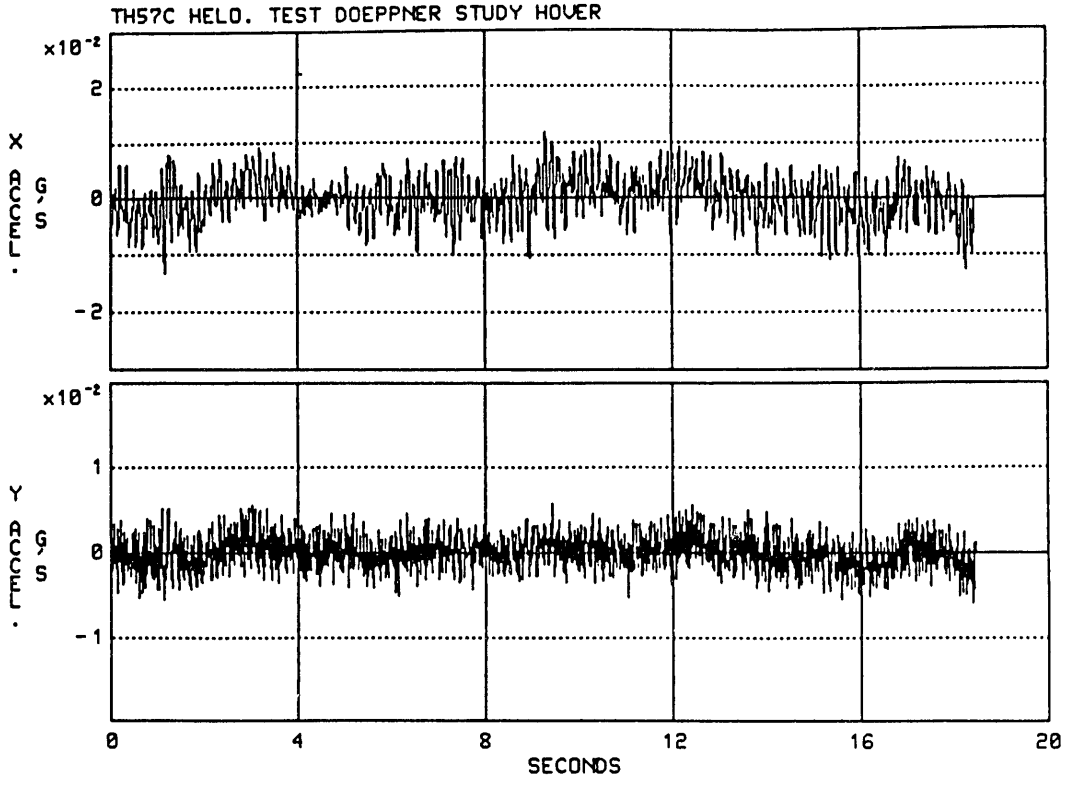

Fig. 2.12. The TH57C helo test Doeppner study hover (x- and y-axis acceleration vs time).

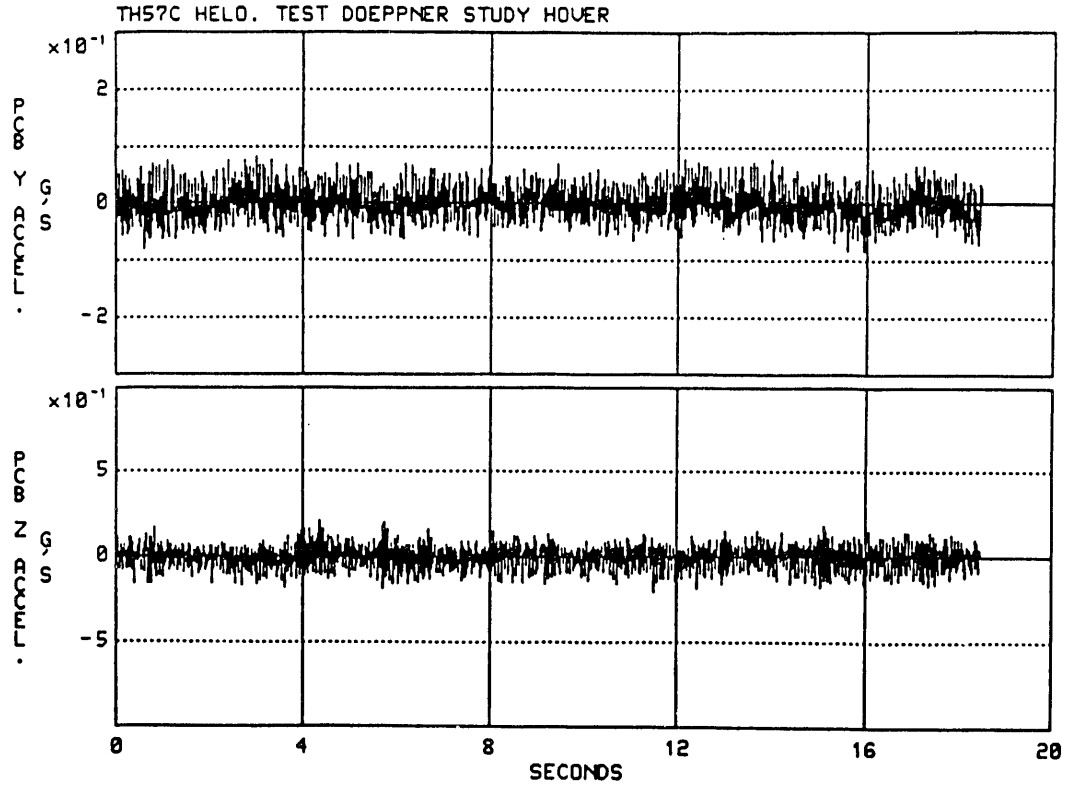

Fig. 2.13. The TH57C helo test Doeppner study hover (y- and z-axis acceleration vs time).

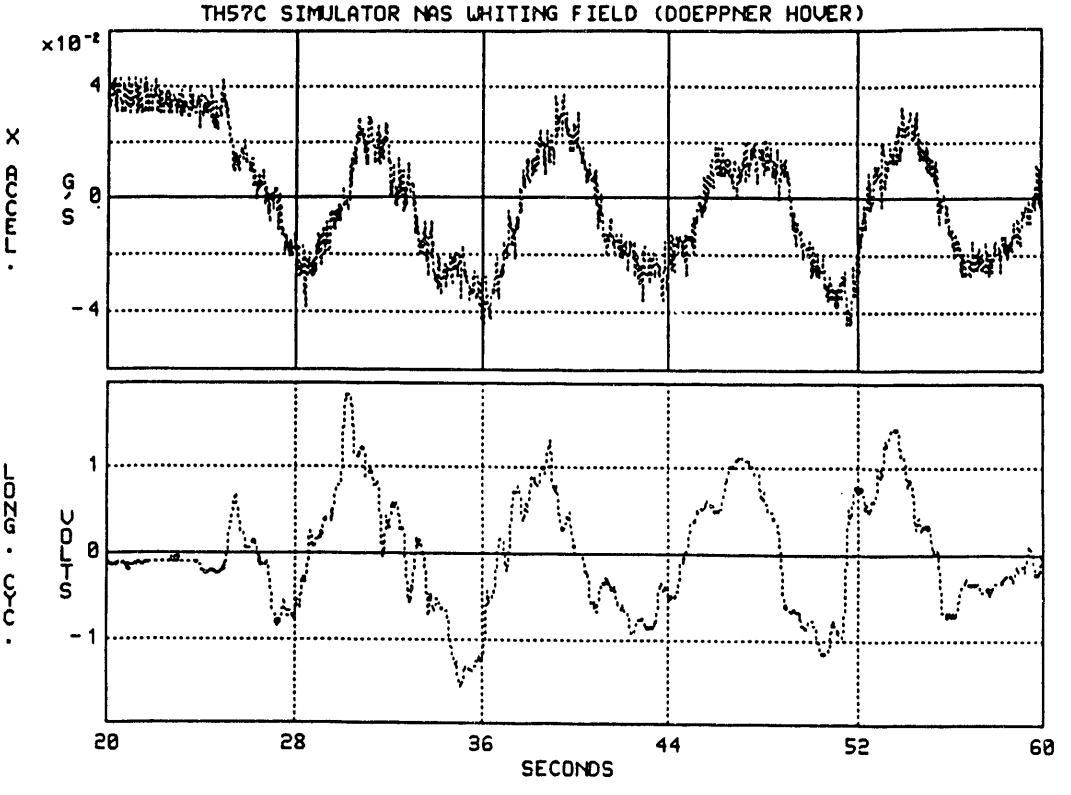

Fig. 2.14. The TH57C simulator Naval Air Station Whiting Field (Doeppner Hover).

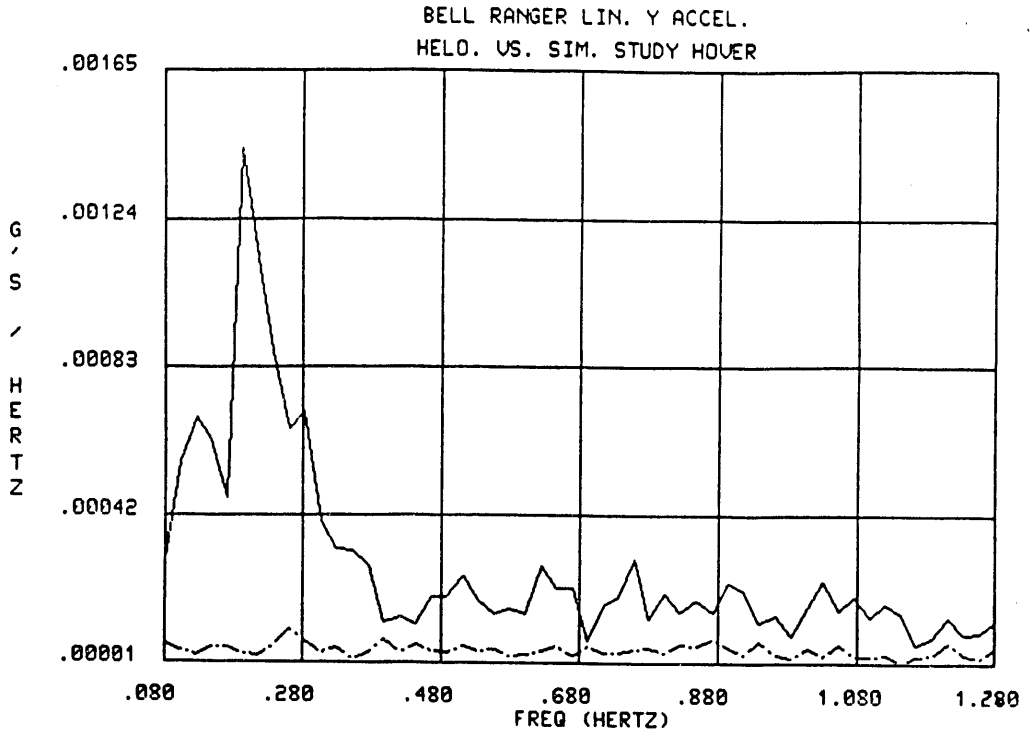

Fig. 2.15. Bell Ranger linear y-accelerator helo vs simulator study hover.

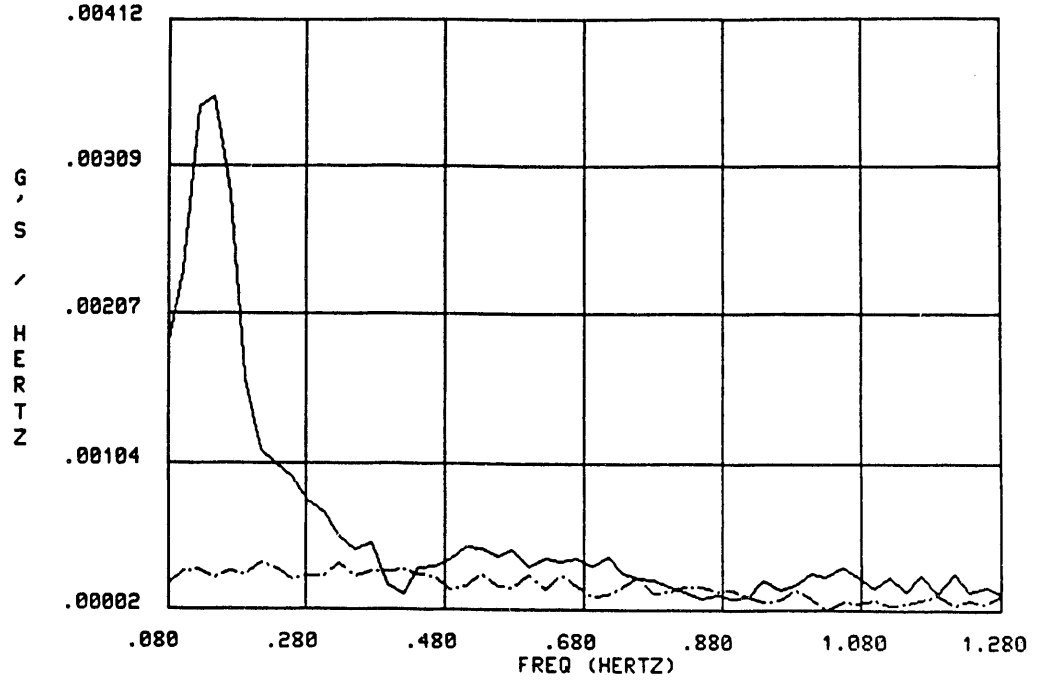

Fig. 2.16. Bell Ranger linear x-accelerator helo vs simulator study hover/HLH (Event 15).

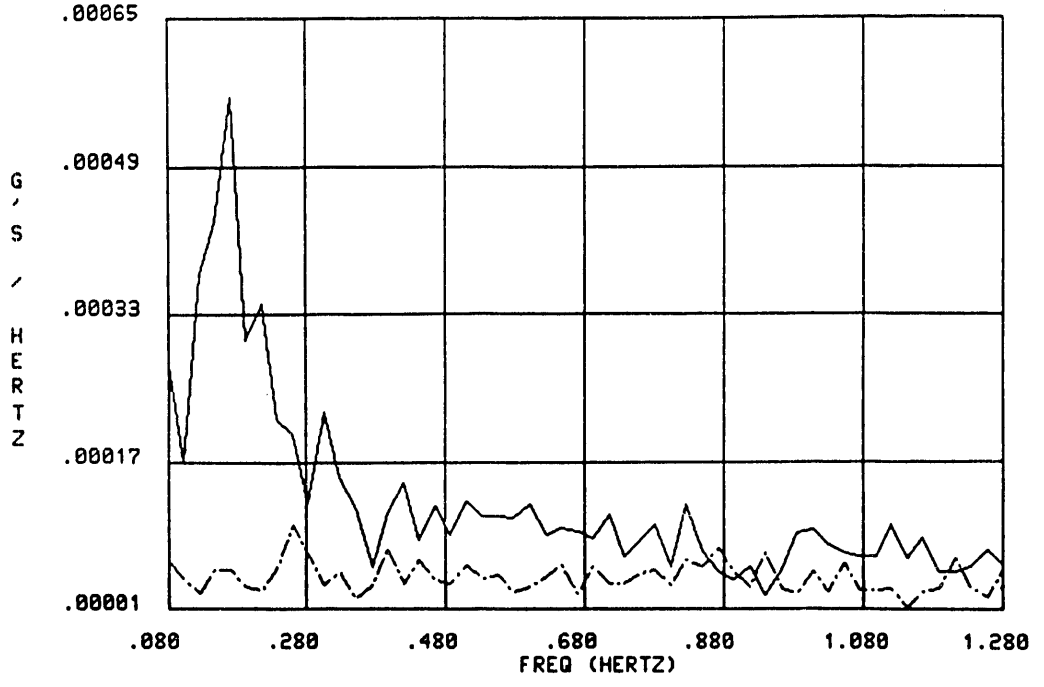

Fig. 2.17. Bell Ranger linear y-accelerator helo vs simulator study hover/HLH (Event 15).

It is obvious from the preceding analysis that the simulator exhibits characteristics predicted by the *Latency/Cue-Conflict Model.* This result, coupled with the high incidence of simulator sickness, supports the arguments that sensory modalities are in temporal conflict, creating an environment of sustained sensitivity to those factors that cause simulator sickness. These anomalies can be attributed to the interaction of the human and simulator where perceptions based on learned expectations are violated. These precepts can be classified as either associated with learned pilot skills or formative interaction.

2.4 EXPERIMENTAL DESIGN

The experiment was designed to support two parallel tasks: (1) an engineering study and (2) a field evaluation of simulator sickness. The engineering study required measuring the motion base dynamics (angular/linear acceleration) and performing a complete analysis of data in support of the behavioral analysis. This study included visual data in the form of logic signals and recorded visual scenes captured during the hops (to be measured during off-test periods). The simulator sickness field evaluation required incorporating into the testing syllabus two scenarios with theme variations to establish bounds for simulator use. In each, a 72-min hop with students in right and left seats were simulated. In the initial hop, students used instruments with visuals for only 20 min. In the second, they performed tasks requiring a high degree of sensory information coupling, as in shipboard and cal-site landings. The theme variations were day, night, and twilight conditions. To facilitate this variation, the experimental design was developed to (1) evaluate whether the initial instrument flight simulation provided some protection from sickness during the second hop, (2) compare day and twilight scenarios to determine whether twilight hops are less

provocative of sickness, (3) make comparisons of pilots who sit in the left vs right seat, and (4) correlate simulator engineering and dynamic traits with incidence and severity of simulator sickness to determine attribute effects and causal relationships that exist.

To accomplish the first objective, all student pilots made the first hop (initial hop included 20 min of visuals) under daylight illumination. On the second, a day later, they made the shipboard landings also under daylight illumination. Half of the pilot pairs switched seats on the second hop. A comparison was made of these two pilot groups. To accomplish the second objective, the pilots made a shipboard landing under twilight conditions, followed by a break of either two or three days and then made another shipboard landing with the exception that the hop was under daylight illumination. The break helped guard against adaptation. Comparisons were then made among all pilots for both hops, with primary interest in those who had no prior visual experience. Finally, comparisons were made between pilots in left and right seats across all events.

Pilot requirements were that all participants should be in their usual state of fitness and wearing flight gear normally worn during training. Students were requested not to discuss testing procedures or outcomes of their hops to eliminate biases introduced by associations. The experimental analysis included incidence, severity, and duration of simulator sickness symptoms and tabulated symptom clusters to include postural stability data. The engineering data package analyzed acceleration profiles (linear and angular) and spectral estimates of energy distribution for each syllabus hop and provided measures of correlation for these data.

2.5 DATA ACQUISITION TECHNIQUES

2.5.1 Simulator System

Figure 2.18 shows the basic equipment configuration employed during the testing of the 2B42 simulator. As shown, a complete facility for recording, analyzing, and displaying system parameters was available that included the ability for real-time and pre- and post-processing data. This distributed data acquisition system (DDAS) environment ensured data integrity across all events.

The state of the system is defined by the simulator's linear and angular acceleration, pilot control signals (longitudinal cyclic, lateral cyclic, rudder), gyro-pitch signal, stick linear acceleration as measured by the PCB linear accelerometers, and graphic CPU timing sequences (i.e., chin, right, left, forward window, and master sync pulse). These parameters represent a minimal observable set for the simulator. The equipment was set up in the upper bay area of the 2B42 Facility. After a point-to-point continuity check was performed on the DACS, the test simulator was brought to an operational state with full motion and visual systems. Then, a complete system-integrity check was established for both the simulator and test equipment, which required functional tests on all control, visual, and measurement signals. The location of the accelerometer packages in the 2B42 cab is shown in Fig. 2.19.

2.5.2 Bell Ranger Helicopter

A Bell Ranger Helicopter was instrumented for the comparative study. The Navy uses the aircraft to teach basic helicopter flight operations and skills to student pilots. To record the flight dynamics of the helicopter, a specially configured instrument package was

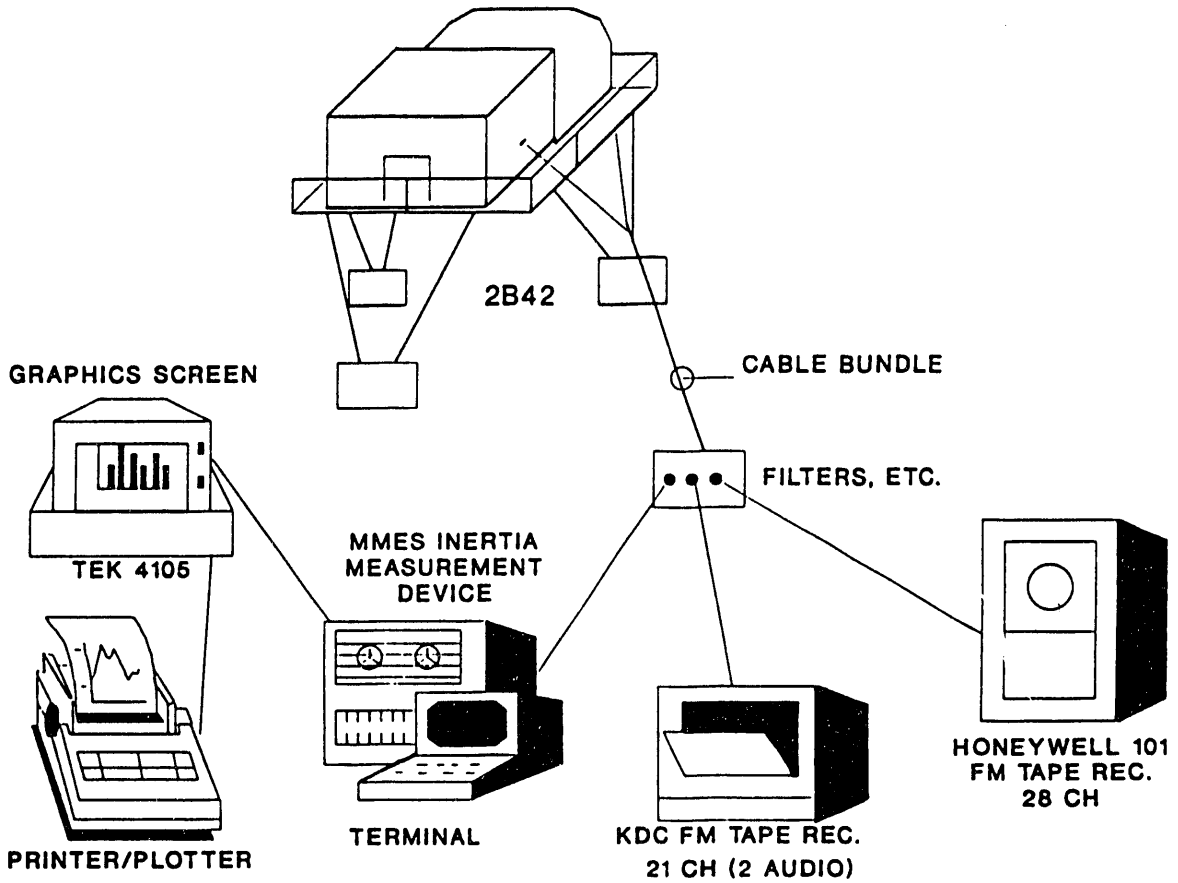

Fig. 2.18. Equipment configuration for 2B42 Acceptance Test, Naval Air Station Whiting Field.

developed. This package consisted of a portable 21-channel FM recorder with power pack, complete set of antialiasing filters (gel-cell design), triaxial linear accelerometers for measuring the platform, and triaxial solid state (PCB) linear accelerometers for measuring stick movement.

The triaxial accelerometers were located behind the pilot's seat as close as possible to the original configuration used on the 2B42 simulator. A structural integrity test was performed on the aircraft to ensure that no structural resonance would compound accelerometer signals. The solid state accelerometers were placed on the pilot's cyclic for correlating stick movements (step inputs) with system response. This nonintrusive measurement technique provided a means to ascertain task skills proficiency in each particular event identified by the hop syllabus.

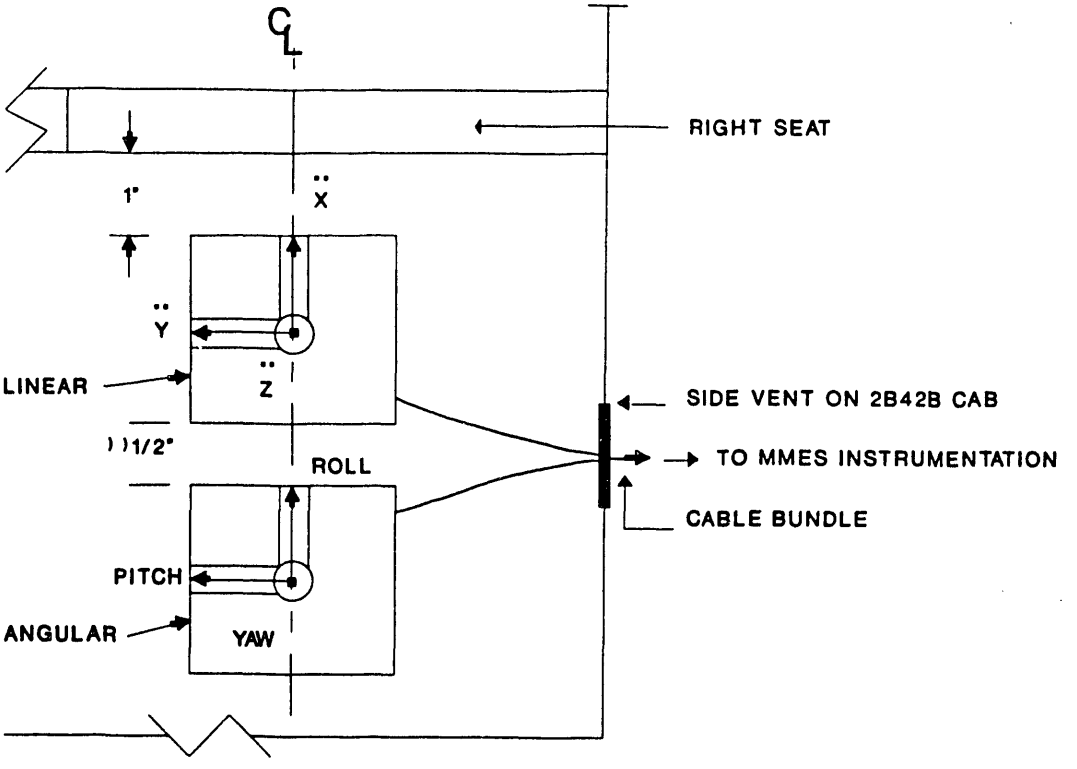

Fig. 2.19. Location of accelerometer package in the 2B42 simulator cab.

3. BEHAVIORAL ATTRIBUTE SELECTION BASED ON THE BEHAVIORAL AND SYSTEMS MODEL

3.1 INTRODUCTION

"You are what you think" is a simple but elegant truth describing the perceptual differences that act as contrast elements, separating one person's behavioral characteristics from those of another. In this context, "think" is defined as those elements of reactive thought that act as a descriptor of one's self—colored perception of the environment, conditioned response to stimuli, and those particular elements of our "residual memory" that make instances of time and space important to us as individuals. Also, behavioral characteristics have a broadened scope which includes any and all behavioral elements that would serve to distinguish one's personality. These traits include personal nuances, preconditioned expectations, and any physical differences that impact our response mechanisms. Of course, this research dismisses any elements of the human population that suffer genetic and cognitive impairments. (Although it is known that their interaction with the environment will play heavily on their perceptions and response, they are excluded to allow a more tractable base for the behavioral model).

This chapter expands upon the definitions given in the preceding paragraph and, using the behavioral and systems model identified in Chap. 1, develops the necessary reasoning to support the selection of particular behavioral attributes acquired during the simulator sickness study. These parameters form the basis for the associative and nonassociative behavioral vector used in the development of the N-tuple neural net.

This treatise does not, an any way, attempt to uncover the morphological changes that occur in the memory trace circuits or address the neurophysiological aspects that accompany memory store. Its specific purpose is to elucidate, in a simple manner, those attributes of human "self" that possess the necessary interactive qualities to act as stable predictors of simulator sickness in a subject population. Some of the reasoning presented extends from basic intuitions developed from the author's personal flying experiences, while other assertions extend from accepted reasoning.

3.2 NEUROBIOLOGICAL IMPLICATIONS OF LEARNING

Lasting behavioral traits are the result of environmental interaction and are descriptively presented as a process in which humans learn important interactive correlates; commit them to memory; and on the occasions where stimuli solicit, respond according to this neural store of information. Psychologists claim that this process can exist in several forms and that the implications are of great importance when the neural mechanisms of learning and its impact on experimental validation are considered. The focus of this research is on a single binary categorization of learning (Thompson 1986), which is used in developing the behavioral model and, subsequently, the selection process for the behavioral attributes.

The paradigm divides learning into two basic processes: associative and nonassociative learning. Nonassociative learning is identified with single-event structures that create environments where humans *habituate* (decrease response in) or *sensitize* (increase response in) themselves to repeated stimuli. Associative learning, on the other

hand, is a causal relationship precipitated by events occurring in the environment and is usually categorized as Pavlovian (classical) or instrumental conditioning. In Pavlovian conditioning, two stimuli—conditioned and unconditioned—are presented with the conditioned response onset preceding the unconditioned response onset. The learning model integrates particular aspects of nonassociative with Pavlovian conditioning to develop the reasoning model.

3.3 REASONING PARADIGM BASED ON THE BEHAVIORAL AND SYSTEMS MODEL

The behavioral and systems model initially presented in Chap. 1 is again shown with modifications reflecting a more formal structure (see Fig. 3.1). A comparison of these two systems shows that accommodation has been expanded to include nonassociative behavior. This change provided the basis for developing arguments for the behavioral model.

A major premise of human experience is that a rich store of neural information is developed during the formative years. This information provides much of our reactive mechanisms that we expect in dealing with any physical system. These data form the sensory (visual/vestibular/tactile) accommodation to walking, running, and the general neural and physiological cognitive pairing of information that accompanies our interaction with the environment. Our lives continue to support these hypotheses (conscious and subconscious thought) and reinforce the resulting expectations. In addition, continued stimuli over the years habituate certain reactive elements in the human neural/physiological response mechanisms. Consider, for example, that walking invokes an oscillatory motion in an x-z plane, which is actually considered to be soothing (rocking). Yet, this same oscillatory motion for (prolonged) periods of time in the y-axis (lateral) would precipitate a hostile reaction and create an environmental imbalance that affects walking or standing. Thus, we come prepared for simulator training (or learning) with a complete, intact store of neural information and expectations based upon previous experiences. It is this trust in expectations that is violated by simulator use.

The behavioral and systems model presented in Chap. 1 provides some insight as to what happens to a pilot during a simulator flight. The effects on the pilot are presented again with supporting arguments for the paradigm and the generation of perceptual errors when events do not match the neural store of expectations.

During a simulator hop, a pilot is subjected to what is perceived as discordant sensory information. Figure 3.1 represents this perception as a conformal mapping of two interdependent processes onto the pilot's associative memory store. The first (process) is a causal expectation, $E[*]$, a result of (generated) predetermined control inputs $[U(t)]$ to the system reflecting a goal task. The second (process) is an interpretive mapping of the concordant information from the visual and vestibular systems [×1, ×2], which provides a feedforward signal in collaboration with the causal expectations. The convolution of these two signals provides the interpretive measures by which a pilot establishes continuity or perception of reality.

If differences are detected, a bimodal error signal is generated, passed through a set of dynamic gains, and then sent as an estimate of the energy contained in the perceptual error to a level of cognitive reasoning where situational awareness [or focused attention] is abstracted with environmental awareness. This metalevel inferencing establishes a measure of confidence or uncertainty in the error perception.

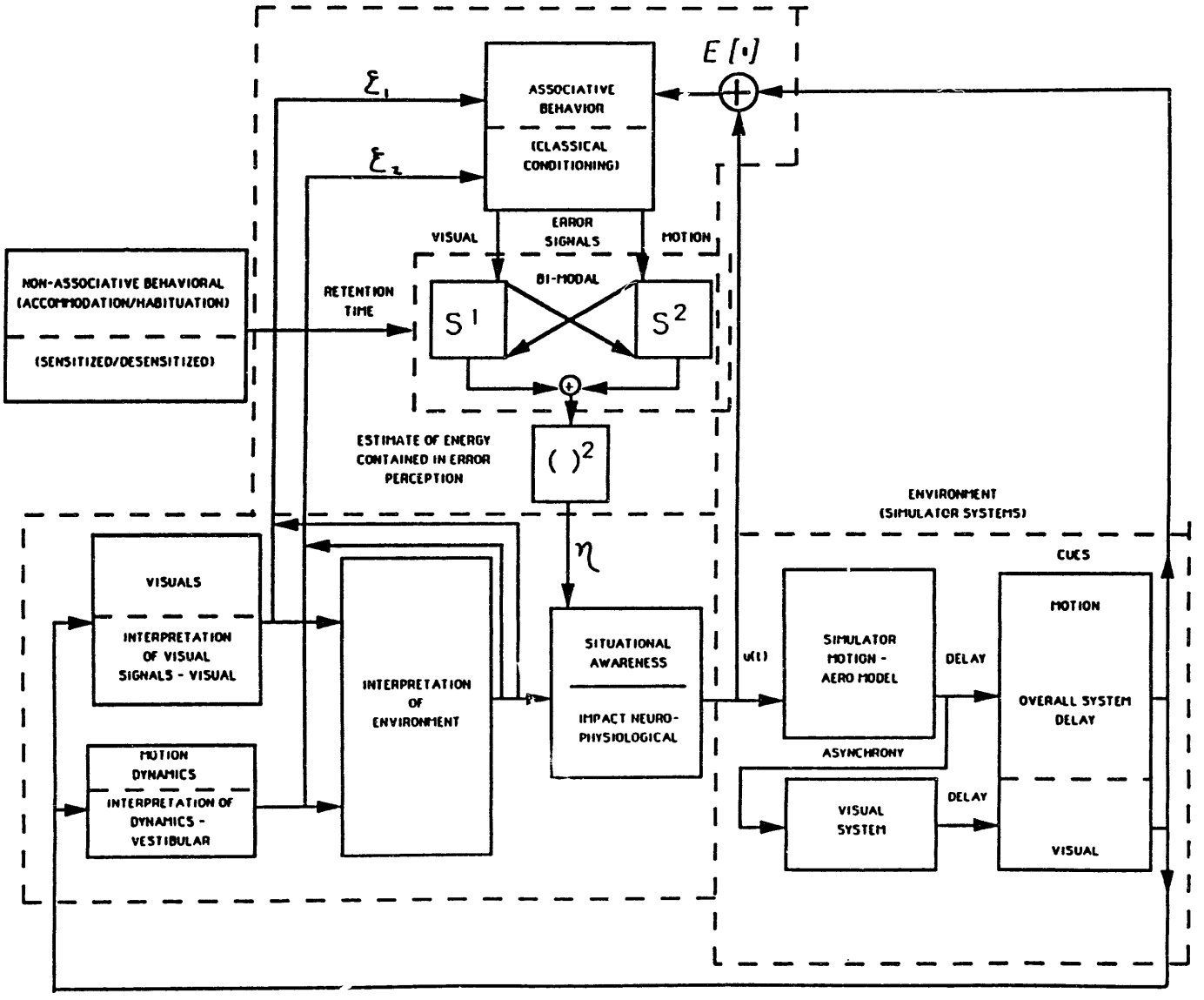

Fig. 3.1. Behavioral and system model.

Environmental awareness provides the basis for establishing assignment criteria to the generated error, with situational awareness conditioning these estimates. If the environment is a simulation, as in the case of the OFT, then it would be expected that perception is discordant with sensory projections. Any error distribution over events (syllabus hop structures) would be accepted by our consciousness. Conflict arises, though, when this perception is colored by a conditioning element based on situational awareness, wherein conscious thought is overridden by a subconscious diversion directing attention to the goal task. In the case of the simulator, the *simulator abstraction* would be replaced by tasks of hovering, landing, or approaches; thus, the corroborating evidence of error is eliminated. This diversion has the effect of acting as a genesis of simulator sickness. Thus, the onset of the disease will occur even in the presence of supporting evidence (conscious thought) that the environment is not real.

The dynamic gains (S_1,S_2), identified earlier, are those elements of nonassociative behavior that act to habituate or sensitize the individual events that are orthogonal to expectations. These variables have a triplet of attributes associated with them that bind the *gains* with a particular behavior/event structure and perceptual error. In this paradigm, the triplet (event β, threshold, time-constant) provides the information required for the subconscious conditioning of the individual. To provide a mathematical description of the process, this relationship is formalized in

$$(\{[\text{event } \beta, \text{ threshold, time-constant}] \Leftrightarrow [S_1\ S_2]\} \cap \{\text{behavior} \cup \text{event } \varepsilon\} \equiv \Delta \rightarrow$$

$$\{\text{decision}_j \in [\text{habituation, sensitization}]\}) \ . \qquad \textbf{(3.1)}$$

An example will serve to illustrate the model. To begin, an expected event (event ε), based on the neural information store (behavior), is compared with the occurring event (event β). If these events are colinear (or nearly colinear), the generated error (Δ) is minimal and below a perceptual threshold value used to condition nonassociative behavior. In this instance, the event is noncompelling and provides an environment (decision_j = habituation) in which habituation can occur (i.e., the dynamic gains are reduced over repeated exposures). If event β is orthogonal to event ε, the error is large and above the perceptual threshold and the nonassociative behavior is sensitized (decision_j = sensitization) to the event (dynamic gains increase with repeated exposures). Repeated exposures will only exacerbate the situation, increasing susceptibility and level of simulator sickness over events. In each case, a time constant correlated with the nonassociative behavior provides a retention time (or event memory) for the stimulus and gains. This time constant is a function of the number of repeated occurrences, event structure, and behavior.

The model described above serves to provide the basis for the selection of the behavioral attributes. A correlation of these parameters with specific elements of the paradigm is given in the next section.

3.4 BEHAVIORAL ATTRIBUTE SELECTION

Table 3.1 lists the behavioral attributes collected during the experiment. It contains 29 elements divided into three categories specific to the pilot, syllabus hop, and simulator system. In addition, seven of the pilot's variables (pilot ill in past week, number of beers in the past 24 hours, ounces of wine in the last 24 hours, ounces of liquor in the past 24 hours,

Table 3.1. Experimental behavioral attributes

Pilot	Syllabus hop	Simulator system
Total fixed wing hours	Pilot/copilot seat	Simulator on freeze
Total rotary wing hours	Event structure	Minutes on freeze
Number days since most recent flight	Day vs twilight	Number freeze events
Number days since most recent in simulator	% Time as pilot	Unusual events
Usual fitness	% Time looking out windows	Stick/throttle control
Experience vection	% Time on instruments	Instruments operational
	% Time navigating	Wait in simulator
	% Time same in aircraft	Minutes in wait
Preselection variables		
Ill during past week		
Number of beers during past 24 h		
Ounces of wine during past 24 h		
Ounces of liquor during past 24 h		
Medication during past 24 h		
Hours of sleep previous night		
Sleep sufficiency		

medication taken in the past 24 hours, hours of sleep during the previous night, sleep sufficiency) were extracted from the attribute list to form a preselection filter. This filter is used to eliminate from the model's data base those individuals already biased toward an incidence of simulator sickness.

On the basis of the previous definition of the system model and subsequent correlation between the behavioral attributes and the system paradigm, the following list identifies the parameter selection for inclusion in the N-tuple neural net model.

Associative Behavior

Total number of fixed wing hours

Total number of rotary wing flight hours

Usual state of fitness

Percentage of time in activities same as in aircraft

Situational Awareness

Percentage of time as pilot

Percentage of time on instruments

Percentage of time looking out windows

Percentage of time navigating

Number of times simulator on freeze, number of minutes

Unusual event occurrence

Instruments operational

Stick/throttle control adequacy

Nonassociative Behavior

Number of days since most recent flight

Number of days since most recent simulator hop

4. APPLICATION OF ADVANCED COMPUTATIONAL METHODS AND OTHER ANALYTIC TECHNIQUES IN SIMULATOR SICKNESS STUDIES

4.1 INTRODUCTION

The current research effort resulted from earlier attempts that used advanced computational methods and other analytic techniques to provide insight into the causal relationships that exist between whole-body energy spectra and the incidence and level of simulator sickness. This research focused, in particular, on quantifying those elements identified in Fig. 4.1 and using them in conjunction with other methods to predict the occurrence of simulator sickness in a user population. This simple paradigm was developed to focus attention on the complexity of issues related to the malady and not just the binary aspect of 0.2-Hz acceleration identified in MILSTD 1472D—the prevalent argument used in determining causality. The weakness of the single-element argument is that it fails to identify the process interdependency of behavior, space, and time as causal elements in the evolution of simulator sickness.

Three analytic techniques are presented, two (energy model/binary decision tree) supporting certain elements of this research, and the third (finite-difference) forming the

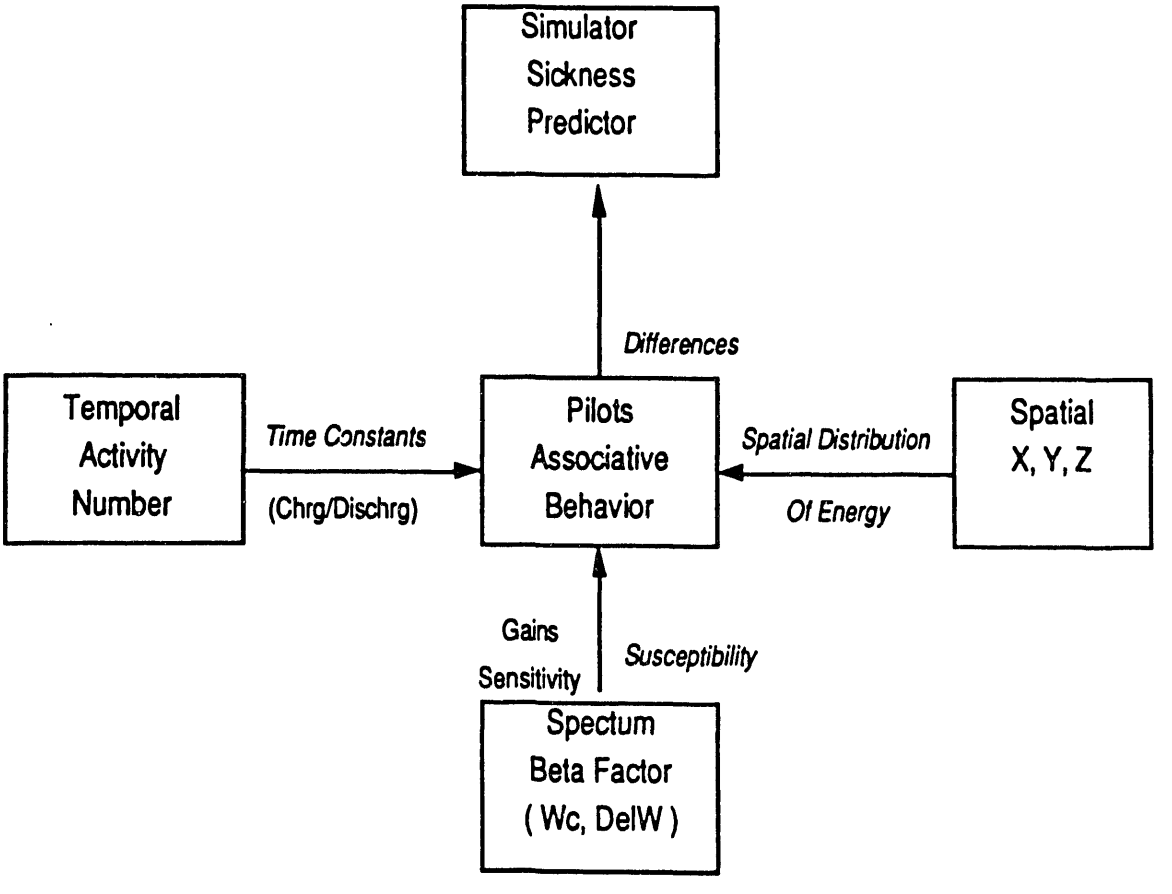

Fig. 4.1. Predictive model for simulator sickness.

basis for characterizing the human-system interactive dynamics. The first is an energy model correlated with select behavioral attributes that provide a simple decision model for class structures. The second is a binary decision tree based on inductive inferencing of system and behavioral attributes. The third is a complex, finite-difference model that uses spatial, temporal, and spectral arguments to provide a measure of susceptibility for the user population based on simulator dynamics.

4.2 STATISTICALLY CORRELATED ENERGY MODEL

To determine the validity of a the whole-body energy model, a simple statistically correlated paradigm was developed (see Fig. 4.2) to test the significance of energy spectra (z-axis using MILSTD 1472D as basis) as a function of simulator sickness susceptibility. In this model (developed by R. S. Kennedy and the author at the Essex Corporation facility in Orlando, Florida, in December 1988), pilots where classified as having either high or low *susceptibility,* depending upon their scores on the Motion Sickness History Questionnaire (MSHQ). Scores were compared with the median MSHQ score and classified accordingly.

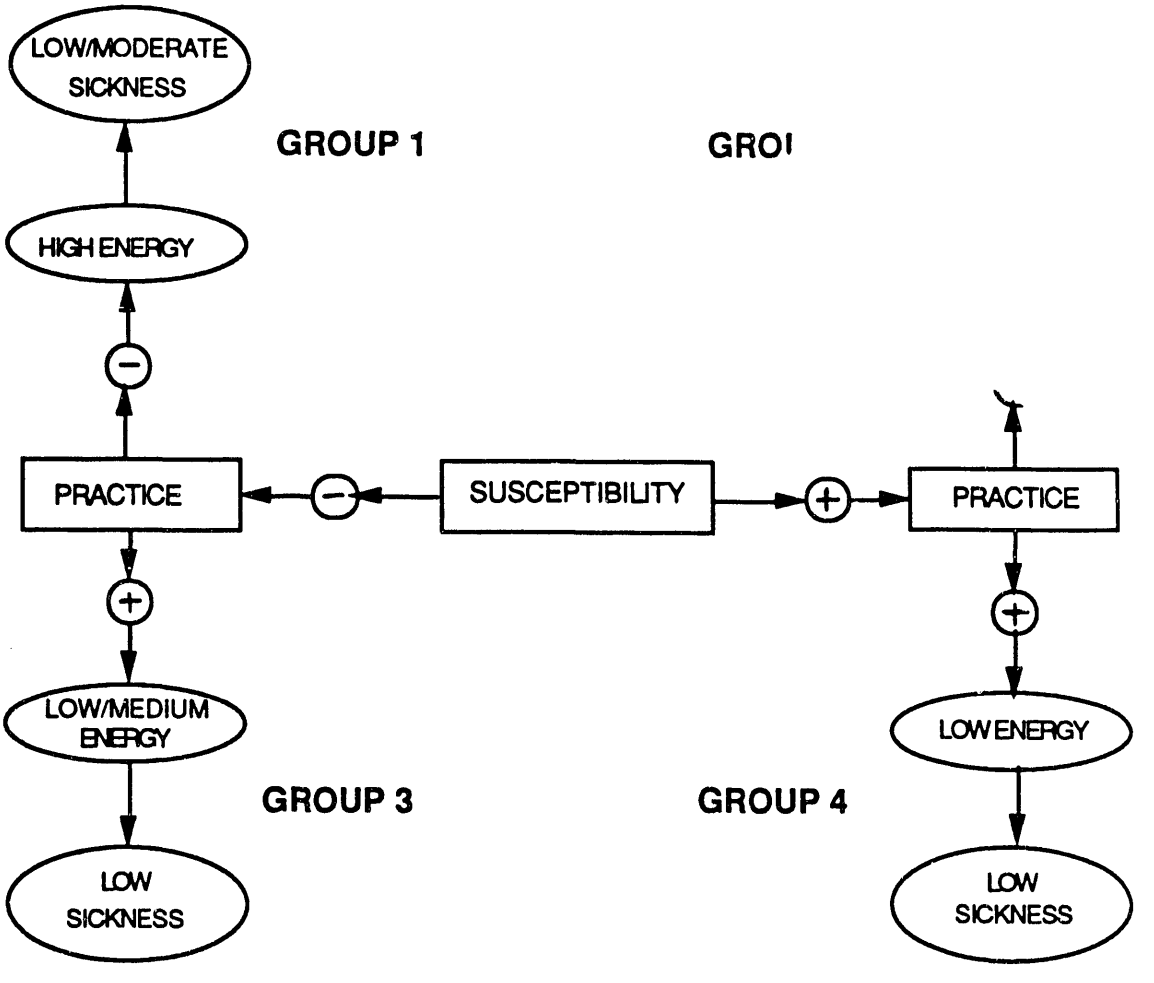

Fig. 4.2. Correlated energy model.

Pilots were also grouped according to the number of *recent flight hours*. The threshold for this attribute was set at 20 h, where a pilot whose recent flight-time was above 20 was categorized as having high flight hours and low if below this threshold.

With this characterization, the model predicts that pilots with low susceptibility and low practice [recent flight hours] (Group 1) will experience low to moderate sickness. This prediction is based on the premise that, although the pilots may experience a high whole-body energy spectrum (low practice), they will be relatively unaffected. Accordingly, pilots with high susceptibility and low practice (Group 2) will experience the highest level of sickness because they will experience a rough ride and be most susceptible to the energy spectrum. Pilots with low susceptibility and high practice (Group 3) will experience low to medium energy and low sickness. Intuition supports this Group 3 characterization since these pilots' abilities to control the nauseoginic environment are at a maximum, reducing the whole-body energy absorption and thus the level of simulator sickness. It should be noted that the reduction of the energy spectrum is not necessary for Group 3 to experience low sickness. Their low susceptibility compensates for high energy profiles, reducing the need for control compensation. The final group includes pilots with high susceptibility and high practice (Group 4). Their training will allow for control compensation given simulator dynamic anomalies, reducing the energy spectrum and providing a low sickness level.

A preliminary analysis (Kennedy) of data collected at several simulator sites supports, to some degree, the model hypothesis defined in Fig. 4.2. In the case of Group 1, an even distribution of high and low energies across the user population resulted in moderate sickness: 11 of 20 Group 1 pilots experienced some level of sickness, while 9 did not; in the Group 2 category, a 70/30 high-low energy spectra resulted in 21 of 32 users being sick; in Group 3, a 50/50 split on high-low energy had 29 of 37 users experiencing no sickness; and in Group 4, a 45/55 split on high-low energy resulted in 18 of 22 users experiencing simulator sickness.

Comparing the data with the model shows a strong correlation for Groups 2 and 3 with the predicted outcome. Group 1 data indicate moderate closure, and Group 4 data indicate a high incidence of simulator sickness, even with low energy spectrum. Arguments can be made that better closure can be gained by increasing the order of the model [including time and space (x- and y-axes)]. But since the intent was to (1) develop a first-order approximation and (2) determine whether the model provided significant structure, further work was forgone to support a more useful and flexible model.

4.3 INDUCTIVE INFERENCING MODEL

One of the major obstacles in studying simulator sickness is the combinatorial explosion that occurs in the functional analysis of the behavioral data and process measurements collected at a simulator site during an experiment. This is compounded by the fact that the data are in both discrete and continuous forms. The discrete forms are the answers to questions posed to the pilots (see Chap. 3). They can be in a yes/no format or subjective evaluations of a system's performance. The continuous data are measurements taken from linear and angular accelerometers and are used primarily to characterize the simulator's dynamics. The formulation of such a problem requires that a qualitative as well as quantitative analysis be brought into focus to identify those elements important in the characterization of simulator sickness.

Machine-learning methods have been employed in instances such as this to synthesize functional relationships that exist between system parameters. In these methods, training examples consisting of attribute values and corresponding class structures are used by the machine-learning algorithm to correctly classify (formulate a knowledge base) examples on the basis of a sequence of tests performed on the attributes. From this knowledge base, a tree (see Fig. 4.3) composed of nodes (tests) and possible outcomes (branches) is developed and used as an evaluator to determine class membership of unknown samples. This determination is achieved by starting at the top node and moving down the branches until a terminal node is reached, resulting in a class membership assignment. Generally, the nodes have many branches for the query. For this problem, however, a binary decision tree is constructed (i.e., only two possible outcomes are generated from the query).

The technique used in developing the decision tree (Horn, Birdwell, and Allgood 1990) is the inductive inferencing method (Quinlan 1986). This method, is a recursively applied algorithm that starts at the top node, finds the sample attribute that gives the largest information gain, partitions the set on this attribute, and then proceeds in the next step to apply this same reasoning to the remaining subset of attributes. This method is a heuristic algorithm that constructs a decision tree that completely and correctly classifies a sample data set or concludes that correct classification is not possible.

This method can be applied to the development of a binary decision tree. The method uses attributes of a class-labeled sample data set to define queries of the form:

$$q_j : A_i \leq \alpha_{ij} ,$$

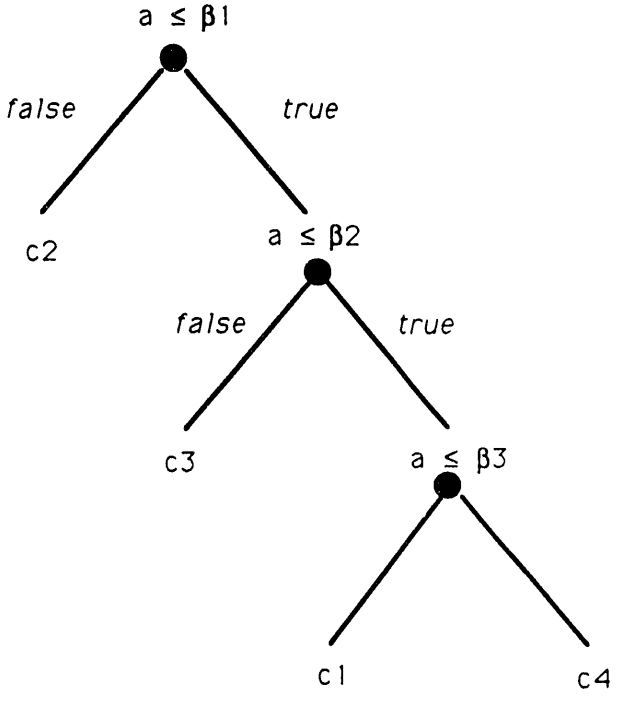

Fig. 4.3. Binary decision tree example.

where q_j is the j^{th} query to be inserted in a decision tree, A_i is the i^{th} attribute, α_{ij} is a real valued threshold, and the result of the query on the given partition of the sample data set is either true or false. For a given partition P, attribute A, and query q, the information gain, I_{gain}, is

$$I_{gain}(P, A, q) = I_{required}(P) - E(A, q) ,$$

where $I_{required}(P)$ is a constant for the particular sample set partition. The conditional entropy, $E(A, q)$, is defined as

$$E(A, q) = -\sum_{r \in \{yes, no\}} n_r / n \sum_{k \in C} n_{r,k} / n_r \log_2 n_{r,k} / n_r ,$$

where n is the number of data objects in the sample set and, within P; C is the set of data classes; n_r is the number of objects with query result r; and $n_{r,k}$ is the number of objects with query result r, which are the members of class k. This formulation makes evident that at each node the attribute A_i and threshold α_{ij} that yields the minimum conditional entropy provides the largest information gain for the query and thus the best partition of the sample set.

This method was used to investigate the relationship(s) that exist(s) between simulator sickness and system motion dynamics, which in turn serve(s) to link associative and nonassociative behavior patterns of the user population with the phenomenon. In this analysis, the mean-square value outputs of a set of bandpass filters [mapping frequency ranges associated with simulator sickness (MILSTD 1472D)] were used to provide the attributes for the training set.

A subset of the available system data was used in the analysis. Those elements considered for inclusion were the x-, y-, and z-axes linear acceleration measurements formulated as a weighted vector norm:

$$\sqrt{ax^2 + by^2 + cz^2} .$$

Also selected were particular elements of the pilot's associative behavior. The two attributes chosen were the number of helicopter flight hours and the number of hours of sleep the previous night.

Before constructing the tree, an attribute data base was developed by filtering the acceleration data from each simulator hop and computing the mean-square value. A total of 45 digital filters covered a range from 0.1 to 1.0 Hz in increments of 0.02 Hz. Each filter had a Q of 8.

The tree is constructed in a stepwise recursive optimal fashion by starting at the top node and determining the attribute that best classifies (largest change in entropy) the 25 samples (number of simulator hops) into two subsets. At this and each successive node, the inferencing algorithm determines the attribute that best classifies the sample set into two subsets. This determination is accomplished by a query of the form, "Is the attribute value less than or equal to the threshold?" The determination is made only after an exhaustive search of the 45 filter mean-square values and the two behavioral attributes.

The result of applying this inferencing algorithm to the selected attributes is presented in Fig. 4.4. Shown are those attributes selected by the algorithm that best assigns

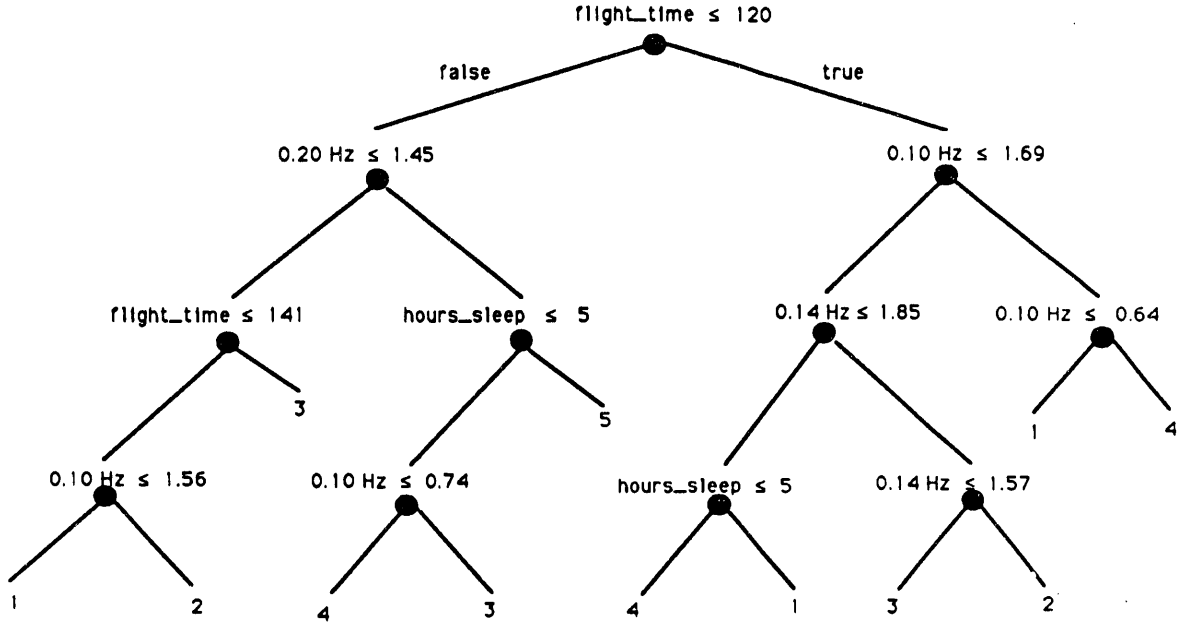

Fig. 4.4. Decision tree producing simulator sickness symptomatology score.

motion-sickness symptomatology to the x-, y-, and z-axes acceleration data, pilot flight hours, and sleep hours. The specific filters selected by the program have center frequencies of 0.10, 0.14, and 0.20 Hz. (Threshold values are scaled by a factor of 1000.)

The decision tree developed by the inductive inferencing algorithm provides strong correlation for the hypothesis set forth in this research effort. Of particular interest is that the first test (top node) uses an associative behavior parameter to split the sample set, attaching significance to the importance of past experience in the genesis of simulator sickness.

4.4 FINITE-DIFFERENCE MODEL: THE "WHOLE BODY ENERGY ABSORPTION MODEL"

The previous works emerged from the author's ideas and efforts to develop a whole-body energy absorption model that characterizes a pilot's ability to shed/absorb energy over a syllabus hop—in particular, modeling the human as a variable filter that fatigues over time, allowing more of the dynamic energy at any instant to be absorbed (internally) by the pilot. The effects would be seen as neurophysiological impacts, integrated over the time course of the syllabus hop. The importance of such a model is characterized in Fig. 4.5, where the whole-body energy dynamics of the pilot is pictured as a function of time.

As indicated in the figure, two extreme possibilities can occur for a pilot, resulting in a simulator-sickness dichotomy. In the first (top curve), the pilot experiences most of the simulator dynamics (activity) in the early stages of the hop. The pilot, modeled as a simple exponential function with charge/discharge time constants, could upon exiting from the simulator experience little, if any, symptomatology because of the ability of the human to shed the effects of the hop during the next hour as the body recovers from the experience. In the second case, the pilot could exit the simulator complaining of discomfort (and other

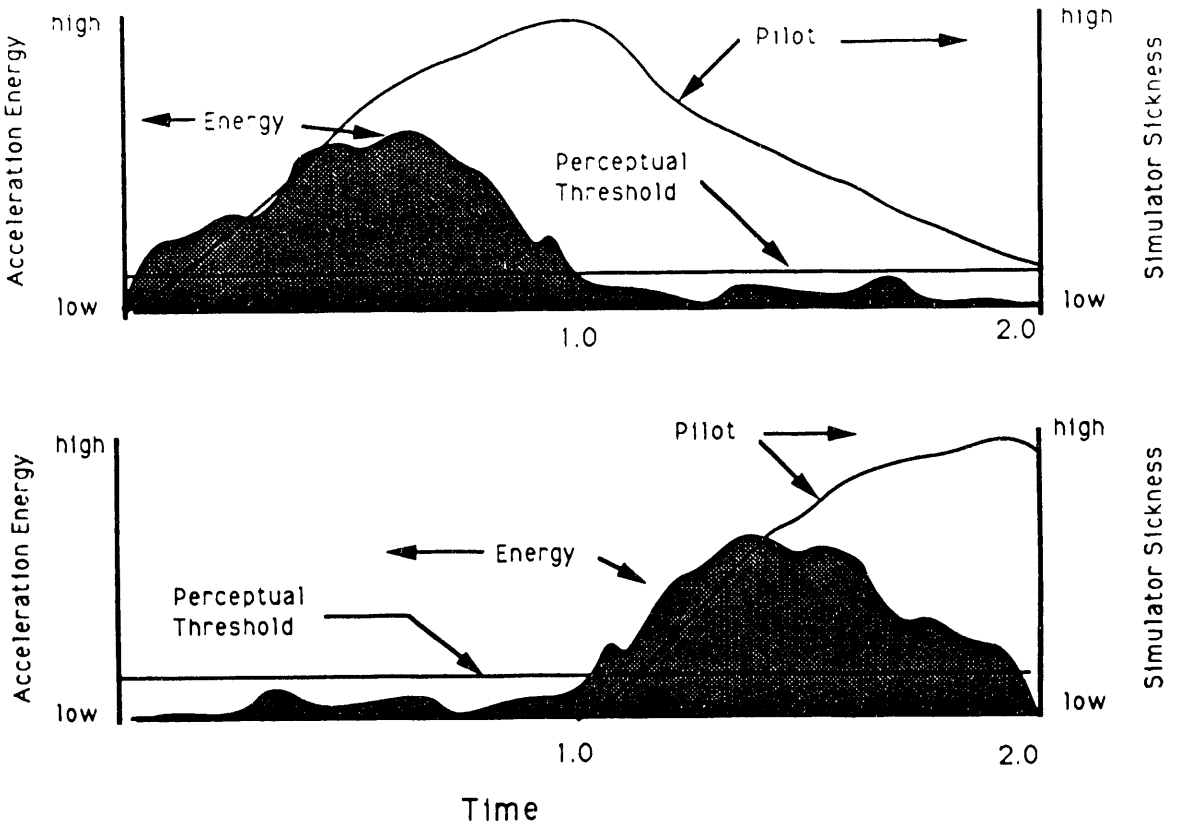

Fig. 4.5. Dichotomy of simulator use acceleration energy vs time.

symptoms) because the activity in the simulator was in the latter stages of the hop sustaining the effects of the ride. In both cases, assumptions are made that (1) the pilot possesses those behavioral attributes that make the pilot susceptible to simulator sickness, (2) the pilot has experienced levels of acceleration energies guarded against by MILSTD 1472D, and (3) all other environmental agents that could act as causal elements for the malady are equal. If an analysis were performed strictly on the basis of spectral energy content averaged over time (ensemble average), both hops would have the same quantitative estimates over the time period. Yet, in one instance the pilot could exit the simulator with little or no adverse effects and in the second could exit the simulator complaining with symptoms associated with simulator sickness. A dichotomy would then exist because the energy spectral estimates would be the same but the response (recollection of simulator experience) quite different.

To overcome this problem, a model was developed that took into account the temporal, spatial, and spectral interdependencies that impact the human's central nervous system. The model is presented diagrammatically in Fig. 4.6, showing particular elements in block form. A basic assumption of the paradigm is that the human acts as a variable filter that fatigues over the course of the simulator hop, allowing more of the instantaneous energy to be absorbed by the body. In addition, the human is assumed to have exponential characteristics that allow for different charge/discharge time constants: $(\{t_{ci}, t_{dci}\} \mid i$ = physical, neural systems). Therefore, a doublet of time constants is required to define both sets of dynamic equations that describe the neurophysiological systems.

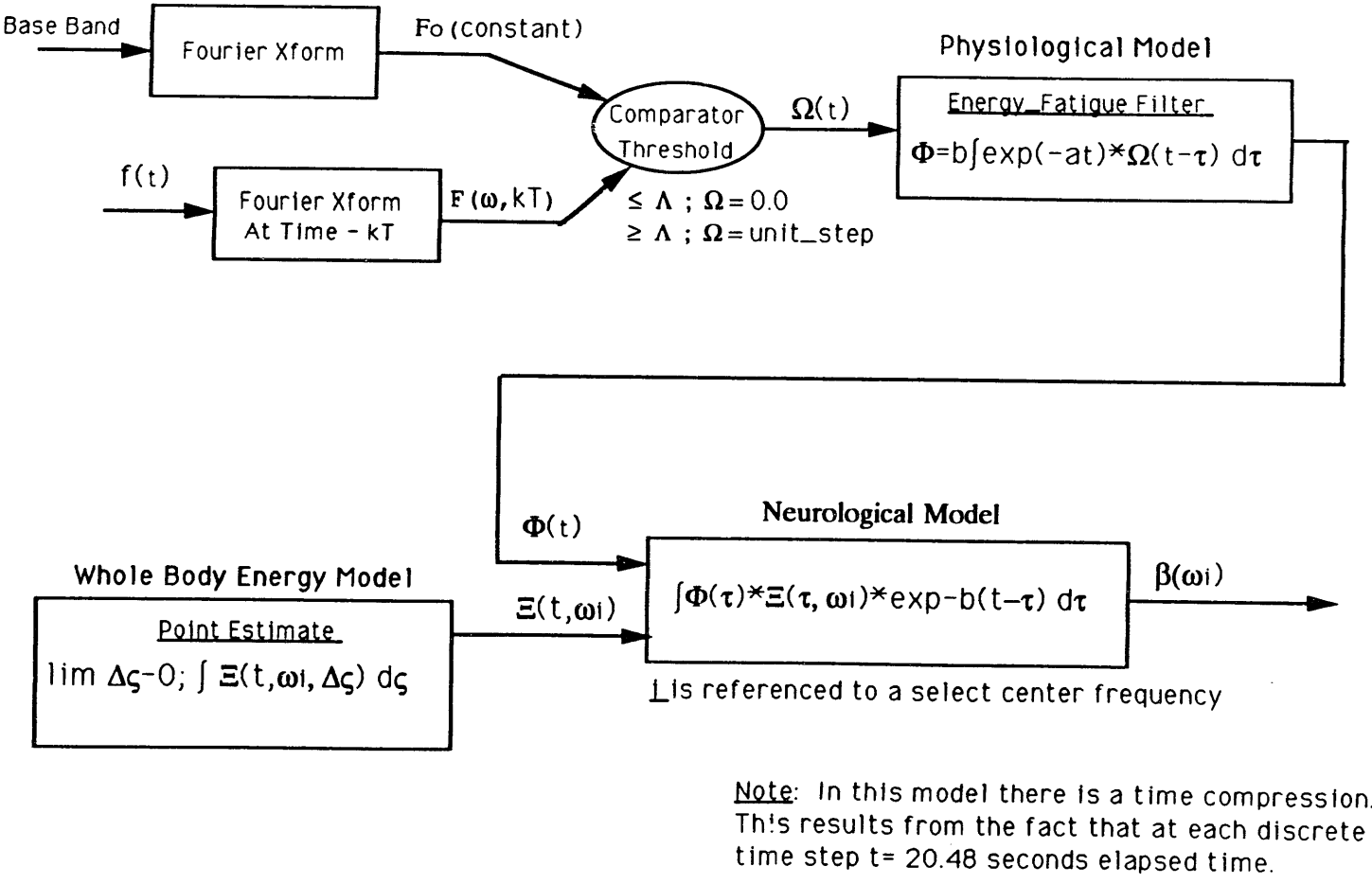

Fig. 4.6. Model block diagram.

Since the model is based on the simulator's imparting dynamic energy to the pilot, it must have the capability to discern when the system is active (i.e., movement in x-, y-, and z-axes). This is accomplished by performing a noise analysis (Fourier transform) on all axes when the system is brought up on rams. This analysis is then stored as a noise spectral estimate energy pattern. Then, at each instance of time in the analysis, a comparison is made between the Noise Spectral Estimate, F_0, and the current spectral energy estimate, $F(\omega)_k$, for each axis. The difference, defined over a select narrow spectral band, is compared with a threshold function, L, which has been calculated and set to a value that allows the model to correlate static downtimes with a forcing function, $\Omega(t)$, equal to zero. This forcing function calculated from the system observance function is then applied to an equation modeling the energy-fatigue (physical) filter, $\Phi(t)$. The charge/discharge time constants ($\{t_{ci}, t_{dci}\} \mid i$ = physical) are set to 7.5 and 45.0 min respectively. (These choices were made on the basis of the author's experience in the simulator). The neurological filter is developed in a manner similar to that of the physiological model with the addition of a term representing a point estimate for whole-body energy absorption (see Eq. 4.1). The time constants ($\{t_{ci}, t_{dci}\} \mid i$ = neural) are equal to 3.5 and 15.0 min, respectively, for charge/discharge. It should be noted that a set of equations will be required for each frequency analyzed (i.e., $\omega_i \; \forall \; i$ = select frequencies of interest):

$$\Xi_k(t,\omega_i) = \lim \; \Delta\varsigma \to 0; \; \int \; \Xi(t,\omega_i,\Delta\varsigma)\, d\varsigma \; . \tag{4.3}$$

The finite-difference equations modeling the interactive neurophysiological process is as follows:

$$\text{for } k = \; 0, \; 1, \; 2, \; \ldots, \; \Gamma \; ,$$

where $k^*\Delta T$ spans the period of activity (i.e., $\Gamma^*\Delta T = t_{final}$) and ΔT is the sampling interval; and for F_0 the Fourier analysis of the noise signal level for a particular axis.

4.4.1 Energy-Fatigue (Physiological) Filter at Each Time Step

If

$$\mid \; F(\omega)_k - F_0 \; \mid \; \geq \; \Lambda \; , \tag{4.2}$$

where $\Lambda = \Sigma \; \omega_j$ and j is defined for some select narrow band frequency, then

$$\Omega \; (k\Delta T) = \text{Unit\_Step else} \; ,$$
$$\Omega \; (k\Delta T) = 0.0 \; .$$

The Physiological model is then defined as

$$\Phi_k \; = 0.95^*F_{k-1} + 0.46^*\Omega(k\Delta T) \tag{4.3a}$$

for $\Omega \; (k\Delta T)$ = Unit_Step, and

$$\Phi_k = 0.99*\Phi_{k-1} + 0.008*\Omega(k\Delta T) \quad \textbf{(4.3b)}$$

for Ω (kΔT) = 0.0.

4.4.2 Neurological Model at Each Time Step

$$\beta_k = 0.91*\beta_{k-1} + 0.089*\Xi_k(t, \omega i)*\Omega(k\Delta T)*\Phi_k \quad \textbf{(4.4a)}$$

for Ω (kΔT) = Unit_Step, and

$$\beta_k = 0.99*\beta_{k-1} + 0.011*\Xi_k(t, \omega_i)*\Omega(k\Delta T)*\Phi_k \quad \textbf{(4.4b)}$$

for Ω (kΔT) = 0.0.

This set of equations, developed for each select frequency band analyzed, represents the neurophysiological model developed for this research. This is the first set of developed equations that incorporate temporal, spectral, and spatial arguments as well as behavioral attributes in a closed form specifically to predict simulator sickness from system dynamics.

The application of this model to two select syllabus hops is presented in the following series of graphs. The first, Fig. 4.7, represents the 1R1 x-axis Physiological model; three parameters are presented: output, $\Phi(t)$; observation function; and forcing function, $\Omega(t)$. The output, represented by the bottom graph, shows the physical response—or fatigue—over the duration of a syllabus hop. As shown, activity was sustained at levels significant enough to create an environment where the physiological impact of whole-body energy absorption was maintained above 0.90 for the hop. (In this model, complete fatigue is equal to a value of 1.0; that is, all energies presented to the body are absorbed with no attenuation.) The top graph represents the forcing function for the model. If it is correlated with the time record for 1R1 x-axis linear acceleration (see Fig. 4.8), it obviously coincides with the activity on this axis. The middle graph represents the observance function and is indicative of the energy present in the low-frequency band. As is evident in the latter stages of the hop, the overall energy contributions are diminishing, indicating a more stable control of the device (a result of pilot efforts or a change in the syllabus hop structure).

The next series (Figs. 4.9–4.11) presents the 1R1 x-axis Beta function calculations for the x-, y-, and z-axes respectively. Beta1, Beta2, and Beta3 (Beta4 = 0.244 center frequency is not presented) are representative of 0.097, 0.147, and 0.197 center frequencies. Visual analyses of these graphs identify certain elements characteristic of the model. The first is the charge/discharge phenomenon that accounts for attenuation in the whole-body energy absorption if energies in a select frequency are absent or at a minimum. (See Beta function values over latter part of hop; compare Beta function across events.) The second is that the high-activity regimes are accounted for by the peaked distributions of the Beta function for the defined time periods. The third is that the dynamics of interaction are accounted for during the complete time period. The fourth is that contributing elements of space, time, and frequency are contained in the model. (Figures 4.12–4.14 are the beta function calculations for run 2R10 analyzed using this paradigm, presented for comparison only.)

A complete set of Beta curves for each of the 20 syllabus hops flown in the TH57C simulator was generated and used in the formulation of the N-tuple neural network (see Chap. 5).

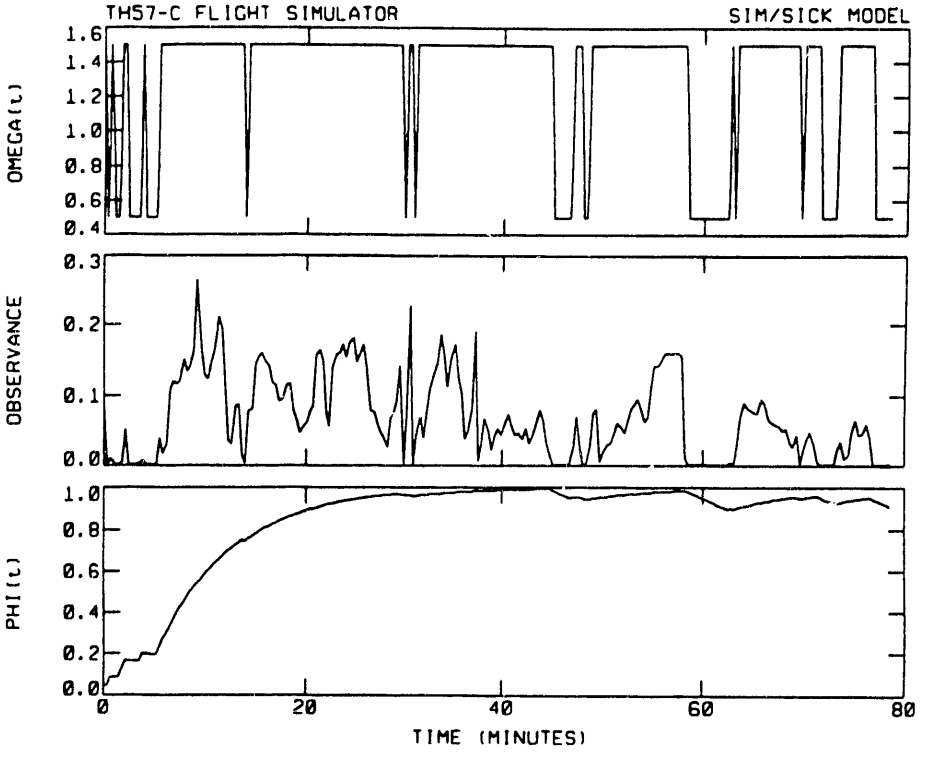

Fig. 4.7. 1R1 x-axis physiological model.

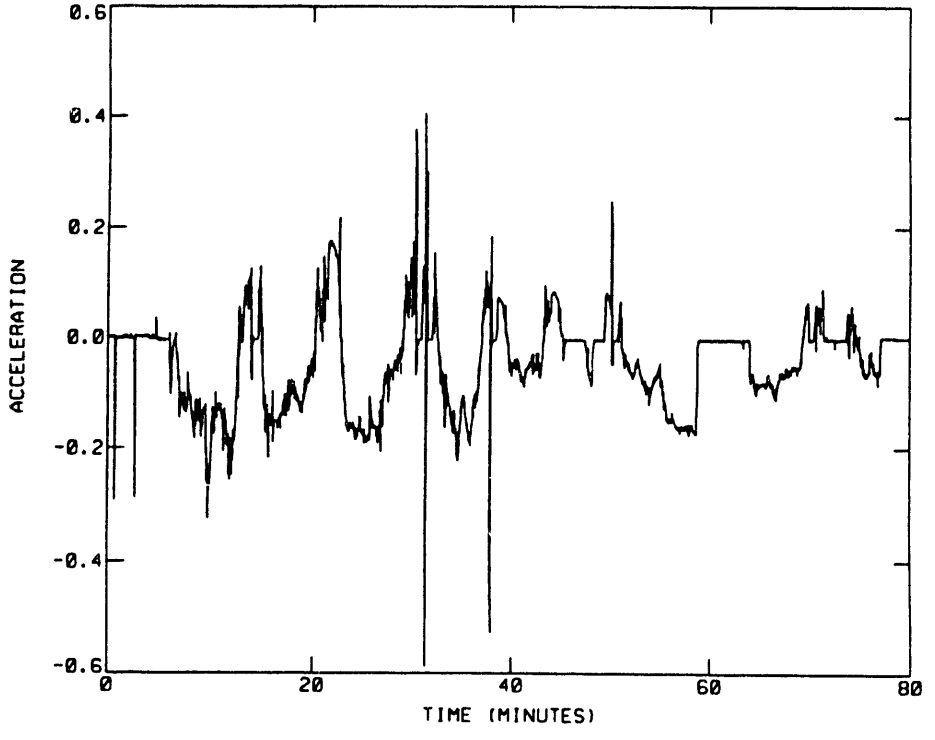

Fig. 4.8. 1R1 x-axis linear acceleration.

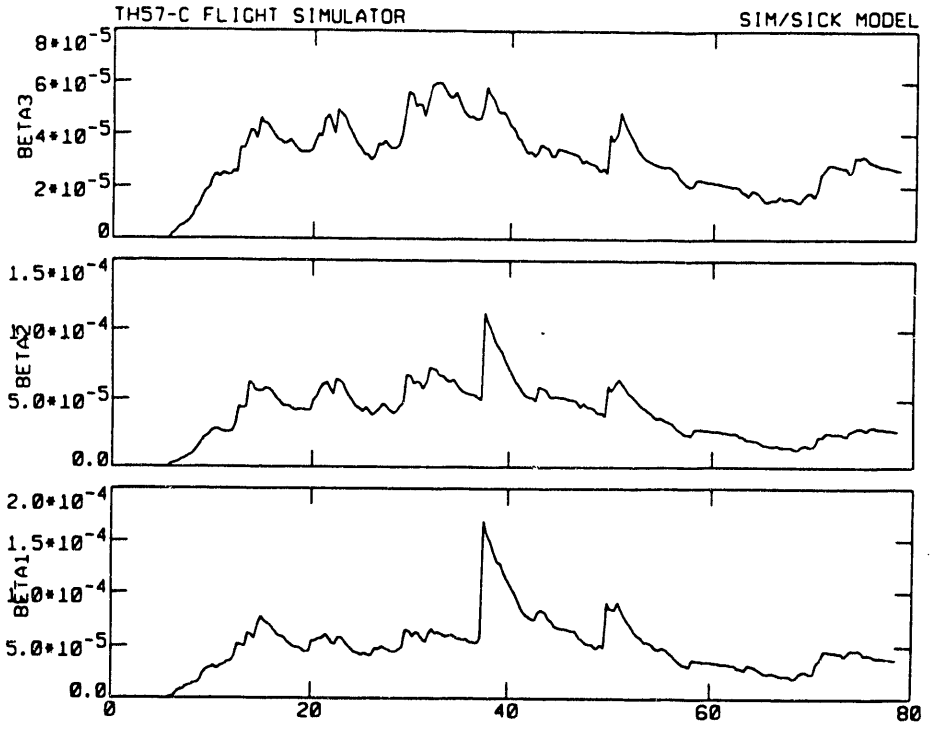

Fig. 4.9. 1R1 x-axis beta function calculation.

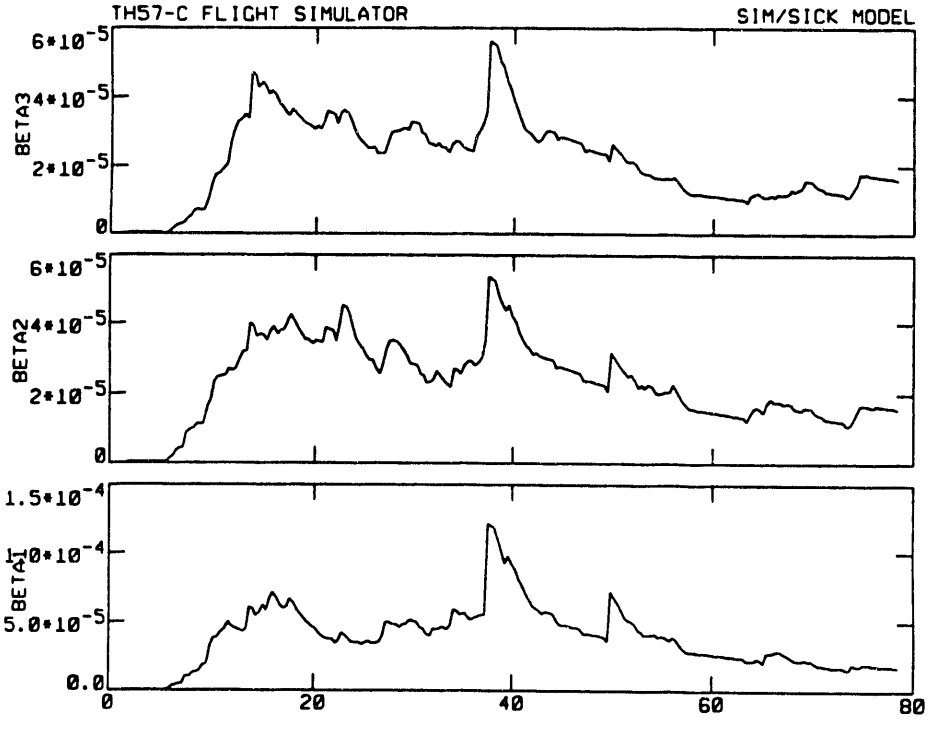

Fig. 4.10. 1R1 y-axis beta function calculation.

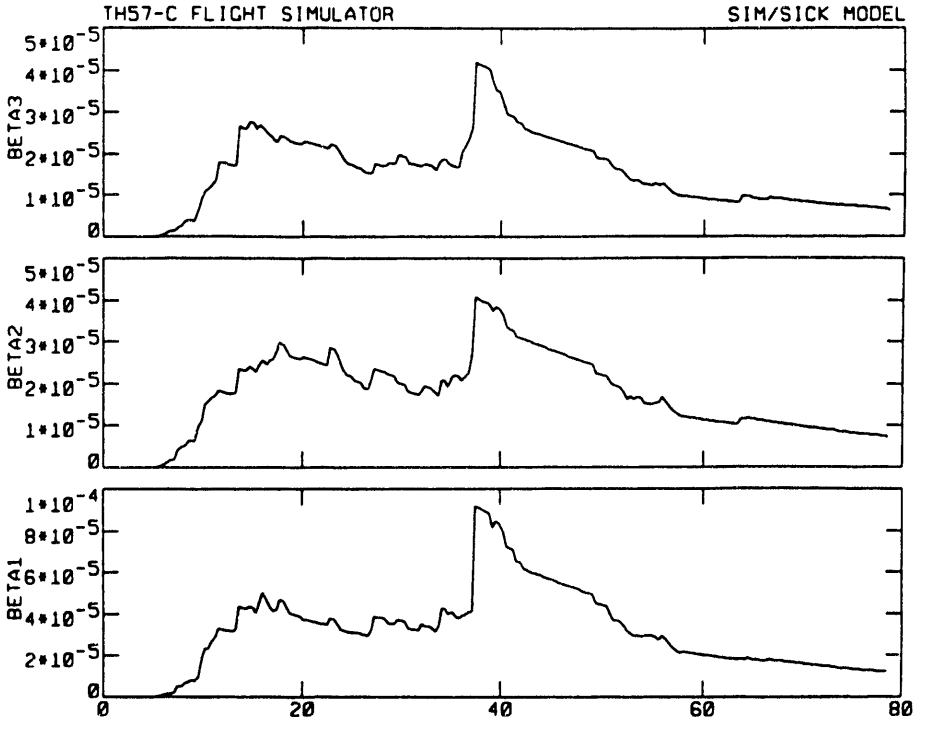

Fig. 4.11. 1R1 z-axis beta function calculation.

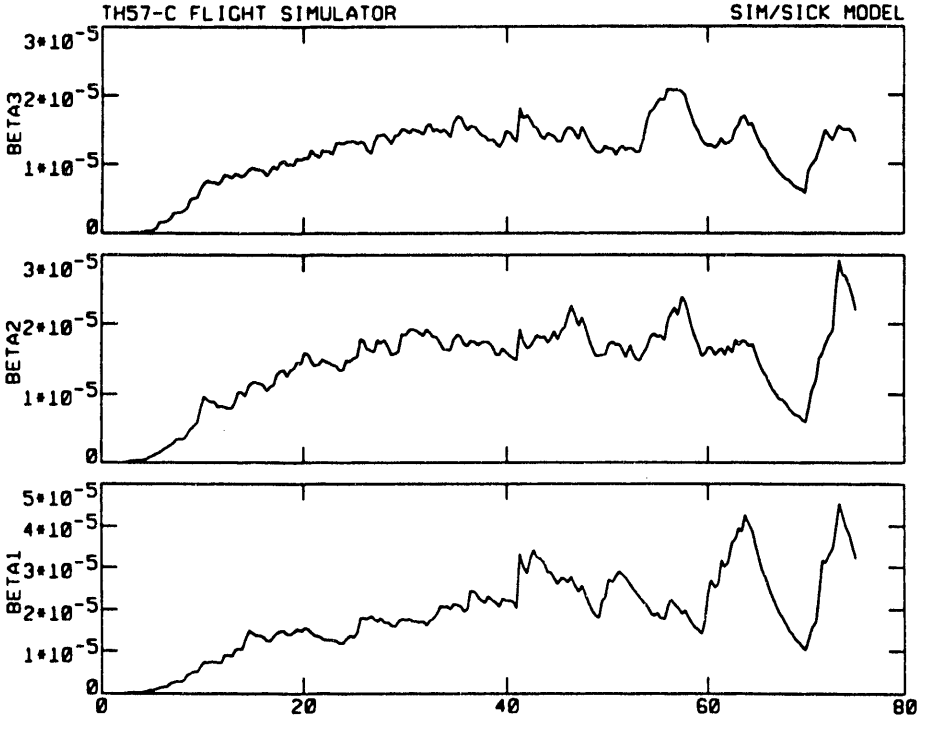

Fig. 4.12. 2R10 x-axis beta function calculation.

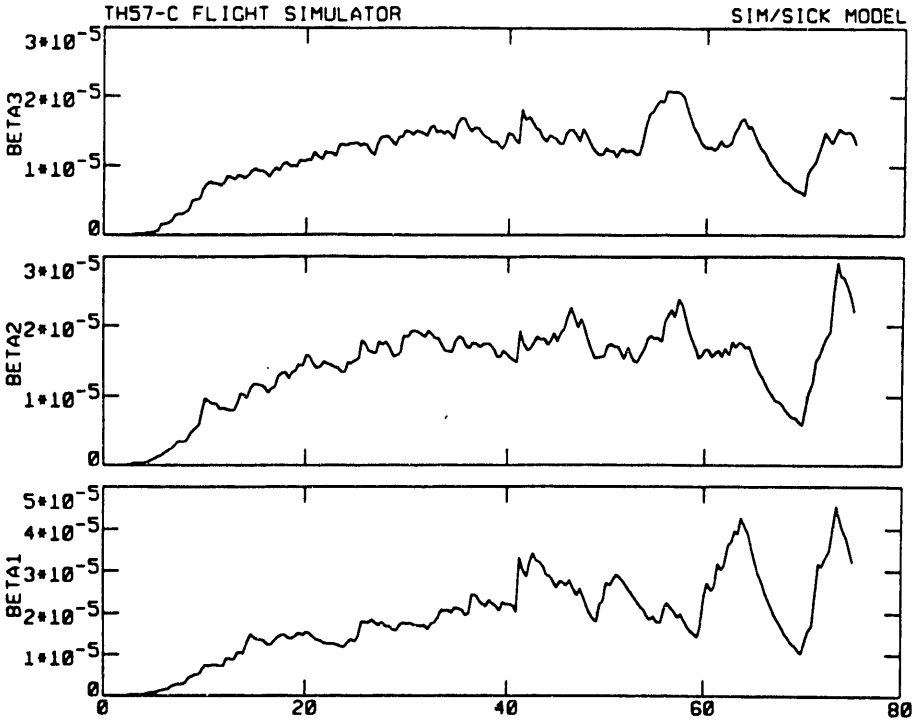

Fig. 4.13. 2R10 y-axis beta function calculation.

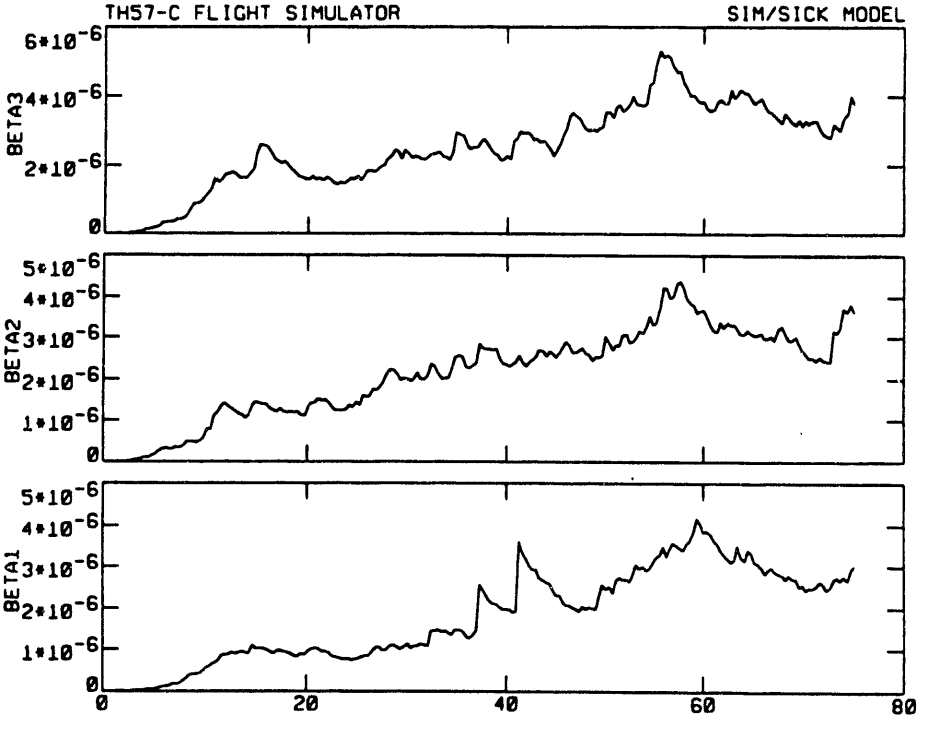

Fig. 4.14. 2R10 z-axis beta function calculation.

5. SIMULATOR SICKNESS PARADIGM: A NEURAL NETWORK STRUCTURE

5.1 INTRODUCTION

Real-time state-space estimates for complex systems [in this sense, nonlinear, dynamical systems whose state projections are not crisp (simple decision boundaries)] are difficult because of the analytic requirements for adequately describing existing functional relationships. At issue is the ability to interrogate or monitor a system, apply interpretive measures of assessment, and make quantitative and qualitative judgments in real time about existing and transitional states. For *simulator sickness*, this translates into an ability to use system dynamics, associative and nonassociative behavioral data, and previous simulator experience to predict the onset and level of the disease in a user population. Of particular importance is the development of a self-organizing mechanism by which the model can synthesize and evolve to a solution.

Analytic models have limited applications to the simulator sickness problem because of their inability to accurately model with mathematics or logic that which is so aptly described with our own grammar—for instance, pilots who fly these devices describe feeling *out of balance* or *uneasy after the hop*. These observations are conditioned on an individual's perception and become context-dependent descriptors for that particular day, hop, pilot, and simulator. These descriptors are colored by personal behavioral attributes and experiences and give rise to different meanings or interpretations. Other problems encountered are the on-line requirements for identifying system parameters and variables and the systematic development of consistent structures that accurately model the observed system. Considering the nature of simulator sickness and the complex structure that exists, developing a strictly analytic predictive model is prohibitive. However, a method exists that has had success in tasks similar to this: the *artificial neural network*. Artificial neural networks are connectionist schemes modeled after the biological structures that exist in the human's central nervous system. These paradigms take advantage of the highly parallel, selective computing mechanisms that allow the human to be successful at either feature extraction or pattern recognition or both. The strength of the paradigm lies in its ability to form its own internal representation of the process and make judgements accordingly. These models are robust in the sense that the failure of (several) computing elements (neurons) and/or connection strengths (synapses) do not necessarily degrade performance significantly (distributed knowledge). The mechanisms by which these structures are developed lend themselves quite readily to the task of real-time and on-line learning or training (adaptive mechanisms by which knowledge is acquired). Also, by providing a basic grammar, the system can deal with fuzzy logic or intuition—as in the case of pilots' comments. Once taught, state assessments can progress in time frames commensurate with system requirements when the proper net structure has been selected. It should be noted that a hybrid-system configuration to deal with both the front-end and output conditioning is usually needed.

Neural nets have an ability to provide temporal correlation with system attributes, which can enhance the capability of the net to project and estimate states and state transitions. This ability also provides a mechanism by which, in the classical sense, the probability of estimating an interesting state increases as the systems gains more information.

As with any model, developmental issues must be considered before implementing a neural network as an observer. First, time requirements for net convergence must be

considered. These times will vary depending upon the number of neurons, connections, structure invoked, and learning rule employed, which are serious considerations for proper selection. Another issue is the need for front-end preprocessing to overcome nonorthogonal data structures that may exist. In some networks such as the Adaptive Resonance Theory (ART) and Kohonen, the input data features are crucial to the net's classification capabilities and become more sensitive as the input is normalized and scaled. The saturation of the net in its ability to learn and reason as well as the ability to forget as the net evolves is also important. These and other issues can be overcome by an appropriate selection and combination of nets whose structures are specifically designed for certain classes of problems.

5.2 BIOLOGICAL MODEL ANALOG: THE ARTIFICIAL NEURAL NETWORK

The structure of artificial neural networks (ANNs) is modeled after the organization of the central nervous system (CNS). The analogies drawn for development of the ANN networks from the neuralphysiological system are slight when the complexities and intricacies existing in them are considered. What is known is information about the basic building block (neuron), interconnectivity (synapses, dendrites), major pathways, and the mechanism by which memory is achieved (morphological changes in synaptic strengths). Current research is extending this knowledge through efforts targeting the structure/form correlates that exist in the central nervous system. The goal is to better understand how cognition and concept formation occur. These studies have provided useful and diverse models of mental activities that are based on the modular interactions of the nervous system (form, visual images, attention, belief/concepts).

By analyzing the biological/physiological process, an enhancement of existing and development of new paradigms can be achieved. By understanding the structure/form correlates that exist (e.g., the *visual system* where form, color, and spatial information is processed along three independent pathways in the brain), enhanced mathematical formulations of select neural attributes can be developed. In addition, answers can be given to questions about such processes as adaptation/habituation and its impact on plasticity, associative behavior and learned expectations and how it colors perception, and situational awareness and how its environmental focus can enhance or detract from the reasoning process.

5.3 HUMAN BRAIN STRUCTURE

The human brain contains over one hundred billion processing units called neurons (computing elements) whose communication is conducted over nerve fibers called synapses. The neuron is the fundamental building block of the nervous system and is similar to all other cells in the body, but it is specialized in its ability to perform the computational and communication functions within the brain. It consists of three parts: cell body, axon, and dendrite. The dendrite sums the information, receiving signals from other cells at terminal points called dendritic spines. Here, information is passed along the axons, across the synaptic cleft, and onto the dendrite leading to the active neuron. [Research has shown that in certain instances the morphological changes that accompany learning create instances where the axons terminate directly on the soma (cell body).] The signals are then passed to

the cell body, where they are averaged with other such signals. If the average of a short interval is sufficient to overcome a resting potential (threshold), then the cell fires, thus producing a pulse that is passed down its own axon to succeeding cells.

The synapses, which form the interconnected pathways by which information is carried across the net, provide signals that act as enhancers or inhibitors. This interplay among the signals and the electrochemical process occurring at the synaptic cleft mediates the learning process and cellular activity that occurs in the brain. Figure 5.1 is a diagrammatical representation of the biological paradigm.

5.4 MATHEMATICAL REPRESENTATION OF THE BIOLOGICAL PARADIGM

Like the biological paradigm, artificial neural networks consist of many interconnected units (neurons) where learning occurs; and as a result, memory stored (connection weights). Since all the networks encountered align with this definition, the mathematical description presented describes general properties of these models with no inference to any particular structure. Figure 5.2 shows the general topology of a neural net.

As shown in Fig. 5.2, the net structure consists of an input layer, an output layer, and in this case, two hidden layers of neurons. These neurons are considered highly connected since each lower level neuron is connected to every neuron in the next layer. It should be noted that no internode feedback occurs in this model, although occurrence is possible.

The output, Θ_{ij}, of neuron$_{ij}$ depends upon the inputs that the unit receives. In this representation, i is defined as the layer number and j the particular neuron present. Exceptions are input neurons and any neuron that is clamped at a fixed output level. The inputs to a neuron are the outputs of neurons in the preceding level, which are communicated over connection strengths, W_{ij}. Therefore, the net input level, $\lambda_{i+1,\,j}$, of neuron $_{i+1,\,j}$ is defined as:

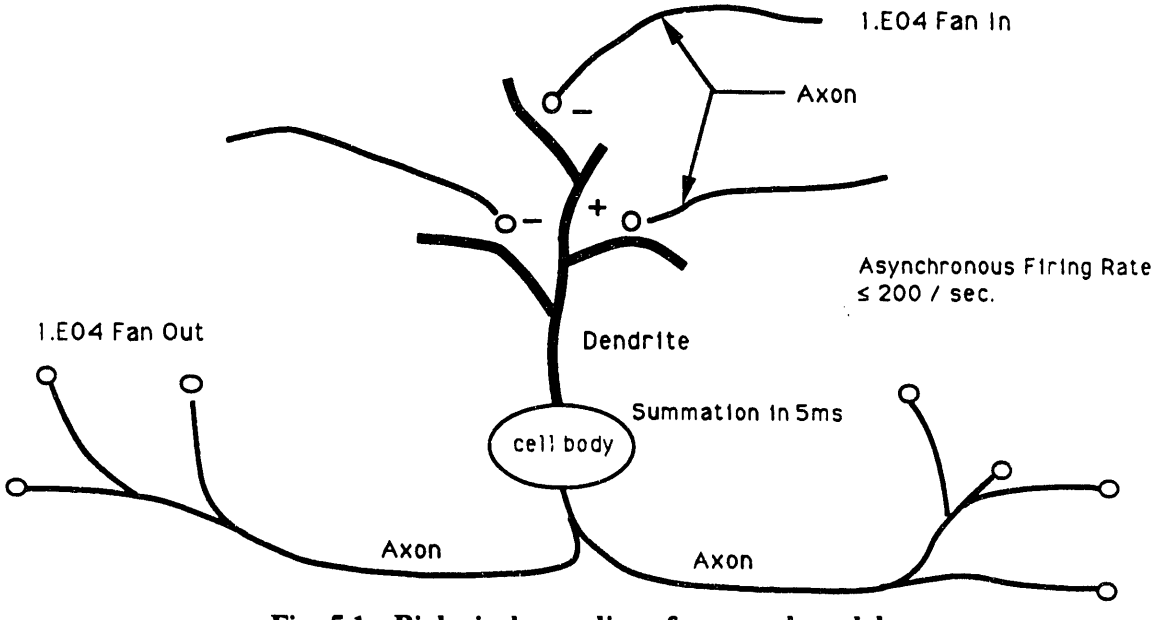

Fig. 5.1. Biological paradigm for neural model.

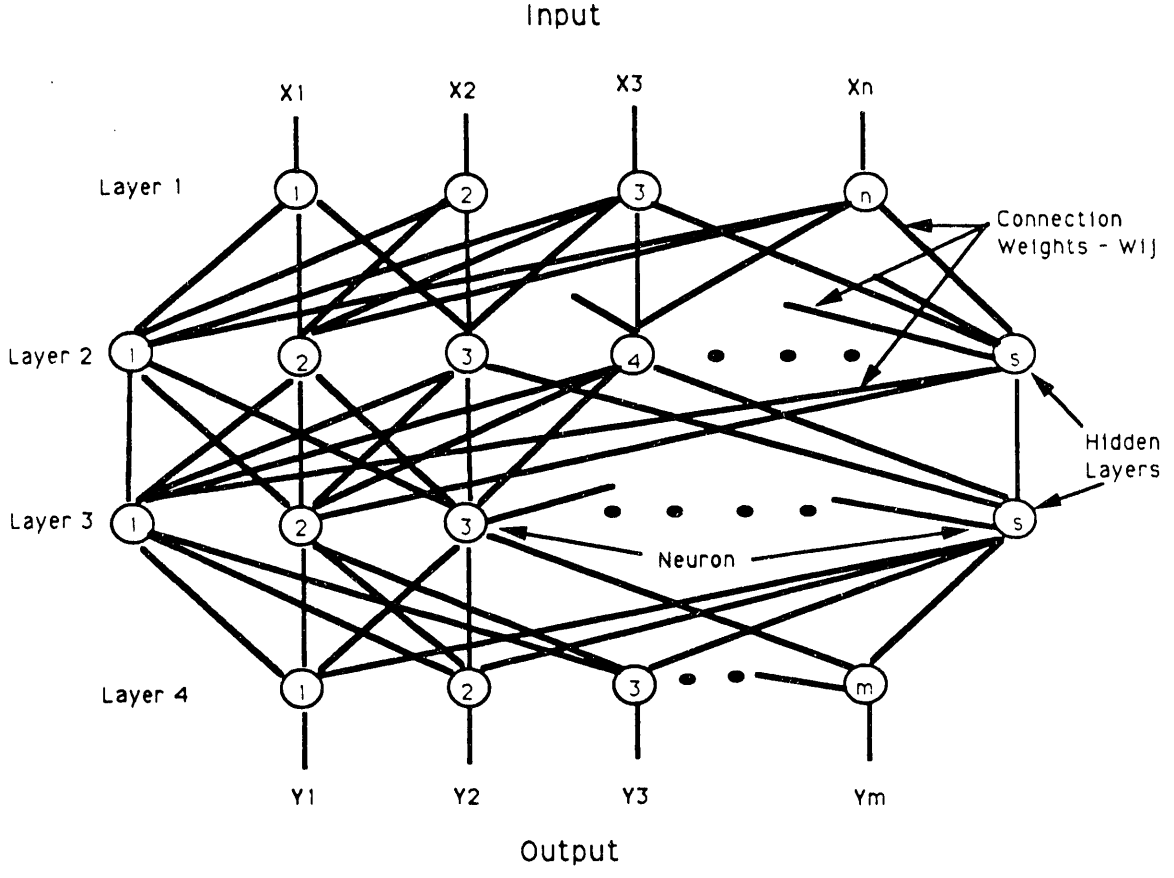

Fig. 5.2. Basic neural net topology.

$$\lambda_{i+1,\,j} = \sum W_{ij} * \Theta_{ij} \text{ : summed over } i \text{ .}$$

In this development, symmetry is assumed in the connection strengths (i.e., $W_{ij} = W_{ji}$). This condition is not necessary for network development but it is usually employed because it leads to the existence of an *energy function*. (It should be noted that asymmetric networks have a potentially richer behavior.) Each connection weight can be excitatory, $W_{ij} > 0$, or inhibitory, $W_{ij} < 0$. Connection weights can also be defined as discrete or continuous and bounded or unbounded.

The connection strengths, W_{ij}, are the key elements in the learning behavior of the net. They represent the distributed memory and are initially chosen randomly and set to small values. Then, through some interactive scheme, they are dynamically adjusted as the network learns in response to a set of training data.

As stated earlier, Θ_{ij} is functionally depended in some way on λ_{ij}.

$$\Theta_{ij} = \Xi (\lambda_{ij}) .$$

However, a change in λ_{ij} does not necessarily result in an instantaneous change in Θ_{ij}. Depending upon the update mechanism employed, the state of each neuron can be updated either immediately or later. The response will be determined solely on whether the system is synchronously (immediately) or asynchronously (randomly) updating the state estimates of

the neurons. An asynchronous mechanism is equivalent to updating, in a random sequence, each neuron with an equivalent constant probability per unit of time, independent of all others.

The equivalence of Θ_{ij} to a value may be either deterministic or stochastic. In the deterministic case, it is a simple assignment of the functional value of the $\Xi(\ )$ function to Θ_{ij}. In the stochastic case, it is with probability $\Xi(\lambda_{ij})$.

The range of $\Xi(\lambda_{ij})$ must be the domain of Θ_{ij} in the deterministic case and [0,1] in the stochastic case. Usually, $\Xi(\ )$ is made nonlinear and monotonically increasing. For the case of a binary discrete range $(-1, +1)$, the transfer function is a simple step function:

$$\Xi(\lambda j) = \text{sgn}\ (\lambda_{ij} - a_{ij})\ ,$$

where a_{ij} is the threshold parameter for unit j.

For continuous valued neurons, the practice is to use the sigmoidal function,

$$\Xi(\lambda_{ij}) = \tanh(\beta\lambda_{ij})\ ,$$

in the range $[-1, +1]$. For [0,1], the corresponding function is

$$\Xi(\lambda_{ij}) = [1 + \exp(-2\beta\lambda_{ij})]^{-1}\ .$$

This last function is normally used for the stochastic case.

5.5 NETWORK PARADIGMS OF USE

Although the mathematical model presented is simple in nature, it captures the essence of the functional relationships that exist in most artificial neural networks. What varies is the net's morphological structure and the dynamics employed in the learning process. Table 5.1 lists some of the more well known nets that are in use today [for a review of neural nets, see Lippman (1988)].

Table 5.1. Some network paradigms of use

Hopfield	Kohonen's feature map (self-organizing)
Back-propagation	Bidirectional associative memory
Counter propagation	Adaptive resonance theory (ART)
N-tuples	Neuromorphic with terminal attractor
Sparse distributed memory	

Each net has its own unique properties that make it suitable for select classes of problems, but this uniqueness does not come without a cost. As an example, Kohonen's Feature Map is used to associate input vectors (patterns) with output class structures. This

map is an unsupervised learning technique that, once trained, will produce excitation levels in each output neuron; the neuron with the maximum excitation level represents the class.

The uniqueness of reasoning is developed around formulating a point distribution about the input data. If the input vectors (data patterns) are orthogonal to each other, the net will converge and be able to distinguish class structures. As the input vectors become colinear (the inner product of two patterns: $\langle \mathbf{A}^*\mathbf{B} \rangle = |A||B|$), the ability of the net to distinguish and classify input patterns degrades to a point where class features are indistinguishable to the net. In terms of *Kanerva's* Sparse Distributed Memory (associative memory), the input patterns must be h-separable in the vector space (i.e., $\forall$ vectors $\mathbf{x}_i, \mathbf{x}_j \in S \; \exists \; h$ such that $|\mathbf{x}_i - \mathbf{x}_j| \geq h$). Similar to Kohonen's Feature Map, if this requirement is not met, the net's ability to discriminate class structures in the input data is not definite. Other nets experience problems of convergence, memory and storage capacity, speed of operation, data preprocessing requirements, and data formatting requirements (i.e., integer, real, binary, normalization).

The data structures of the simulator sickness model require the net to be able to store large numbers of input data patterns (x-, y-, z-axes; f_{cf} = 0.097, 0.147, 0.198, 0.247; syllabus lengths of 72 min); use real, binary, and integer data constructs in the formulation; and provide an associative mapping of input data to predefined output classes. The network that best supports these criteria is the N-tuple. In the following section, the network is described in some detail to provide a fundamental understanding of its structure.

5.6 N-TUPLE NETWORK

The N-tuple network can be thought of as a binary mapping of images onto a retina and the subsequent development of discriminators (N-tuples) for pattern recognition (see Fig. 5.3) and feature extraction. In this formulation, an image is projected onto a planar retina that has been subdivided into K (= $n \times m$) cells, C (i.e., a matrix of cellular entities addressed by ij). Each cell, C_{ij}, will be in one of two (binary) states—on or off—which assumes that no representation for gray-scaling is enforced. In the on state, the cell will have a value of 1; in the off state, the cell will have a value of 0. These states correspond with the presence or absence of an active image projected onto the pixel respectively. Each cell is then randomly grouped into one of the N-tuple configurations. These configurations are the discriminators of the network and can have 2^N states represented by the decimal equivalent of the binary number projected by the on/off states of the associated cells. As a pattern is mapped onto the retina, the state of each discriminator is recorded and correlated in a memory matrix with the particular pattern representing its experience. Patterns of the same class are learned by or-ing the active cell states (on/off states in the ij space) in the memory matrix. As different patterns are presented and learned, a formal structure for each experience is reflected in the memory matrix. The synthesis capability of the network results not only from those correlated features developed in the N-tuple from similar patterns but also from the fact that there will also be forbidden states not addressed by each particular experience. This feature provides the discrimination needed to learn particular features of each pattern presented and then be able to discriminate between and classify presented unknown patterns.

Classification proceeds along the lines of highest correlation wins. As an unknown pattern is presented, it is translated into the N-tuple discriminator space and compared with existing class-feature constructs that exist in the memory matrix (inner product of the

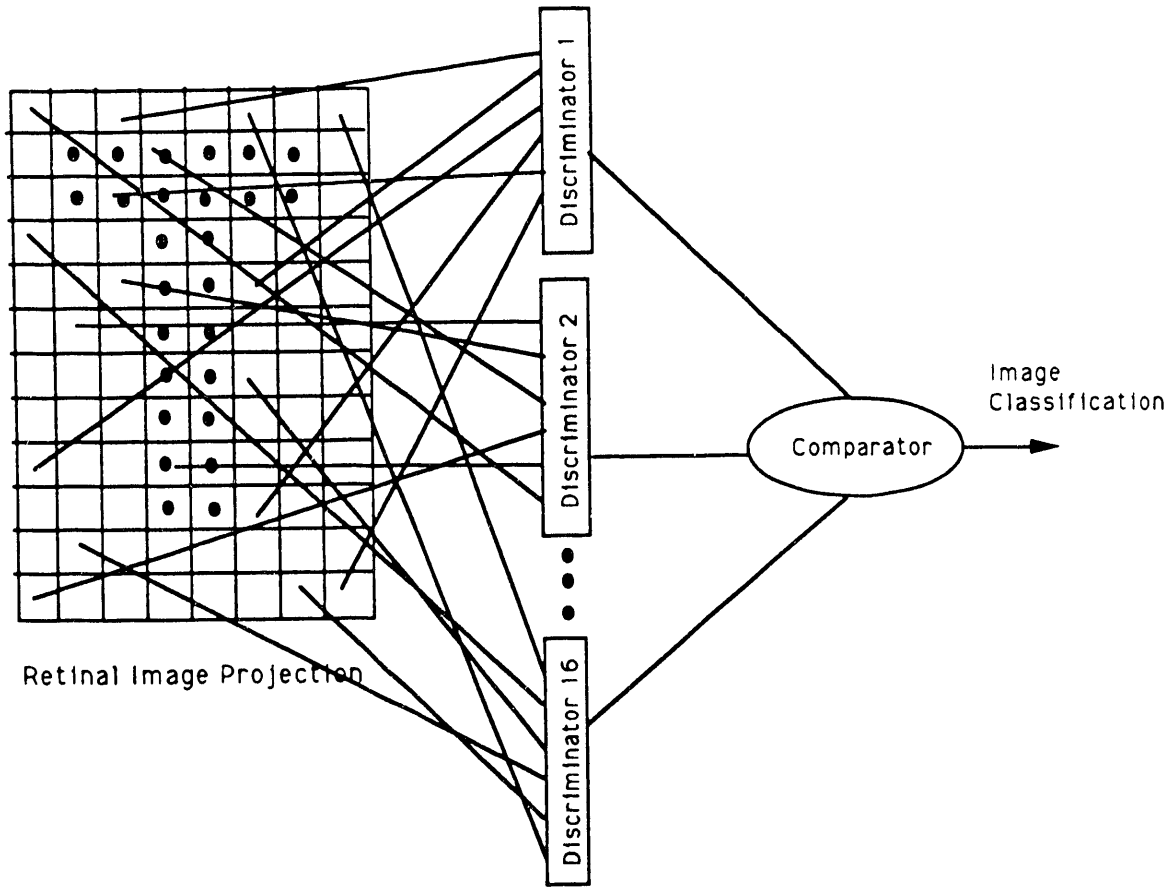

Fig. 5.3. Retinal projection of block T for N-tuple discriminator on 8 × 12 retina.

unknown image vector and the memory feature space vector). The results are stored and then compared to find the highest inner product value. The pattern (or image) is then said to possess, or correlate with, the features of the learned class with the highest score. Ties are abritarily broken.

The following is a mathematical formulation of the preceding argument.

A window of dimension

$$P \text{ (pixels)} = a \times b$$

is defined in an arbitrary picture space.

The pixel elements of the P-window are labeled as matrix entries defined by the subscripted variables ij in the **E** matrix:

$$\mathbf{E} = \{ \begin{matrix} e_{11}, & e_{12}, & \ldots, & e_{1b} \\ e_{21}, & e_{22}, & \ldots, & e_{2b} \\ \ldots & \ldots & \ldots & \ldots \\ e_{a1}, & e_{a2}, & \ldots, & e_{ab} \end{matrix} \} .$$

These elements, e_{ab}, are then grouped in K_d, N-dimensional vectors representing the N-tuple discriminators. Defining the parameter K is an arbitrary decision as well as the

element grouping N (usually randomly chosen). The K_d N-tuples can have 2^{NB} states, where B is the number of bits per pixel. Each state is then characterized by the total bit pattern of the group of N pixels. (In this formulation B will be equal to one, giving the total number of states that any particular K_d discriminator can be as equal to 2^N).

Two types of N-tuple samplings can exist: a *one-to-one* and a cover set. In one-to-one sampling, the selected N pixels are randomly chosen yet are unique to a particular K_d discriminator. In this case, exactly P/N N-tuple discriminators are in the scanned window. The second sampling is a cover set, where the N pixels are again randomly chosen but can be members of several discriminators. In this instance, G which represents the number of N-tuple discriminators in the scanned window can be greater than P/N (i.e., $G \geq P/N$).

For the following formulation, a *one-to-one* structure is adopted. A training pattern,

$$\mathbf{E}^j t = \{ e^{j11}, e^{j12}, \ldots \\ \ldots \\ e^{ja1}, \ldots, e^{jab} \},$$

a part of the training set

$$\mathbf{E}_t = \{ \mathbf{E}^1_t, \mathbf{E}^2_t, \mathbf{E}^3_t, \ldots, \mathbf{E}^T_t \},$$

is applied to the N-tuple. Each $\mathbf{E}^j_t$ will represent a state, $\mathbf{S}^K_t$, for each of the K_d N-tuples. Therefore, each $\mathbf{E}^j_t$ will have a discriminator state space, $\mathbf{S}^{Ejt}$, defined as

$$\mathbf{S}^{Ejt} = \{ \mathbf{S}^1_t, \mathbf{S}^2_t, \ldots, \mathbf{S}^{Kd}_t \},$$

where the superscript variables are correlated one-to-one in a unique matching with the defined N-tuples and the elements $\mathbf{S}^i_t$ are vectors themselves.

When testing with an unknown pattern, $\mathbf{U}^j_t$, a discriminator state vector, $\mathbf{S}^{Ujt}$, is developed for the unknown pattern. From this, a response vector, $<\mathbf{Z}^{Ujt}>_k$, defined as a vector product space unique for each $\mathbf{E}_{jt}$, is derived by performing inner products on each element of the $\{[\mathbf{S}^{Ejt} * \mathbf{S}^{Ujt}]\}$. The response vectors will span the training set (i.e., k = T). The cardinality of $<\mathbf{Z}^{Ujt}>_k$, $I\mathbf{Z}^{Uk}I$, is called the response of the window to the unknown pattern $\mathbf{U}^j_t$. The unknown pattern will be associated with the training pattern, $\mathbf{E}^j_t$, giving the largest cardinality.

This formulation is a simple—yet effective—mechanism by which feature extraction and data compression can be performed over a large operational space, incurring no penalties that are inherent in many of the other neural net structures (e.g., saturation, convergence). As can be expected, drawbacks exist. Memory requirements can have an exponential growth as the number of N-tuple/states and patterns increase. Storage of real numbers, as opposed to integers, can also create memory resource problems. Finally, a formal methodology must be constructed for mapping domain-specific data onto the retina. Even with these restrictions and limitations, this network offers the best solution for mapping the complex operational space of simulator sickness onto a usable structure.

6. DEVELOPMENT ISSUES FOR THE N-TUPLE NETWORK

6.1 INTRODUCTION

In the development of the Simulator Sickness Paradigm, several issues were associated with the structure of the N-tuple network. Some examples are data scaling and sensitivity and memory requirements for class development. This chapter outlines these issues and the approach to resolve them. These solutions can be thought of as generalizations that can be applied in the development of N-tuple networks.

6.2 RETINAL MAPPING: TEMPORAL, SPATIAL, AND SPECTRAL ARGUMENTS

The strength of the N-tuple network is in its ability to map complete histories (time in this case) of variables considered to be causal factors in a process and correlate them for feature extraction. For the Simulator Sickness Paradigm, this required capturing the human-system interaction dynamics (Whole Body Energy Absorption Model) and associative/nonassociative behavioral patterns of the user community. The interaction dynamics required mapping four discrete frequencies for each of three linear acceleration axes (x-, y-, and z-axes), and the behavioral required mapping 14 variables and the 12 energy contributions from the previous run's dynamics. Figures 6.1–6.3 (x-, y-, z-axes, respectively, mapping 0.97, 0.147, 0.197, and 0.244 Hz vertically) show this retinal projection for the dynamics of the 18th hop occurring on the third day of testing.

It is obvious from this projection that one of the first issues to be dealt with is determining the size and extent of the retinal plane. The breadth (y-axis projection) of the planar image was set by the length of the data records representing the temporal extent of each hop. In this case, 242 maximum points for the longest run (72-min hop) compressed down from approximately 250K. This parameter is not a limiting factor in the design for most computer applications but must be considered in the trade-off of the complete projection versus memory and CPU requirements for hardware implementations. Another horizontal-axis design parameter is the full extent or replication of records—that is, should each run be represented as a full 242 points? One answer to this question is to extend the data record to full extent by splicing the last 242-n (where n is the total number of temporal points for a particular hop) temporal data points of the record onto itself. Intuitively, this would give the same topological weighting in the y-axis for all hops (images). The other answer is a one-for-one mapping of the image onto the N-tuple—that is, the extent of the image is based on the length of the actual simulator flight. For this research, the latter was chosen. It was done so to support one of the main premises of this research: that it is just as important to know the temporal extent of the hop as it is to know the energy contributions at any instance of time. Figure 6.4 (x-axis temporal/spectral dynamics) is the planar projection of run 4R27 used in this research, representing a 43-min hop. As can be seen, the projection maps only the temporal extent of the time period itself. If, as stated earlier, the model is sensitive to temporal extent and variation, then the paradigm should extract essential features of the run and predict the extent and level of simulator sickness in the user population.

The depth of the network is functionally related to the number of data records and the resolution (or sensitivity) required. One of the interesting aspects of the N-tuple

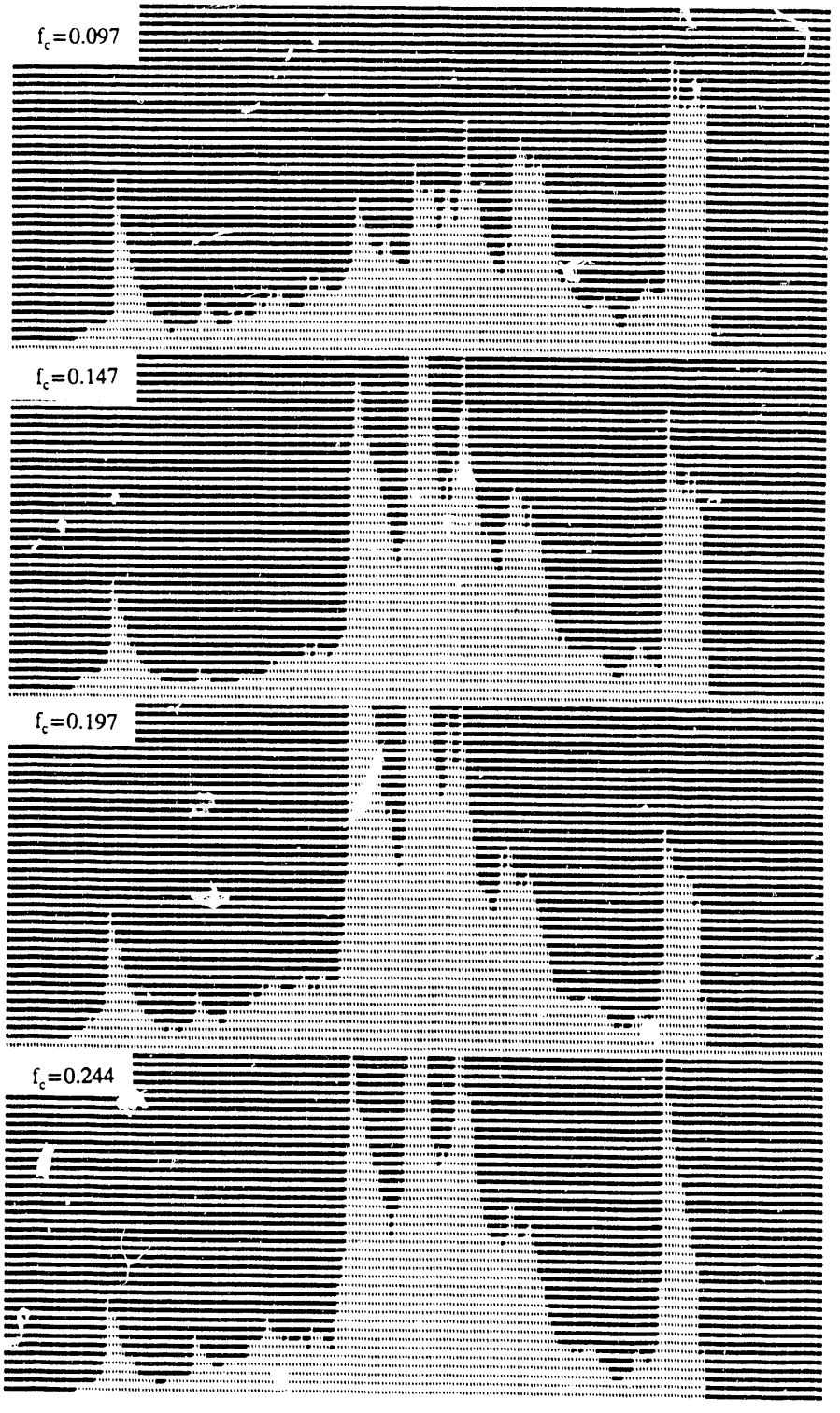

Fig. 6.1. The x-axis whole-body energy absorption model retinal map—hop 3R18.

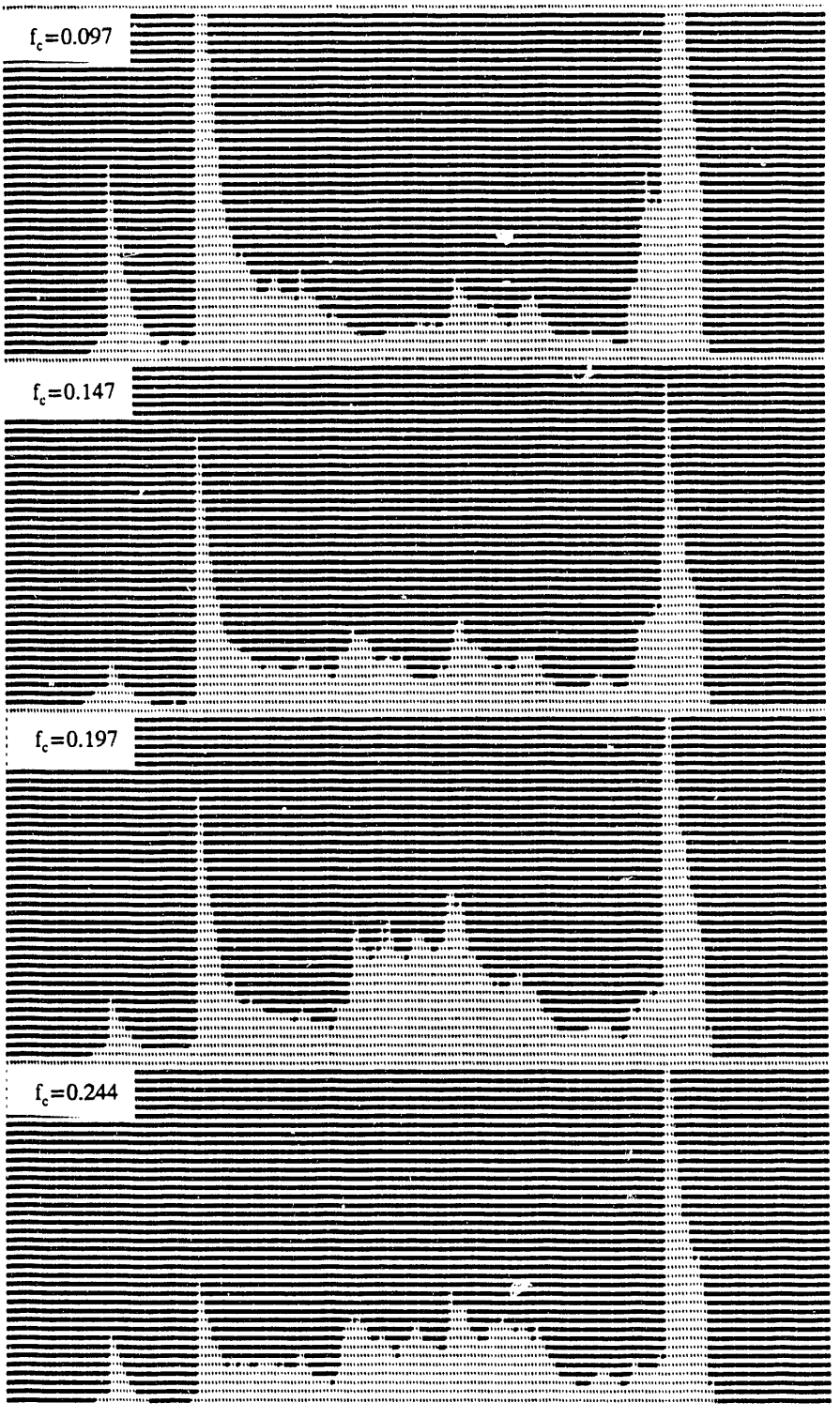

Fig. 6.2. The y-axis whole-body energy absorption model retinal map—hop 3R18.

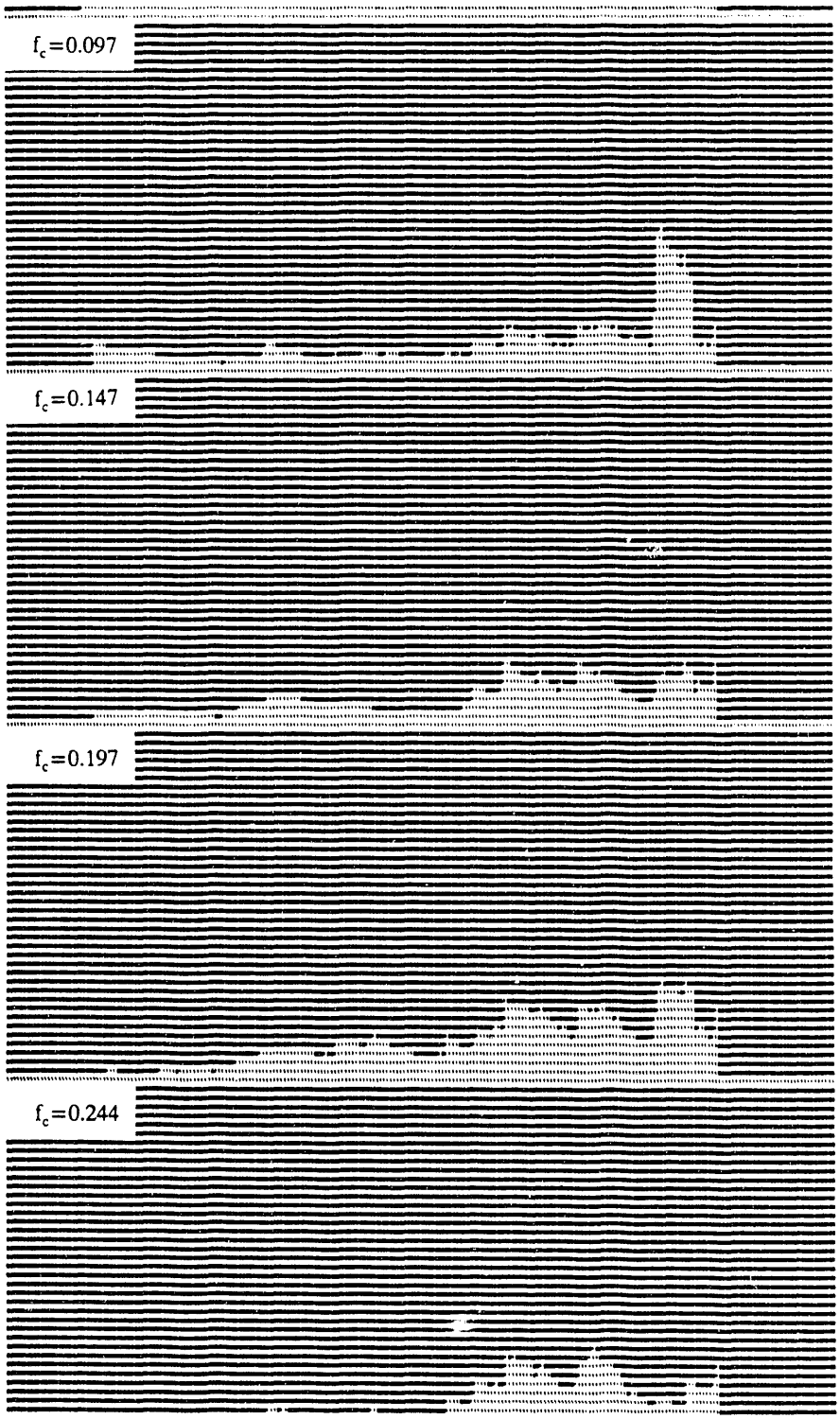

Fig. 6.3. The z-axis whole-body energy absorption model retinal map—hop 3R18.

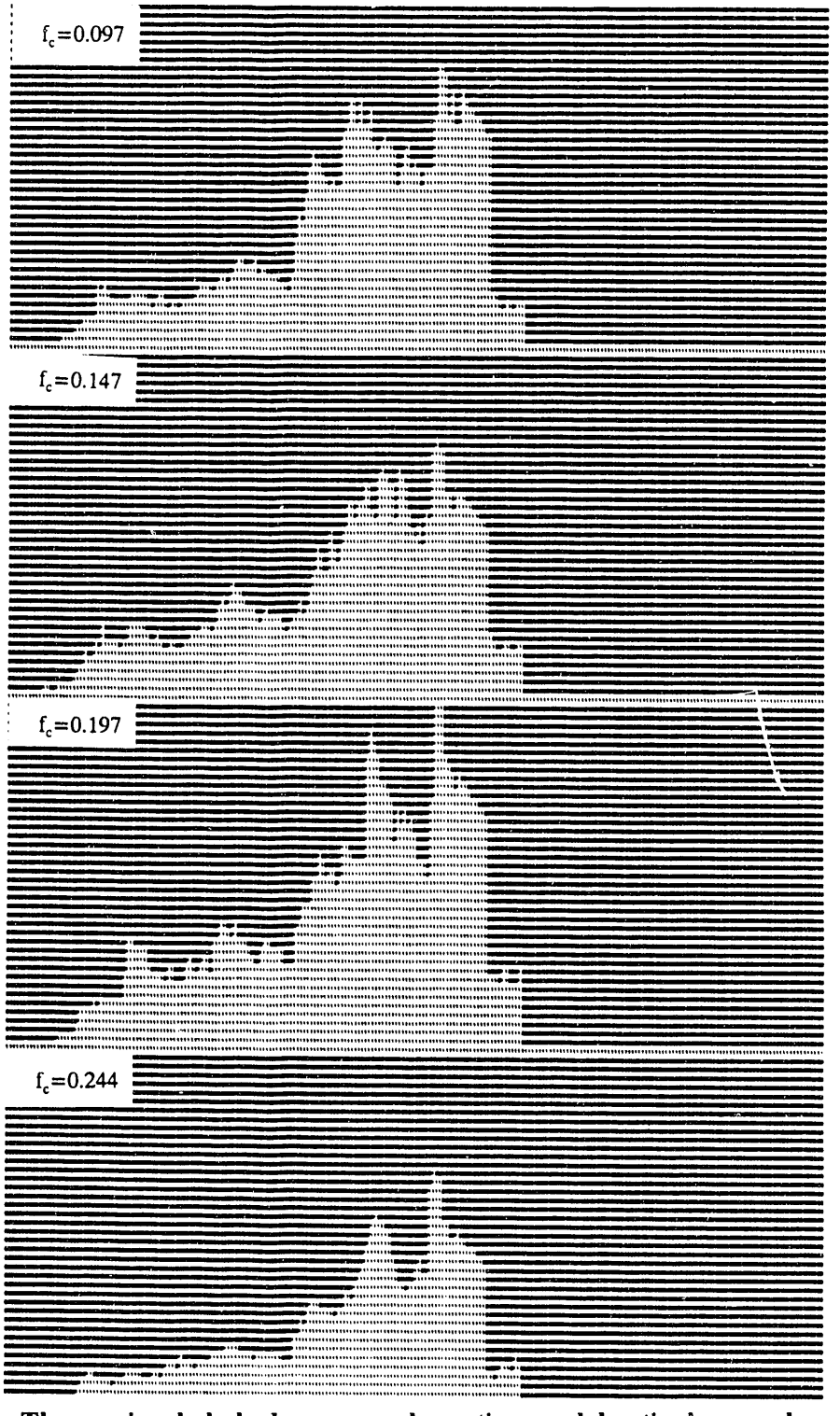

Fig. 6.4. The x-axis whole-body energy absorption model retinal map—hop 4R27.

formulation is that each time record (history) can be dealt with on an individual basis without introducing any artificial biases in the prediction capability. Each record can be scaled differently without impacting the ability of the network to capture and extract image features important to classification (relative variations as opposed to absolute). This overcomes problems associated with mathematical formulations that would be artificially sensitized to scaling variations of data or information. This a particular problem with many neural nets whose synaptic strengths, influenced by scale, represent the distributed knowledge.

For the predictor network, the y- and z-axes were normalized to a unit value equal to the x-axis dispersion. This equated to a scale factor of 7.5 for the y-axis and 140 for the z-axis. As seen, the z-axis acceleration was an order of magnitude down from the other two. Yet, with variable scaling capabilities, the change or variation in the z-axis, which is important for prediction, was facilitated. With the above reasoning and using perceptual variance as a performance measure, a depth of 480 pixels was chosen for this network. It should be mentioned that saturation of the net can occur if each image map projects fully onto the retina (see Fig. 6.5). In this case, no separability of classes exists and, therefore, no feature selection or discrimination capabilities. Therefore, image-variance on the retina is an important parameter for the network structure.

6.3 DISCRIMINATOR ATTRIBUTES

Defining the size of the discriminator(s) (see Chap. 5) is of particular importance when considering a hardware implementation of the net. The choice is impacted by the number of classes; size of retina; states (selectivity) allowed for each discriminator; and in this case, the structure of any parallel net. This is not a concern for most N-tuple formulations when using laboratory or office computer resources because capability is usually bounded by storage and memory. (Time is intentionally left out as an argument since it represents a subjective evaluation relative to the user and system being used.)

For this paradigm, 25 discriminators were constructed. This number was chosen primarily because it allowed an equal distribution or weighting of state projections between the parallel, interactive-dynamic and behavioral networks. Thus, for the dynamic network, each discriminator has 2^{4608} (115.2K pixel projection/25, N = 4608) possible states that it can represent; for the behavioral map, 2^{104} (2.6K pixel projection/25, N = 104).

6.4 CLASS MEMBERSHIP DEVELOPMENT

To facilitate the large storage requirements for each network and its respective discriminators, each class descriptor for each parallel network was developed by using a binary-vector image map. Each image was a similarity (position sensitive) map produced by storing in retinal position *ij*, the number of times that particular position was identified as significant by the members of the class set. With this structure, training and learning occurred by the application of an exclusive-or function to each retinal element of any image that belonged to a particular class and then inclusion of the similarity attribute. By formulating the network in this manner, a weighted similarity could be included in the analysis.

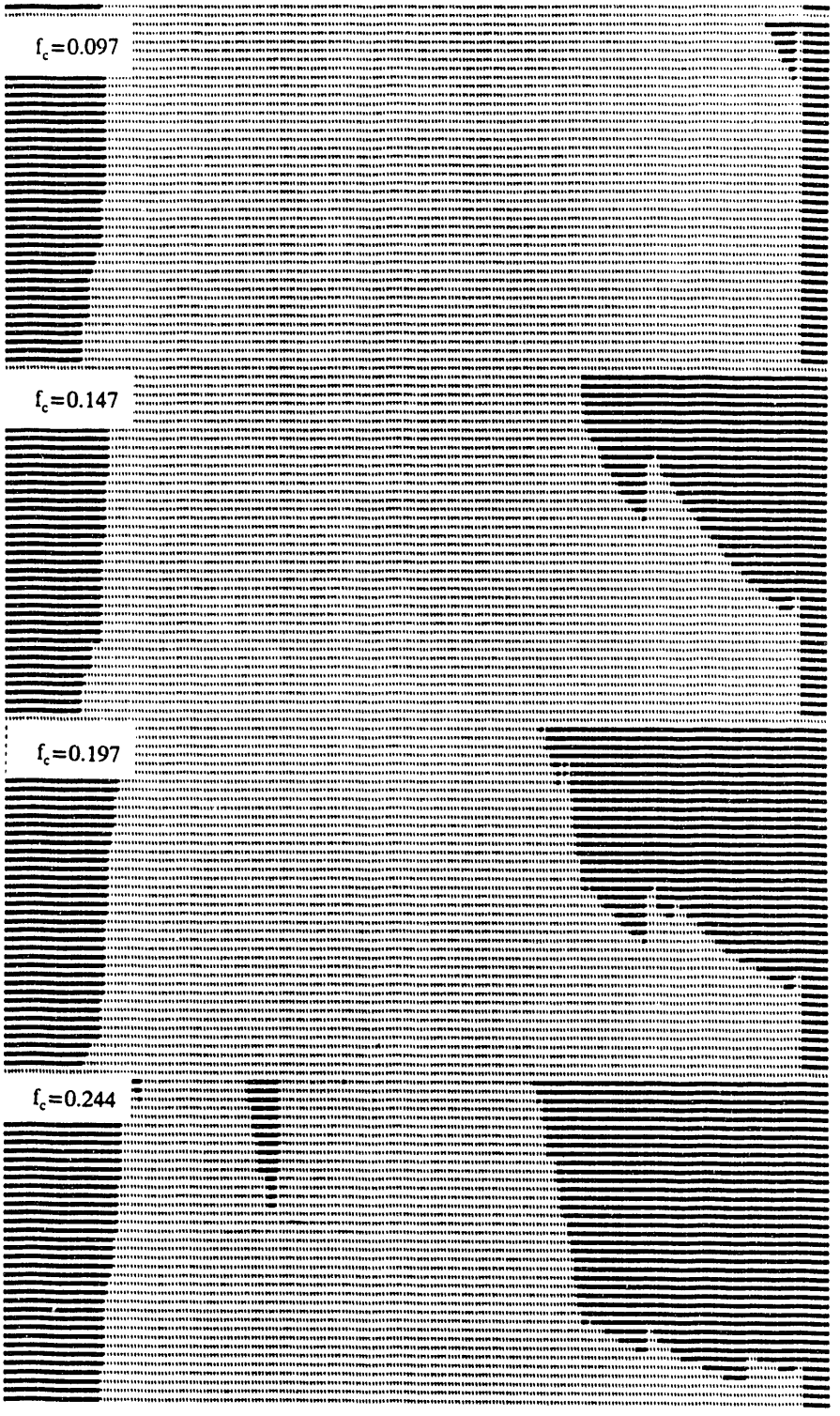

Fig. 6.5. The y-axis whole-body energy absorption model retinal map—hop 1R1.

The universal set (S) of class members consists of 20 simulator flights distributed across 3.125 usage days (8 hops per day, 72 min per hop) and 16 student pilots. Class distinctions were determined by the postsymptomatology scores (Kennedy) for each hop. A post score is computed from a battery of tests administered to check for motor skills and functional mental impairments as a result of the hop. The scores range in value from 0 (no impairment/no functional loss) to 5 (serious impairment). This is a logarithmic scale, so larger values are indicative of serious physical problems. Figure 6.6 shows the frequency distribution of symptomatology for each post score class. These scores were further broken down into specific symptomatology (nausea, visual-motor, and disorientation).
Figures 6.7–6.9 depict the individual attribute scores by hop number for days 1, 2, and 3 respectively. Above each triplet is the logarithmic scale, in parentheses, corresponding to the integer class structure. Figure 6.10 shows the total composite score for each day and each hop.

Given the limited number of members in the data set, integer representations for classes were chosen. Within this, only 1 through 4 were developed—for several reasons. First, having two members from each of the four classes representing available information uses eight members of the set S (40% of the available information). This is sufficient for cover and provides enough unknown cases to test the predictor's capabilities. Second, to use the symptomatology attributes would use most, if not all, the data sets in developing the class structures themselves, leaving an insufficient number to test. Third, by excluding the extreme points (cases 0 and 5), the predictor's capability to extrapolate would be functionally tested, providing a figure of merit for classification.

The classification networks were developed by using the reasoning set forth in the above text. The results are presented in Chap. 7.

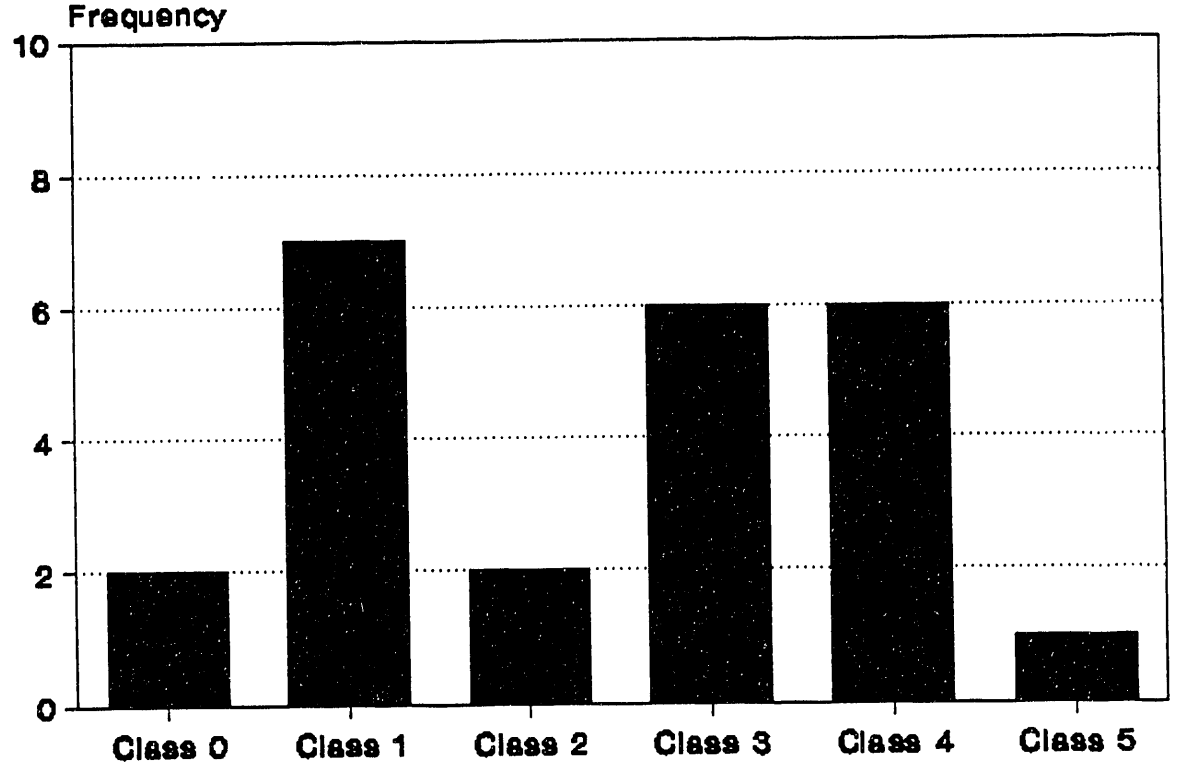

Fig. 6.6. Class membership vs frequency for differential score across all hops.

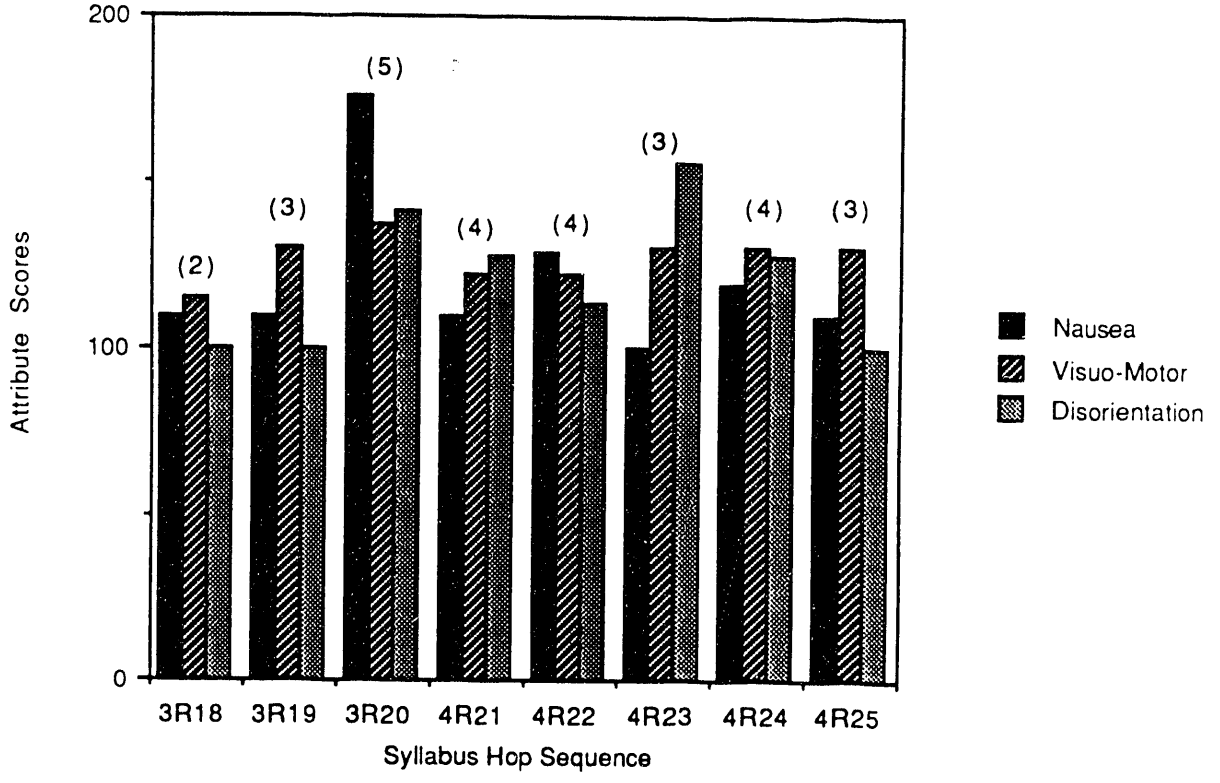

Fig. 6.7. Attribute scores by symptoms by hop number—day one.

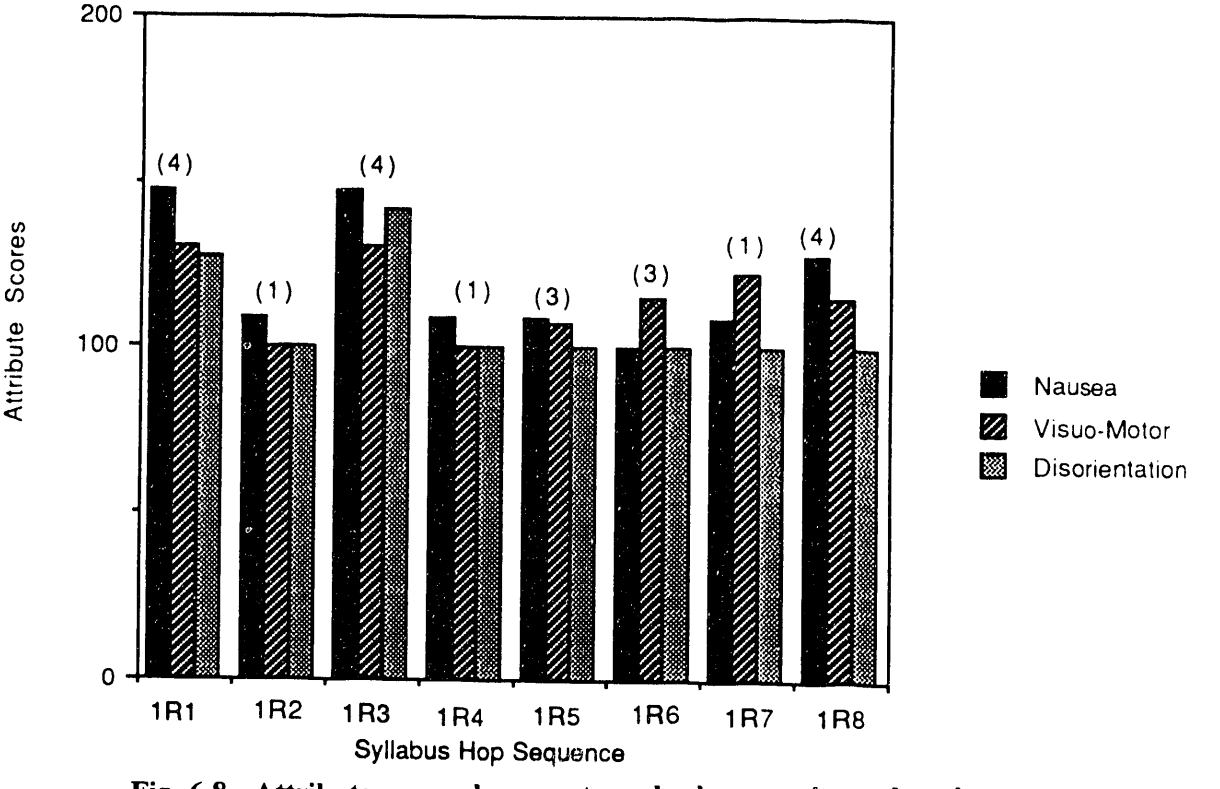

Fig. 6.8. Attribute scores by symptoms by hop number—day three.

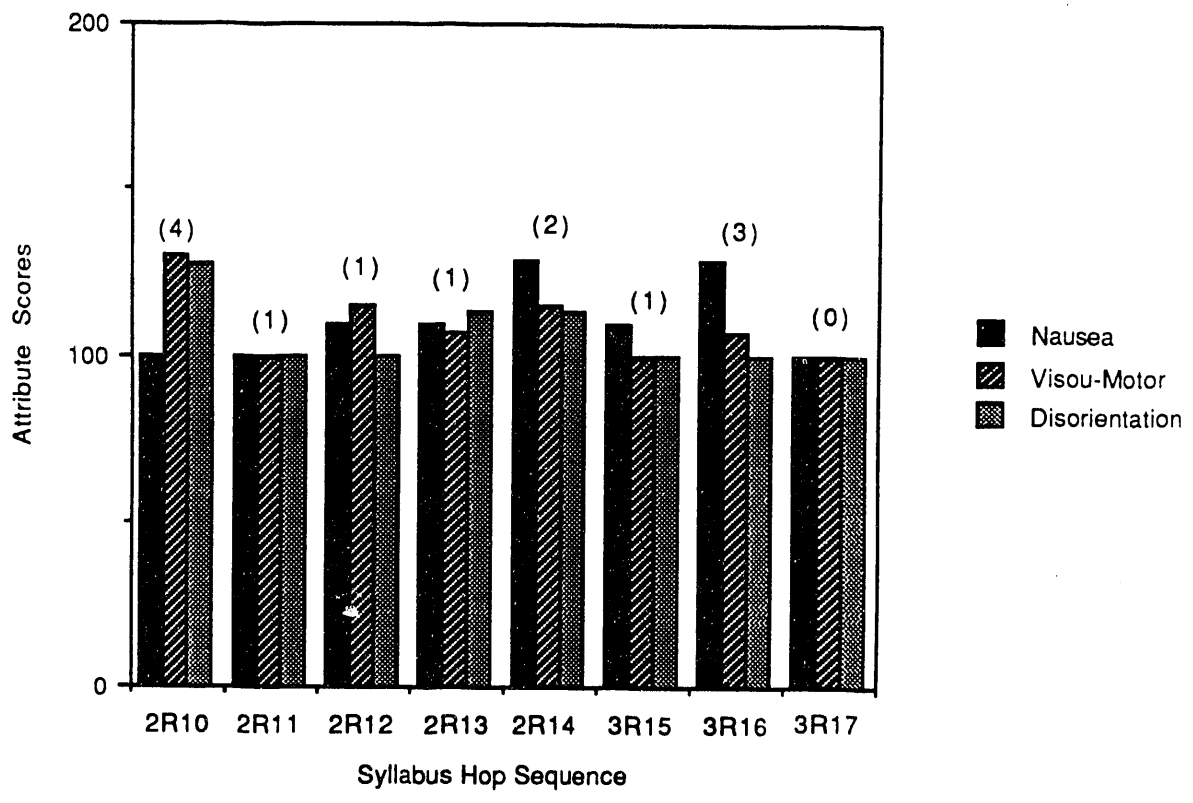

Fig. 6.9. Attribute scores by symptoms by hop number—day two.

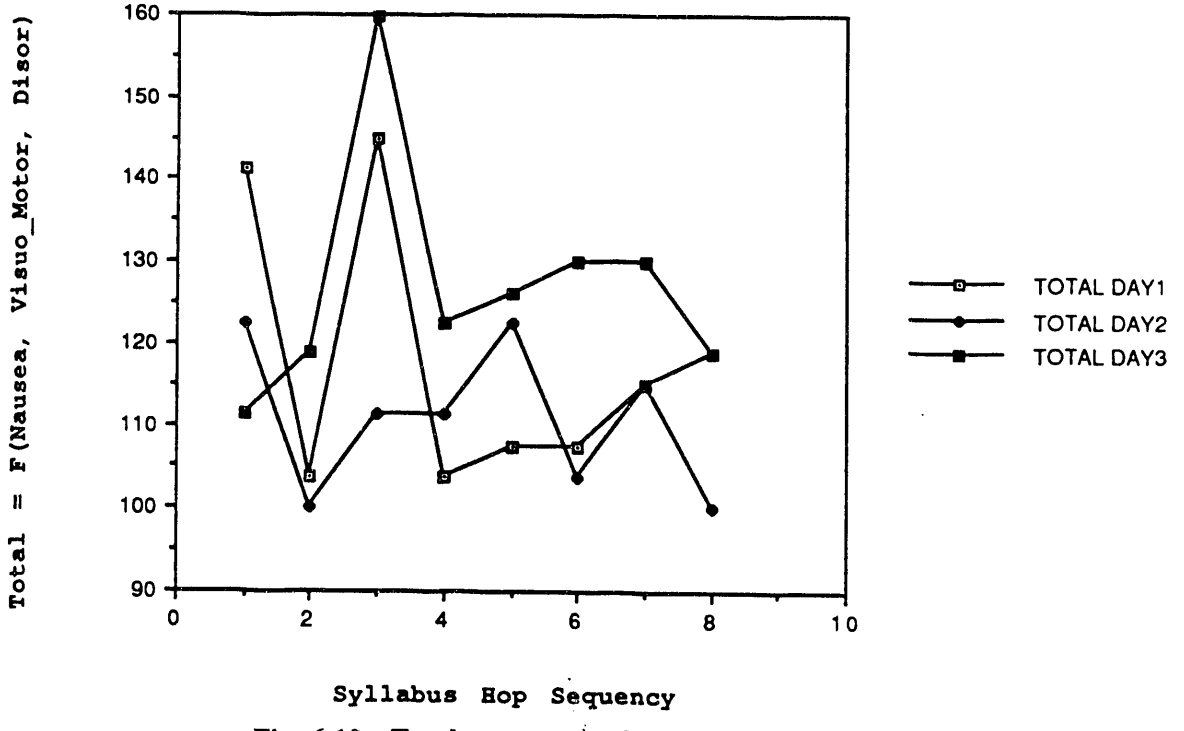

Fig. 6.10. Total symptomatology scores each day.

7. THE N-TUPLE'S PREDICTIVE CAPABILITIES: RESULTS AND CONCLUSIONS

7.1 INTRODUCTION

When the capability of a model or any analytic structure to act as a stable predictor is assessed, a figure of merit must be defined which integrates the relevant aspects of the phenomenon with a functional accountability of interactive parameters that are relevant to the process. In light of this, the performance measure must provide, through qualitative and/or quantitative reasoning, descriptors that can be equally applied to decisions under uncertainty as well as crisp data sets. Along with this provision must come a developing knowledge base for understanding incorrect classifications and the extrapolation of such to enhanced formulations. These requirements, therefore, establish certain functional criteria that must be met by the analytic formulation. These criteria are developed from the broad spectrum of system interactive correlates and are defined for the phenomenon itself, the analytic structure employed, and the available data from which the knowledge of the system is formulated.

When the phenomenon is considered, complexity is the main issue. The resulting criterion, therefore, is one of developing applied (reasonable) expectations. If the phenomenon is a highly complex intercorrelated process and the research represents the initial efforts, then objective measures will not suffice in adequately describing the paradigm's effectiveness in classifying unknown patterns. In this instance, a subjective qualifier is also needed. This qualifier is context dependent on the application and the phenomenon being described. Objective measures may be the number of correct or incorrect classifications or some functional entity tied to these variables. A subjective parameter would be a threshold percentage above which the paradigm's ability to classify would be considered successful. Considering the complexity of simulator sickness and the highly interactive environment in which it exists, a 70% or greater probability of classification would be indicative of the strength of the approach. Conceptually speaking, this subjective evaluation would also account for the extension of results to the next generation predictor.

For the analytic structure, the criterion is one of determining performance measures that are stable across all events. These parameters are functionally related to the model and should possess a formal logic and reasoning as well as intuition that integrate into a mathematically tractable formulation. The associated N-tuple variables will be identified and completely described in the following section.

The data (members of the universal set) will impact the size of the allowable training set and thus the descriptors for each class structure. The resulting criterion will therefore be one of reasonableness in the face of diminishing resources (ensemble class members). This reasonableness is a very subjective parameter that relates numbers of ensemble (class data sets) members available with expectations for classification. As stated, for this research effort, 20 data sets exist from which to develop six classes of symptomatology levels: 0, 1, 2, 3, 4, and 5. Table 7.1 identifies the criterion for each level of simulator sickness, with Table 7.2 providing a further refinement. It should be noted that eight levels are identified for complete scoring, but only six were experienced in the pilot group. If two member data sets were used for each class, exactly one-half of the available data would be used in the model structure. This small amount of data would not allow a sufficient cover set of

Table 7.1. Criteria for categorizing levels of simulator sickness

Category	Criteria
0	No symptoms reported
1	Any simulator sickness symptom reported
2	More than two other symptoms reported
3	One minor plus other symptoms reported
4	One major symptom alone or Two minor symptoms or One major and one minor symptom or One minor plus four other symptoms, of which two or more are stomach awareness, sweating, drowsiness, or pallor
5	One major and two minor symptoms
6	Two major symptoms (including subject's report of emesis)
7	Experimenter's report of emesis

Table 7.2. Diagnostic categorization

Pathognomic symptom	
Vomit	
Major symptoms	
Drowsiness	Severe
Increased salivation	Moderate and severe
Nausea	Moderate and severe
Pallor	Severe
Retch	Severe
Sweating	Severe
Minor symptoms	
Drowsiness	Moderate and slight
Increased salivation	Slight
Nausea	Slight
Pallor	Moderate and slight
Sweating	Moderate and slight
Mental symptoms (minor and other)	
Apathy	Other
Confusion	Minor
Depression	Other
Difficulty concentrating	Minor
Fullness of head	Other

Table 7.2 (continued)

Visual symptoms (minor and other)	
Blurred vision	Other
Difficulty focusing	Minor
Eye strain	Other
Visual flashbacks	Minor
Other symptoms	
Aerophagia	
Anorexia	
BM desire	
Burping	
Character facies	
Dizziness	
General fatigue	
Headaches	
Increased yawning	
Stomach awareness	
Vertigo	

unknown members to test the predictive capabilities of the network. To overcome this problem, only four classes were defined (1, 2, 3, and 4), and two members of each class set were used as defining examples. Therefore, the reasonableness of the paradigm's predictive capability will be determined by its ability to not only classify the existing known members and those unknown members of the same class but also those members associated with each extreme point (0 and 5) and the compression/expansion of each to the closest set member. In this case, 0 should map to 1, and 5 should map to 4.

7.2 N-TUPLE PERFORMANCE MEASURES

The performance measures of the N-tuple that provide stable prediction are developed from set theory. Seven such parameters exist including a signal-to-noise ratio (SNR). The following gives a descriptive analysis and mathematical formulation for each. For this analysis, the first element in each set is associated with the image to be classified and the second with the class itself.

The unknown structure/image (I_u) to be classified is a planar projection defined in terms of zeros and ones:

$$I_u = [0\backslash 1] \; . \tag{7.1}$$

The image or experience of an N-tuple class is captured in a similar form expanded to include information about the number of set members (k) used to define each class:

$$I_c = [0\backslash 1\backslash 2\backslash \ldots \backslash k] \; . \tag{7.2}$$

The noise (Bledsoe) projected by the classification of image I_u by class I_c is calculated by summing the number of doublets of the form (1, 0) or (0, 1). For this analysis, it will be defined as Dissimilar Noise and calculated as

$$E_n = \sum_{\text{instances}} [(1,0) \text{ or } (0,1) \text{ or } \ldots (0,k-1)] \tag{7.3}$$

over all instances. Another noise estimate is the set of (0, k) doublets. This noise is defined as the Orthogonal Noise (on) and is calculated by summing over each discriminator (disc) space the number of these sets that exist:

$$E_{\text{on}} = \sum_{\text{disc } k} \sum_{\text{disc } j \text{ space}} [(0,2)] \; . \tag{7.4}$$

Similarity measures will be defined over four set structures. The first, the Null Set, is the form (0, 0). This set represents the forbidden states associated with the unknown image and is calculated as the sum of these doublets over the range of the image:

$$S_{\text{null}} = \sum_{\text{image}} [\text{existing doublets of the form}(0, 0)] \ . \qquad (7.5)$$

The second similarity set, (1, k), is defined as Similarity Order_k, where once again, k is the number of members from each distinct class used in the formulation of its N-tuple image It is calculated over the image range as

$$S_{o\_k} = \sum_{\text{image}} [\text{existing doublets of the form}(1, k)] \ . \qquad (7.6)$$

The third similarity set is a combinatorial summation over the image range of all possible sets of the form [(1, 1), (1, 2), . . . , (1, k-1)]:

$$S_{o\_k\text{-}1} = \sum_{\text{image}} [\text{doublets of form}(1, 1), \ldots, (1, k-1)] \ . \qquad (7.7)$$

The sixth parameter is a weighted summation of the existing similarity sets, defined as

$$S_{\text{weighted}} = \Sigma\, k \text{ (over range of } S_{o\_k}) + \Sigma\, k\text{-}1 \text{ (over range of } S_{o\_k\text{-}1})$$

$$\text{for each set member } [1, (1 \text{ or } 2 \text{ or } \ldots k\text{-}1)] + \Sigma \text{ (over range of } S_{\text{null}}) \ . \qquad (7.8)$$

The final performance measure used in the classification analysis is an SNR computed as

$$SNR_{\text{ntuple}} = (S_{o\_k} + S_{o\_k\text{-}1} + S_{\text{null}}12)/(E_n + E_{on}) \ . \qquad (7.9)$$

These performance parameters are calculated for each of the two parallel N-tuple nets, Dynamic and Behavioral.

7.3 RESULTS

Appendixes A and B (Cases I and II respectively) represent different classification schemes employed in categorizing the 20 "unknown" test cases using the Simulator Sickness N-Tuple Classifier. For Case I, the metric used to determine class membership is the linear weighted summation over the entire similarity set for both dynamic (dyn) and behavioral (beh) nets Eq. (7.8):

$$\text{Class I}_{\text{metric}} = S_{\text{weighted\_dyn}} + S_{\text{weighted\_beh}} \ . \qquad (7.10)$$

(See Appendix C for Case I Fortran program listing.) For Class II, the metric is a nonlinear relationship in the form of a normalized power law function. The metric is calculated as

$$\text{Class II}_{\text{metric}} = (S_{\text{weighted\_dyn}}/115200 + S_{\text{weighted\_beh}}/2600)^{\log 10(SNR\text{dyn}+SNR\text{beh})} \ . \qquad (7.11)$$

The results of the classification are summarized in Table 7.3. This table lists by run the actual Differential Score, the Case I classification, the Case II classification, and whether a particular run was used in forming the image of the class. For this discussion, only Case I results will be reviewed. (Case II is presented only to provide an example of another method that could be employed in a classification scheme.)

The first thing to notice is that the Case I Classifier is 85% (17 of 20) successful at classifying the differential symptomatology scores for the runs. Classifications can be further broken down into subsets containing those elements used in the formation of each image class and those that are functionally "unknown" classes. For the image maps, Class 1 through Class 4 have a 100% success rate. The "unknown" classes have a 75% success rate. This facet will be further covered later in the section. Earlier, it was reported that only eight members (representing 40% of the universal set) were used to develop the class images for the four Symptomatology Scores. The two extreme points, Class 0 and Class 5, remained with no accountability (knowledge) in the network. The hypothesis was that if the N-tuple did indeed capture the complexity of the human-system interaction, then it could be expected that the network would map the extreme points, 0 and 5, to their closest projections, 1 and 4 respectively. As indicated in Table 7.3, two Class 0 (3R17 and 4R27) and one Class 5 (3R20) are symptomatology incidences. As shown, the N-tuple mapped those in Class 0 to Class 1 and those in Class 5 to Class 4. Finally, recall that in Chap. 6, run 4R27 (Fig. 6.4) was identified as a short (43-min) run. One of the argued performance measures of the N-tuple would be its effectiveness at classifying short-duration runs as well as those occurring over the normal time period (72 min). As shown in Table 7.3, the N-tuple was successful at classifying Run 4R27. (As mentioned, this run is a Class 0 mapped to Class 1).

As reported earlier, the error rate for the "unknown" classes is 25%, generating errors significantly correlated with Class 1 and partially with both Class 3 and Class 4. To understand how these classification errors are developed, one must understand the issues associated with the scoring of symptomatology for each run. Recall that for the class structures, a simple integer-valued scoring based on a logarithmic scaling was used; but this system could also be expanded into a triplet of symptomatology attributes—nausea, visuo-motor, and disorientation. Table 7.4 redefines the integer scoring (Kennedy/Lane) for each run in terms of its associated triplet. Comparison of attribute scores of Runs 3R19 and 4R25 (Class 3 to Class 1 error) shows that they match. But comparison with another Class 3, say 1R6, shows that not only are the triplet values inconsistent but also the total score (107.48 vs 118.70). This inconsistency in class definitions will create problems for the N-tuple as well as any other artificial neural network in the ability to correctly establish class memberships. Given that the inconsistency exists and that it provides a plausible explanation, it is of interest to investigate and compare the image maps of these three runs. Figures 7.1, 7.2, and 7.3 are the N-tuple projections for runs 3R19, 4R25, and 1R6 linear x-axis Whole Body Energy Model respectively. A visual inspection provides an interesting perspective on the N-tuple's ability to extract image information even though the definition across all events of the same nature may be convoluted. Comparing runs 3R19 and 4R25 (Figs. 7.1 and 7.2) shows similarity in the sense that peaked values occur during approximately the last one-third of the syllabus hop. In addition, the expected value would seem to be equivalent across the two events, especially the first two-thirds of the hops. Now, compare these findings with the planar map of Run 1R6 (Fig. 7.3). As is obvious, Run 1R6 presents a visual projection vastly different from those of the other two runs. It then would be expected that runs 3R19 and 4R25 project in a similar manner and Run 1R6

Table 7.3. Classification results of the simulator sickness N-tuple

Run	Differential symptomatology	Case I classification	Case II classification	Member of class image
1R1	4	4	4	Yes
1R2	1	4	4	No
1R3	4	4	1	No
1R4	1	1	1	Yes
1R6	3	3	3	Yes
1R7	1	1	1	No
R10	4	4	2	Yes
2R11	1	1	1	No
2R12	1	1	1	Yes
2R14	2	2	2	Yes
3R15	1	1	1	No
3R16	3	3	3	Yes
3R17	0	1	1	No
3R18	2	2	2	Yes
3R19	3	1	1	No
3R20	5	5	2	No
4R22	4	4	1	No
4R25	3	1	1	No
4R26	1	1	1	No
4R27	0	1	1	No
		(85%)	(70%)	

Table 7.4. Symptomatology scoring in terms of attribute triplets

		Attribute scoring			
Run	Integer	Nausea	Visuo-motor	Disorientation	Total
1R1	4	147.70	130.32	127.84	141.14
1R2	1	109.54	100.00	100.00	103.74
1R3	4	147.70	130.32	141.76	144.88
1R4	1	109.54	100.00	100.00	107.48
1R6	3	100.00	115.16	100.00	114.96
1R7	1	109.54	122.74	100.00	114.96
2R10	4	100.00	130.32	127.84	122.44
2R11	1	100.00	100.00	100.00	100.00
2R12	1	109.54	115.16	100.00	111.22
2R14	2	128.62	115.16	113.92	122.44
3R15	1	109.54	100.00	100.00	103.74
3R16	3	128.62	107.58	100.00	114.96
3R17	0	100.00	100.00	100.00	100.00
3R18	2	109.54	115.16	100.00	111.22
3R19	3	109.54	130.32	100.00	118.70
3R20	5	176.32	137.90	141.76	159.84
4R22	4	128.62	122.74	113.92	126.18
4R25	3	109.54	130.32	100.00	118.70
4R26	1	100.00	115.16	100.00	107.48
4R27	0	100.00	100.00	100.00	100.00

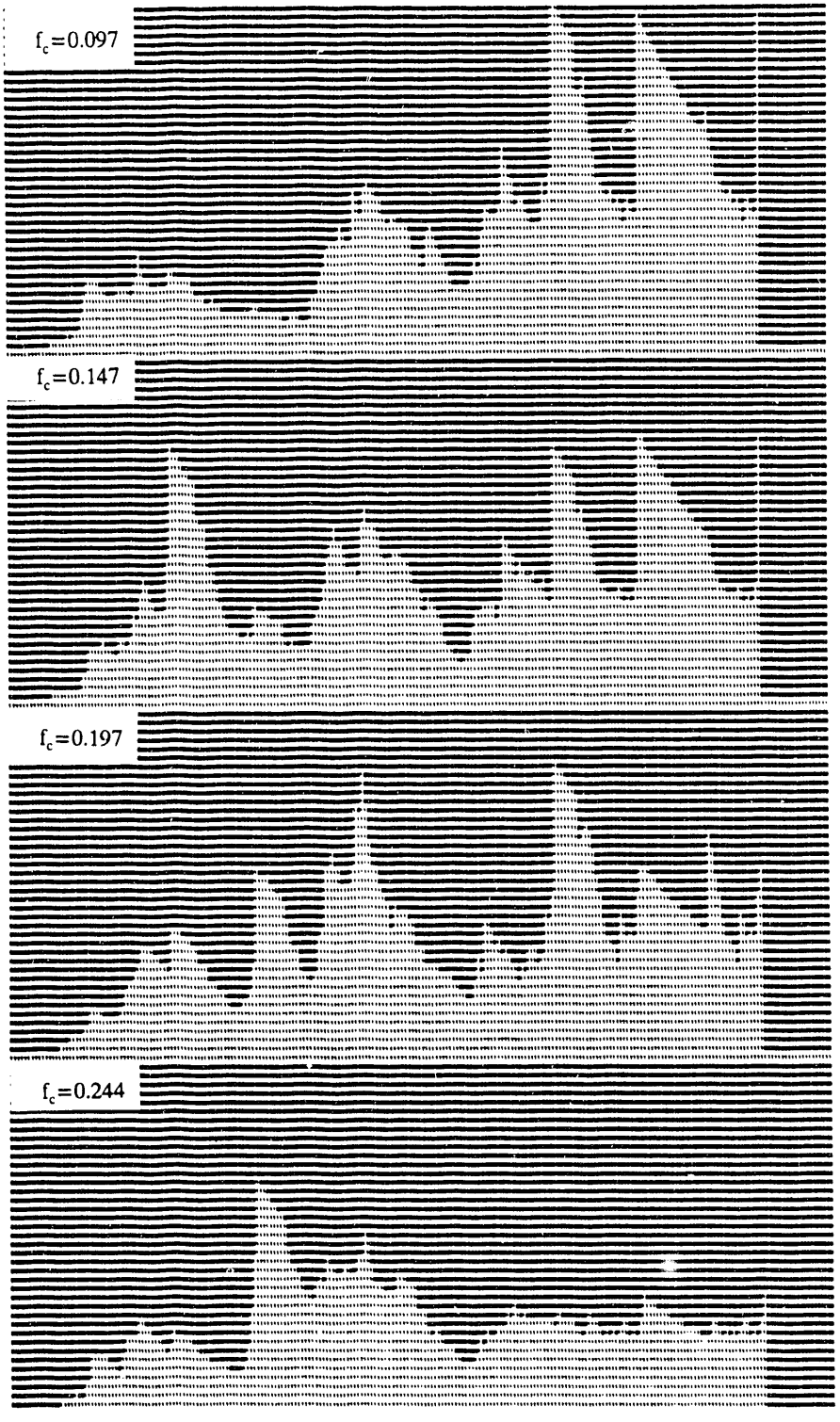

Fig. 7.1. Whole-body energy absorption model x-axis output (Run 3R19).

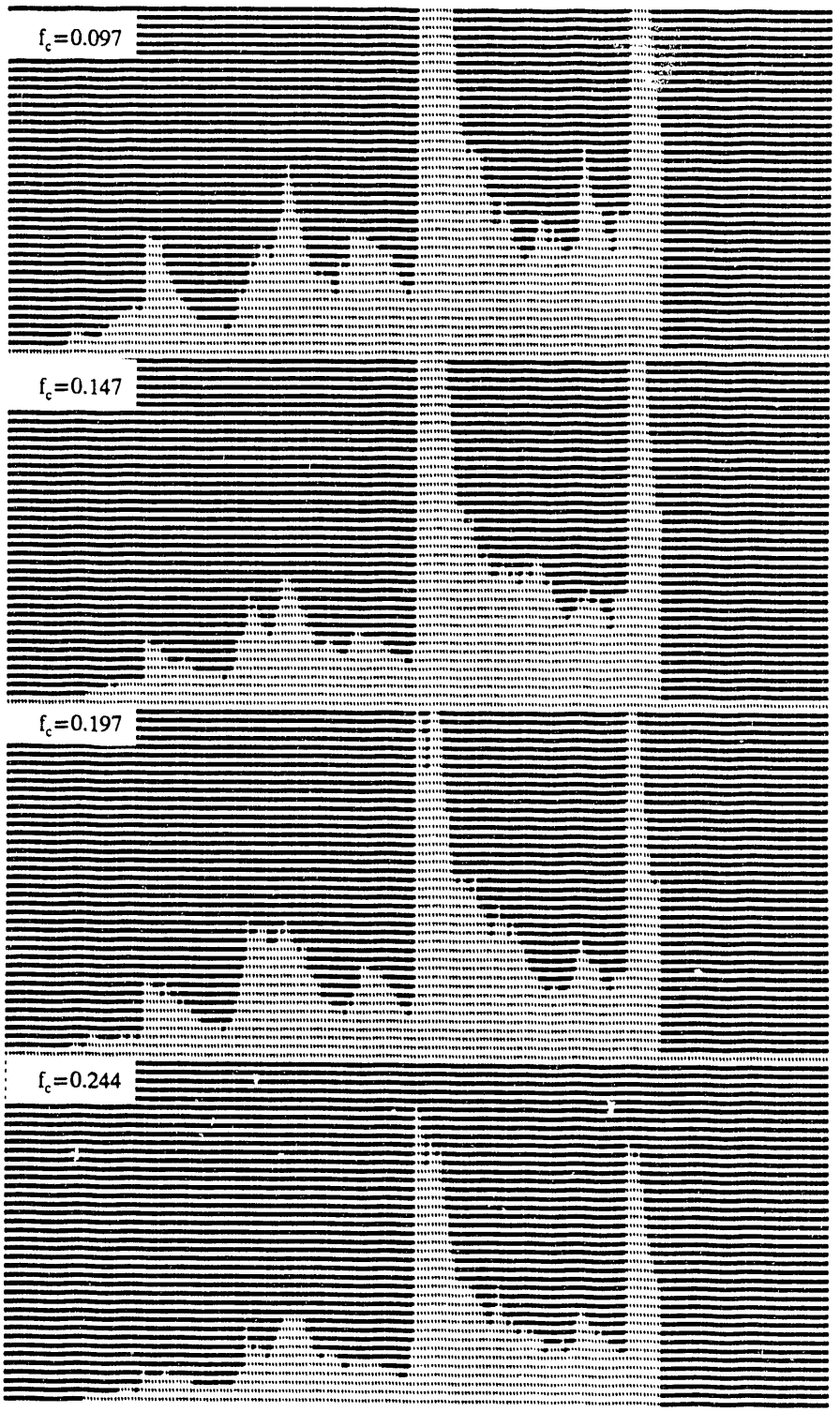

Fig. 7.2. Whole-body energy absorption model x-axis output (Run 4R25).

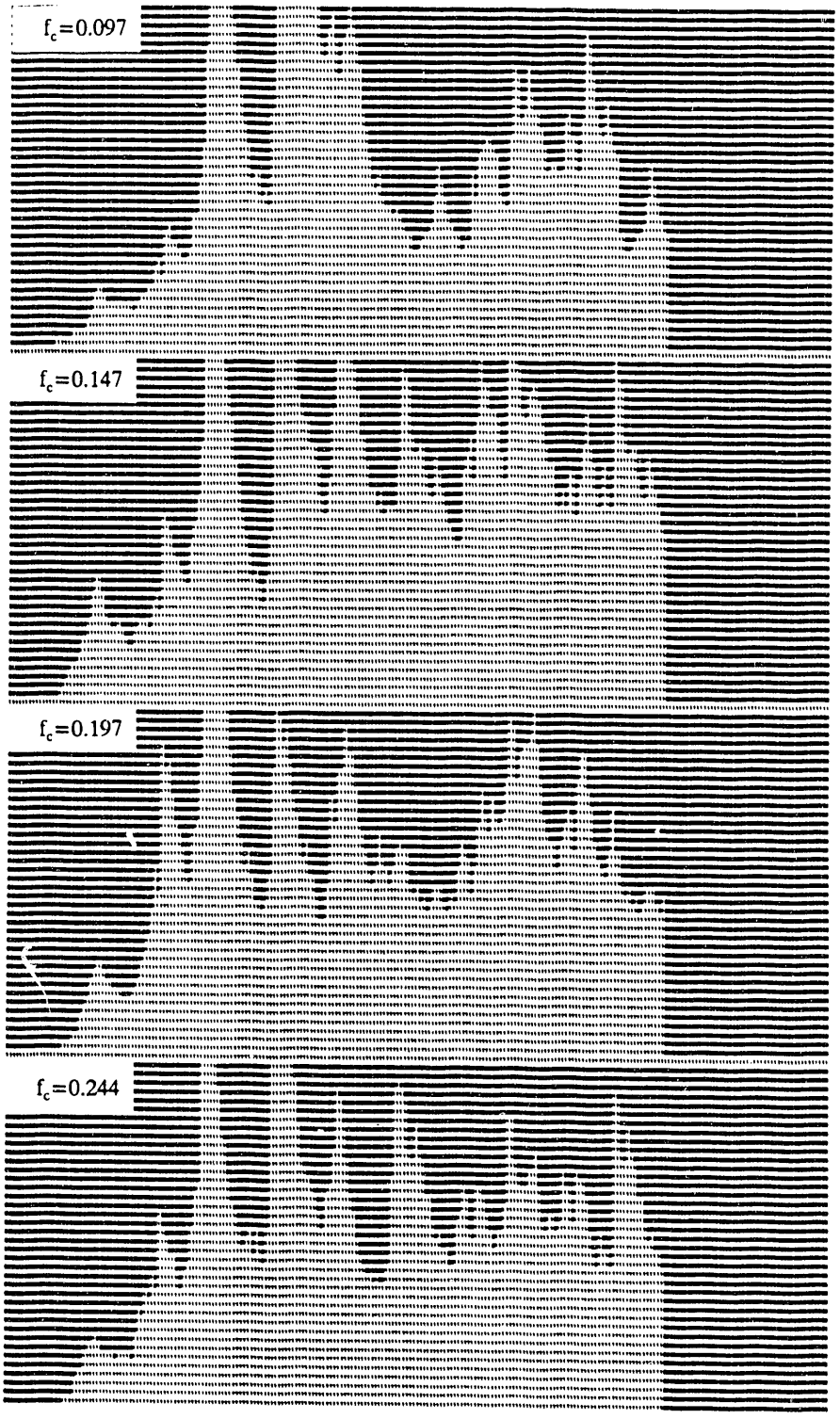

Fig. 7.3. Whole-body energy absorption model x-axis output (Run 1R6).

to be quite different. With this, it is suggested that the image map of Class 3 is captured in the similarity of runs 3R16 and 1R6 (which project as colinear maps) and not runs 3R19 and 4R25 (which are similar for the same reasons). If the convoluted nature of the existing "similar" class images could be rectified by expanding class definitions to include subsets or new classifications, then the N-tuple would converge without ambiguity. These same arguments apply to the Run 1R2 classification error (i.e., better resolution will reduce the uncertainty in the class image maps).

The results are summarized as follows.

1. The Simulator Sickness N-Tuple using Case I metrics had an 85% success rate for classification over the entire universal set. It had a 100% success rate for images used to define classes and a 75% success rate for "unknown" classes.
2. The Classifier projected the Extreme Classes 0 and 5 to Classes 1 and 4 respectively.
3. The Classifier correctly classified the Class 0, 43-min hop (Run 4R27) as Class 1.
4. The N-tuple formulation will capture the image of a class and provide a basis for (similarity/forbidden states) reliable projection. In light of this, the net could, through unsupervised learning, identify previously unknown classes.
5. Errors were explained in terms of the convoluted definitions of classes and could be resolved if more data were available.

7.4 CONCLUSIONS

The main emphasis of this research was to develop a neural net paradigm and behavioral model that would capture the interactive dynamics of the human and the simulator system and predict the level of simulator sickness in a user population. The hypothesis was that the interactive sensitivity of humans to simulator dynamics was not uniform across events and that the whole body energy occurring late in a hop would influence the incidence of simulator sickness more than early occurrences would. To facilitate this research required developing a model (Whole Body Energy Absorption Model) that characterized the temporal, spatial, and spectral interplay of the human and machine. In addition, it was necessary to develop an understanding of the neuro-physiological impacts (associative and nonassociative behavioral patterns) of simulator use and take this understanding into account in the paradigm structure. Once this was achieved, a neural network formulation had to be developed that could not only accommodate a large amount of data (data points >2900) but also correlate and feature extract in a complex hyper-space (n = 38). The success of this research is the development of the Simulator Sickness N-Tuple Predictor.

This N-tuple formulation with the Whole Body Energy Absorption Model has stable predictive powers (see the preceding Results) and provides consistent measures of similarity. This ability is shown in the discovery of the dichotomy that exists in the symptomatology class images. The network has a hardware extension that makes it ideally suited for field deployment (Boolean feature extraction) as a biofeedback monitoring device. The knowledge gained from the Whole Body Energy Absorption Model can augment the existing Military Standard 1472D to expand the concept of 0.2-Hz acceleration energy to include a narrowband, low-frequency region spanning 0.097 to 0.247 Hz. This paradigm can also be used to develop filter design parameters for the simulator system. By passing the x-, y-, and

z-axis acceleration data through predesigned filters and using this as input into the model, the N-tuple formulation can be used to predict the incidence and level of simulator sickness in the user population. With correct filter design, all events can be pushed into appropriate categories, reducing the incidence level across the user group and alleviating the need for enforced travel restrictions.

In closing, I suggest possibilities for future research using this paradigm. First, to establish this as a stable predictor, it will be necessary to apply the model to a different set of data. This new set could be from the same simulator operating under different conditions or from a simulator of different design. If the latter is chosen, then data compression may be necessary because the number of points representing the history of the flight may vary. In either case, by mapping to the same retina, the problem becomes scale and time invariant. Once stable predictability is established, a method would need to be developed to incorporate the model into existing systems at simulator sites. This would also require developing a program to supervise the maintenance of the feedback information. Another possibility is to apply the model to an expanded data base to determine whether correlations exist between the model's predictive output capabilities and the occurrence of latency and flashback. If features can be extracted, then those users who are at risk can be identified and the danger eliminated by alerting them to the problem. The possibility exists that the method needs to be expanded to incorporate angular acceleration into the model. To facilitate this, a literature search would need to be performed to determine what functional relationships exist between angular acceleration and simulator sickness. Once this has been established, a development phase would be undertaken to integrate this additional information into the predictor. Finally, the basic structure of the paradigm could be reduced by eliminating those elements that provide little or no information in the class definition. By developing a method to perform a sensitivity analysis for parameter reduction, the order of the model could be reduced.

8. REFERENCES

Allgood, G. O., et al. 1987a. "In Plant Simulator Sickness Investigation TH57C Operational Flight Trainer," Executive Summary, pp. 11-15 in Report to NAVAIRSYSCOM, Washington, D.C.

Allgood, G. O., et al. 1987b. "The Effects of Very Low Frequency Vibrations on Simulator Sickness," *58th Annual Science Meeting of the Aerospace Medical Association*, Las Vegas, May.

Allgood, G. O. 1989. Unpublished work showing functional relationships that exist between narrowband spectral energy estimates and the incidence of simulator sickness, March.

Allgood, G. O. 1991. Personal conversation with U.S. Department of Transporation representatives at the 4th Symposium on Simulator Sickness, sponsored by NASA, Naval Training Systems Center, Orlando, Fla., March 1991.

Barrett, G. V., and D. D. Nelson 1965. *Human Factors Evaluation of a Driving Simulator—Summary of Human Factors Evaluation*, Goodyear Engineering Report 12400, Goodyear Aerospace Corporation.

Barrett, G. V., and C. L. Thornton 1968. "Relationship Between Perceptual Style and Simulator Sickness," *J. App. Psychol.* **52**(4).

Bledsoe, W. W., and I. Browning 1959. "Pattern Recognition and Reading by Machine," *Proceedings of the Eastern Joint Computer Conference*, presented to the Joint IRE-AIEE-ACM Computer Conference, December 1959.

Casali, J. G. 1986. *Vehicular Simulation-Induced Sickness, Vol. I: An Overview*, NTSC TR 86-010, Naval Training Systems Center, Orlando, Fla.

Casali, J. G., and W. W. Wierwille 1980. "The Effects Of Various Design Alternatives on Moving-Base Driving Simulator Discomfort, *Hum. Factors* **22**(6).

Casto, J. H. 1982. *Simulator Sickness: Weekly Summary of Aircraft Mishaps*, U.S. Naval Safety Center, Report 38, September.

Crampton, G. H., and F. A. Young 1953. "The Differential Effect of a Rotary Visual Field on Susceptibles and Non-Susceptibles to Motion Sickness," *J. Comp. Physiol. Psychol.* **46**(6).

Dichgans, J., and T. Brandt 1973. "Optokinetic Motion Sickness as Pseudo-Coriolis Effects Induced by Moving Visual Stimuli," *Acta Oto-Laryngol.* **76**.

Dolezal, H. 1982. *Living in a World Transformed: Perceptual and Aperformatory Adaptation to Visual Distortion*, Academic Press, New York.

FITRON 124, 1981. "F-14 WST SF112/WAVS Aircrew Adjustment," U.S. Navy Message from FITRON 124 TO COMFITAEWWINGPAC, San Diego, October.

Frank, L. H. 1981. "Simulator Sickness," invited address, NASA Ames Research Center, Moffett Field, Calif., August.

Frank, L. H., J. G. Casali, and W. W. Wierwille 1987. "Effects of Visual Display and Motion System Delays on Operator Performance and Uneasiness in a Driving Simulator," *Proceedings of the Human Factors Society* 492, Santa Monica, Calif.

Hartman, B. O., and C. Hatsell 1976. *Field Study: SAAC Simulator, U.S. Air Force School of Aerospace Medicine*, Brooks Air Force Base, Tex.

Havron, M. D., and L. F. Butler 1957. *Evaluation of Training Effectiveness of the 2FH2 Helicopter Flight Trainer Research Tool*, Tech. Report NAVTRADEVCEN 1915-00-1, Naval Training Device Center, Port Washington, N.Y.

Homick, J. L. 1982. *Space Motion Sickness*, Tech. Report USC 18681, NASA Johnson Space Center, Houston.

Kellog, R. S., C. H. Castore, and R. E. Coward 1980. *Psychophysiological Effects of Training in a Full Vision Simulator*, Aerospace Medical Association, Anaheim, Calif.

Kennedy, R. S., G. O. Allgood, and M. G. Lilienthal 1989. "Simulator Sickness on Increase," AIAA Flight Simulation Technologies Conference, Boston, Aug. 14, 1989.

Kennedy, R. S., et al. 1991. *Simulator Sickness: Reaction to a Transformed Perceptual World, VI, Preliminary Site Surveys* (unpublished manuscript).

Kennedy, R. S., L. J. Hettinger, and M. G. Lilienthal 1990. *Motion and Space Sickness*, CRC Press Corp., Boca Raton, Fla.

Lestienne, F., J. Soechting, and A. Herthoz 1977. "Postural Readjustments Induced by Linear Motion of Visual Scenes," *Exp. Brain Res.* **2**.

Lilienthal, M. G., et al. 1987. "Preliminary Report on the In-Plant Evaluation of Simulator Sickness and Related Human Factors Engineering Issues in the TH57C Training Device," Technical Memo submitted to Martin Marietta Energy Systems, Inc., Oak Ridge National Laboratory, Oak Ridge, Tenn.

Lippman, R. P. 1988. "Neural Network Classifiers for Speech Recognition," *Lincoln Lab. J.* **1**, 107–24.

McCauley, M. E., and R. S. Kennedy 1976. "Recommended Human Exposure Limits For Very-Low-Frequency Vibration," Technical Publication TP-76-36, Pacific Missile Test Center, Point Mugu, Calif.

Miller, J. W., and J. E. Goodson 1958. "A Note Concerning *Motion Sickness in the 2FH2 Hover Trainer*," Report 1, Project NM 7 01 11, Subtask 3, Naval School of Aviation Medicine, Bureau of Medicine and Surgery, Pensacola, Fla.

Miller, J. W., and J. E. Goodson 1960. "Motion Sickness in a Helicopter Simulator, *Aerosp. Med.* **31**.

Money, K. E. 1980. *Flight Simulator Motion Sickness in the Aurora CP 140 FDS*, DCIEM Tech. Communication 80-C-44, Defence and Civil Institute of Environmental Medicine, Downsview, Ontario.

Parker, D. E. 1971. "A Psychophysiological Test for Motion Sickness Susceptibility," *J. Gen. Phychol.* **85** and **87**.

PM Trade 1991. *PM Trade Training Systems and Devices*, PM Trade, Orlando, Fla., Spring.

Precht, W. 1979. "Vestibular Mechanisms," *Ann. Rev. Neurosci.* **2**.

Quinlan, J. R. 1986. "Induction of Decision Trees," *Machine Learning*, Vol. 1, pp. 81-106, Kluwer Academic Publishers, Norwell, Mass.

Reason, J. T., and E. Diaz 1971. *Simulator Sickness in Passive Observers*, Report FPRC/1310, AD 753560, Flying Personal Research Committee, Ministry of Defense, London.

Rosinski, R. R. 1982. *Effect of Projected Distortions on Perception of Graphic Displays*, Tech. Report 82-1, Contract N00014-77-C-0679, University of Pittsburgh, Office of Sponsored Research, Pittsburgh.

Ryan, L. E., P. G. Scott, and R. F. Browning 1978. *The Effects of Simulator Landing Practice and the Contribution of Motion Simulation to P-3 Pilot Training*, TAEG Report 63, Training Analysis and Evaluation Group, Orlando, Fla.

Sinacori, J. B. 1967. *V/STOL Ground-Based Simulation Techniques*, USAAVLABS Tech. Report 67-55, U.S. Army Aviation Material Laboratories, Fort Eustis, Va.

Thompson, R. F. 1986. "The Neurobiology of Learning and Memory," *Articles*, pp. 941-47 (Aug. 29).

Uliano, K. C., et al. 1986. *The Effects of Asynchronous Visual Delays on Simulator Flight Performance and the Development of Simulator Sickness Symptomatology*, NAVTRASYSCEN Report 85-D-0026-1, Naval Training Systems Center, Orlando, Fla.

INTERNAL DISTRIBUTION

1–5. G. O. Allgood
6. H. R. Brashear
7. B. G. Eads
8. D. N. Fry
9. D. W. McDonald
10. D. R. Miller
11. G. N. Miller
12. R. E. Uhrig
13. J. O. Stiegler
14. K. W. Tobin
15. D. F. Craig
16–17. Central Research Library
18. Y-12 Technical Reference Section
19–20. Laboratory Records
21. Laboratory Records—Record Copy
22. ORNL Patent Section
23. I&C Division Publications Office

EXTERNAL DISTRIBUTION

24. Assistant Manager for Energy Research and Development, DOE-OR, P.O. Box 2001, Oak Ridge, TN 37831-8600

25. B. Chexal, Electric Power Research Institute, 3412 Hillview Avenue, Palo Alto, CA 94303

26. V. Radeka, Brookhaven National Laboratory, Instrumentation Division, 535-B, Upton, NY 11973

27. M. M. Sevik, Carderock Division, Naval Surface Warfare Center, Code 1900, Bethesda, MD 20084-5000

28. R. M. Taylor, Leeds and Northup, Sunneytown Pike, North Wales, PA 19454

29–30. Office of Scientific and Technical Information, U.S. Department of Energy, P.O. Box 62, Oak Ridge, TN 37831

DATE
FILMED
9/2/93

END